RESTORING HEARING AND BALANCE IN A MOUSE MODEL OF *SLC26A4* - RELATED DEAFNESS

By

XIANGMING LI

B. S., Wuhan University, Wuhan, P.R. China, 2007

AN ABSTRACT OF A DISSERTATION

submitted in partial fulfillment of the requirements for the degree

DOCTOR OF PHILOSOPHY

Graduate Biochemistry Group

KANSAS STATE UNIVERSITY

Manhattan, Kansas

2013

Abstract

Mutations of *SLC26A4* are the most common cause of the hearing loss associated with enlargement of the vestibular aqueduct. *SLC26A4* encodes pendrin, an anion exchanger expressed in the cochlea, the vestibular labyrinth, and the endolymphatic sac of the inner ear. *Slc26a4*$^{\Delta/\Delta}$ mice, devoid of pendrin expression, develop an enlarged membranous labyrinth which leads to the failure to develop hearing, thereby recapitulating the human disease. Identifying the ionic composition of the endolymph and evaluating the importance of pendrin expression at various sites are initial steps towards developing strategies for preventing enlargement of the endolymph volume and subsequently restoring the inner ear functions. The major aims of the present study are 1) To determine the ionic composition of inner ear fluids during the developmental phase in which the enlargement of the endolymph volume occurs; 2) To test the hypothesis that pendrin expression in the endolymphatic sac is more important than its expression in the cochlea and the vestibular labyrinth. Here, we determined the Na^+ and K^+ concentrations in the cochlea and the endolymphatic sac with double-barreled ion-selective electrodes and generated a mouse model that restores pendrin expression in the endolymphatic sac while lacking expression in the cochlea and the vestibular labyrinth. High Na^+ and low K^+ concentrations were found in the cochlear endolymph during the embryonic stage. A rise of the K^+ concentration along with a decline of the Na^+ concentration occurred shortly before birth. The site-specific restoration of pendrin to the endolymphatic sac prevented enlargement and rescued hearing and balance. In conclusion, these data demonstrate that endolymph, in the phase of luminal enlargement during the embryonic development, is a Na^+-rich fluid that is modified into a K^+-rich fluid just before birth; restoration of pendrin in the endolymphatic sac is sufficient for developing normal inner ear function. Furthermore, these data suggest enlargement of endolymph volume caused by the loss of *Slc26a4* is a consequence of disrupted Na^+ absorption. Moreover, pharmacological strategies that correct fluid transport, as well as spatially and temporally limited restorations of pendrin, might restore normal inner ear functions in humans carrying mutations of *SLC26A4.*

RESTORING HEARING AND BALANCE IN A MOUSE MODEL OF *SLC26A4* - RELATED DEAFNESS

by

XIANGMING LI

B. S., Wuhan University, Wuhan, P.R. China, 2007

A DISSERTATION

submitted in partial fulfillment of the requirements for the degree

DOCTOR OF PHILOSOPHY

Graduate Biochemistry Group

KANSAS STATE UNIVERSITY

Manhattan, Kansas

2013

Approved by

Major Professor

Dr. Philine Wangemann

Department of Anatomy and Physiology

Copyright

Abstract

Mutations of *SLC26A4* are the most common cause of the hearing loss associated with enlargement of the vestibular aqueduct. *SLC26A4* encodes pendrin, an anion exchanger expressed in the cochlea, the vestibular labyrinth, and the endolymphatic sac of the inner ear. *Slc26a4*$^{\Delta/\Delta}$ mice, devoid of pendrin expression, develop an enlarged membranous labyrinth which leads to the failure to develop hearing, thereby recapitulating the human disease. Identifying the ionic composition of the endolymph and evaluating the importance of pendrin expression at various sites are initial steps towards developing strategies for preventing enlargement of the endolymph volume and subsequently restoring the inner ear functions. The major aims of the present study are 1) To determine the ionic composition of inner ear fluids during the developmental phase in which the enlargement of the endolymph volume occurs; 2) To test the hypothesis that pendrin expression in the endolymphatic sac is more important than its expression in the cochlea and the vestibular labyrinth. Here, we determined the Na^+ and K^+ concentrations in the cochlea and the endolymphatic sac with double-barreled ion-selective electrodes and generated a mouse model that restores pendrin expression in the endolymphatic sac while lacking expression in the cochlea and the vestibular labyrinth. High Na^+ and low K^+ concentrations were found in the cochlear endolymph during the embryonic stage. A rise of the K^+ concentration along with a decline of the Na^+ concentration occurred shortly before birth. The site-specific restoration of pendrin to the endolymphatic sac prevented enlargement and rescued hearing and balance. In conclusion, these data demonstrate that endolymph, in the phase of luminal enlargement during the embryonic development, is a Na^+-rich fluid that is modified into a K^+-rich fluid just before birth; restoration of pendrin in the endolymphatic sac is sufficient for developing normal inner ear function. Furthermore, these data suggest enlargement of endolymph volume caused by the loss of *Slc26a4* is a consequence of disrupted Na^+ absorption. Moreover, pharmacological strategies that correct fluid transport, as well as spatially and temporally limited restorations of pendrin, might restore normal inner ear functions in humans carrying mutations of *SLC26A4.*

Table of Contents

List of Figures

List of Tables

Acknowledgements

I would like to thank Dr. Philine Wangemann, my major professor, who introduced me to biomedical science and helped me grow into an independent scientist. I am very grateful to her for giving me the opportunity to work in her outstanding laboratory and providing tremendously support in the course of my learning and research. Also, I would like to thank the professors in my committee. Dr. Anna Zolkiewska, Dr. Bruce Schultz and Dr. Peying Fong provided valuable advice during my Ph.D program. Thanks to Dr. Larry Hollis for acting as my outside chair-person as well as Dr. Andrew J. Griffith, Dr. Daniel C. Marcus and Dr. Taku Ito for constructive suggestions during my research work. Also, I would like to extend my gratitude to the past and current lab members. Donald Harbidge, Fei Zhou, Gayathri Krishnamoorthy, Hyoung-mi Kim, Joel Sanneman, Julie Hix, Kalidou Ndiaye, Katrin Reimann, Ruchira Singh, Sara Billings and Takayuki Kudo have given me priceless help. Moreover, I would like to thank all my friends in Manhattan, Kansas, who have been with me and made my time here unforgettable. Last but not the least, I would like to thank my mother Yuanhui Xiang and my father Baoli Li, the most precious people in my whole life.

Chapter 1 Introduction

Organization of Chapter 1

This chapter provides an overview of inner ear anatomy, physiology and genetics with an emphasis on the hearing and balance function. It starts with an introductory section on the inner ear anatomy, development and physiology, followed by a summary of the environmental and genetic factors that cause hearing impairment. The last section focuses on the gene *SLC26A4*[1], that when mutated contributes to the hearing loss associated with enlarged vestibular aqueduct (EVA).

Inner ear anatomy

The mammalian ear is comprised of the three parts: the outer ear, middle ear and inner ear (*Figure 1.1A*). The outer ear is comprised of the pinna, the external auditory canal and the surface of tympanic membrane. The pinna collects and directs the sound through the ear canal to the tympanic membrane. In some mammals with mobile pinnae, each pinna helps to localize the direction of the sound. In humans, the direction of the sound is localized by the central nervous system. The ear canal is important to direct and concentrate the sound wave. Blockage of the ear canal results in the

---

[1] In compliance with the guideline for human gene nomenclature from HUGO gene nomenclature committee (http://www.genenames.org/) [1] as well as the guideline for mouse gene nomenclature (http://www.informatics.jax.org/mgihome/nomen/) , the symbols for human genes are represented with italicized upper-case letters and the symbols for murine genes are represented in italicized letters with only the first letter being capitalized. e.g. *KCNQ1* represents the gene in human, and *Kcnq1* represents the gene in mouse.

The symbols to corresponding proteins are represented as all upper-case letters, but are not italicized for either human or mouse. e.g. KCNQ1 represents the protein expressed in both human and mouse.

Exception: In Chapter 1, instead of using SLC26A4 as the symbols for encoded protein, pendrin represents the encoded proteins in both human and mouse.

dampening of hearing. The outer portion of the skin in the ear canal produces earwax which provides physical and biological protection.

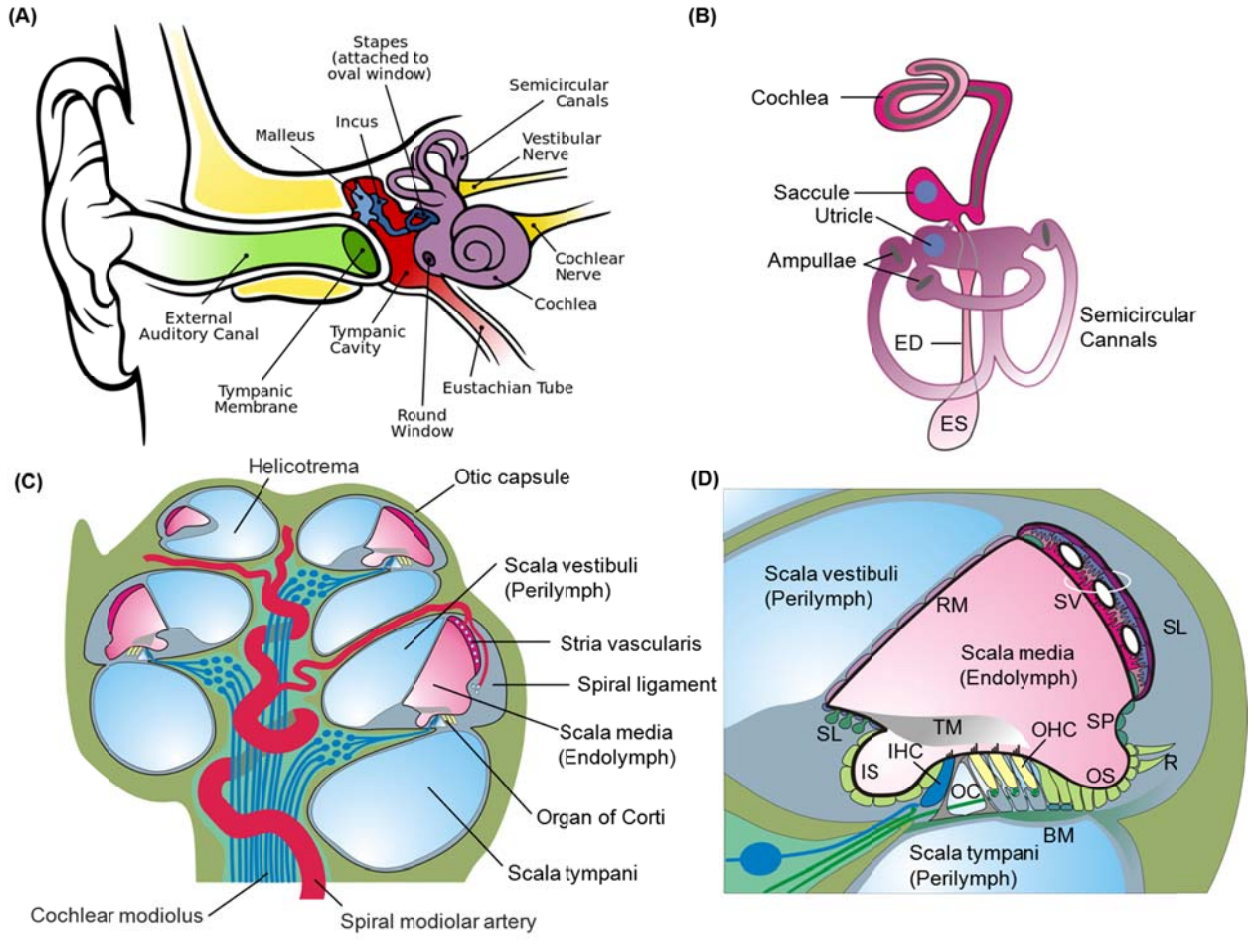

Figure 1.1: Schematic diagram of the anatomy of auditory apparatus.

(A) The overview of the outer ear, middle ear and inner ear. This image is adapted from Chittka et al. 2005 [2]. (B) The membranous labyrinth of the inner ear. Artwork by Dr. Philine Wangemann, adapted from Kim and Wangemann 2001[3]. (C-D) The cross sections of the membranous labyrinth in cochlea to demonstrate the internal structure. Artwork by Dr. Philine Wangemann, adapted from Marcus 2012 [4]. (C) The middle modiolar section of the cochlea to show four cross-sections of the membranous labyrinth. (D) Enlarged view of one cross-section of the membranous labyrinth to show the heterogeneity of the epithelia. ED: Endolymphatic duct. ES: Endolymphatic sac. RM: Reissner's membrane. SV: Stria vascularis. SL: Spiral ligament. SP: Spiral prominence. R: Root cell. OS: Outer sulcus. BM: Basilar membrane. OC: Organ of Corti. OHC: Outer hair cell. IHC: Inner hair cell. IS: Inner sulcus. SL: Spiral limbus. TM: Tectorial membrane.

The middle ear, also known as tympanic cavity, is an air-filled cavity behind the tympanic membrane that is connected to the oral cavity through the Eustachian tube. The Eustachian tube is normally closed but briefly opens during swallowing, which equalizes the pressure between the tympanic cavity and the atmosphere. The middle ear contains three ossicles, malleus, incus and stapes, that connect the tympanic membrane to the oval window of the cochlea. Sound, which consists of periodic air-pressure variations, induces movements of the tympanic membrane, which in turn induce a "chain-movement" of the three ossicles. The last of the three ossicles, the stapes, contacts the oval window and transmits the movements to the inner ear fluids.

The inner ear, resides in the temporal bone. It houses the membranous labyrinth, which consists of two epithelia-lined fluid compartments (*Figure 1.1B*). One compartment consists of the cochlea for detecting sound, the saccule for detecting linear acceleration, and the endolymphatic sac, a non-sensory structure believed to be involved in fluid regulation [5]. The other compartment consists of the utricle for detecting linear acceleration and three ampullae with semicircular canals for detecting angular acceleration. The lumen of both compartments is filled with endolymph and the two epithelial structures are surrounded by perilymph. Perilymph is essentially a common compartment that is defined by the temporal bone. The epithelia of the membranous labyrinth are heterogeneous consisting of sensory cells as well as a variety of supporting cells that define the structure, determine the composition of the luminal fluid, and set the transepithelial voltage (*see section* "Inner ear physiology").

The two major fluids of the inner ear, endolymph and perilymph, are very different in their composition. Endolymph contains high K^+, Cl^-, and HCO_3^- concentrations and low Na^+ and Ca^{2+} concentrations, which is an unusual composition for an extracellular body fluid [6]. In contrast, perilymph contains high Na^+ and Cl^- concentrations similar to other extracellular fluids in the body.

The cochlea is a snail-like structure consisting, in humans and mice, of two and half turns (*Figure 1.1B*). In the cochlea, by sectioning along the cochlear modiolus from the apical to the basal turns, four cross-sections of the membranous labyrinth can be visualized (*Figure 1.1C*). Scala media is the term for the membranous labyrinth in the

cochlea. Scala media is surrounded by two open perilymph-filled fluid spaces, scala vestibuli and scala tympani. Scala vestibuli and tympani are connected throughout the length of the cochlea via the interstitial fluid of the spiral ligament. In addition, scala vestibuli and scala tympani are connected at the cochlear apex. This connection is termed helicotrema. In the cochlea, scala media is enclosed by the sensory and non-sensory epithelia cells (*Figure 1.1D*). The sensory epithelia consisting of inner and outer hair cells are located in the organ of Corti and the non-sensory epithelia consist of a variety of supporting cells that define the cochlear structure, maintain endolymph composition and transepithelial voltage (*see section* "Inner ear physiology").

Inner ear morphogenesis

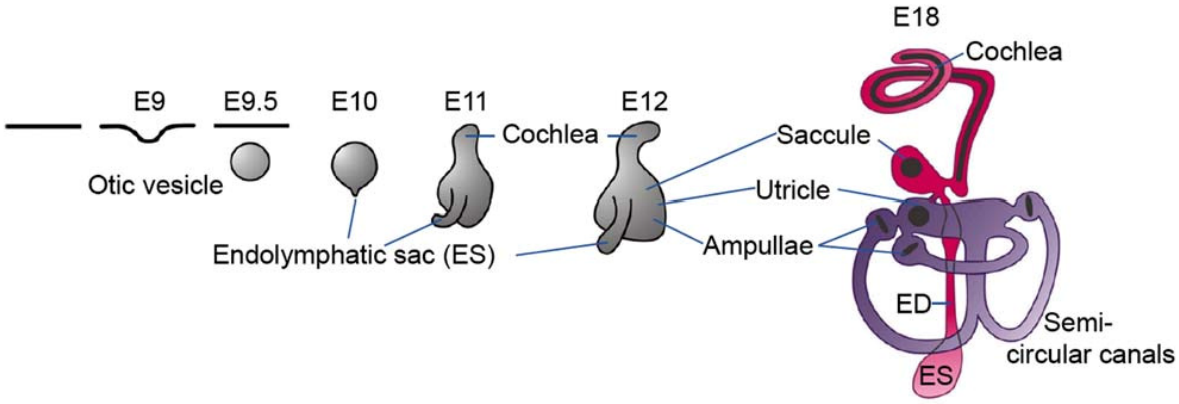

Figure 1.2: Embryonic morphogenesis of the murine inner ear.

ED: Endolymphatic duct. Artwork by Dr. Philine Wangemann, reproduced from Wangemann 2011 [7].

The knowledge about the development of the inner ear has mainly acquired from the study of animal models (*see textbook* "Development of the Inner Ear" *[8] for review)*. For example, the morphology of the inner ear at different developmental stages from the formation of the otocyst onward, has been established, by using the paint – filled technique, which enables the visualization of the fluid space enclosed by inner ear epithelia [9]. The development of the murine inner ear begins with the formation of the otic pit at embryonic day (E) 9, which is formed by the invagination of ectodermal cells (*Figure 1.2*). The continuous bending and eventual closure of the otic pit at E9.5, forms

a spherical structure, termed otocyst. The morphogenesis of the inner ear from the otocyst, is guided by factors from the adjacent hindbrain and mesenchyme. This process starts at E10 with a protrusion from the dorsal side of the otocyst that forms the primordium of the endolymphatic duct and sac system. At E11, a protrusion from the ventral side of the otocyst appears and forms the primordium of the cochlear duct. In the next 6-7 days, the primordia of the endolymphatic duct and sac system, as well as the cochlear duct, continue to elongate to achieve their full structures.
Contemporaneously, the middle portion of the otocyst gradually forms the vestibular labyrinth, including the saccule, the utricle, and the semicircular canals [10]. Between E16.5 to17.5, the closure of the duct between the saccule and utricle separates the membraneous labyrinth into two fluid-compartments with one compartment composed of cochlea, saccule and endolymphatic sac and the other one composed of utricle and semicircular canals [11].

Inner ear physiology

The inner ear contains both sensory and non-sensory epithelial cells, which enclose the endolymphatic space. Sensory cells are responsible for transducing mechanic signals of sound and acceleration into electric signals - a process termed mechanotransduction. Nonsensory cells are essential for supporting this mechanotransduction by maintaining the ion composition in endolymph and generating a high endolymphatic potential.

Mechanotransduction

The sensory hair cells are responsible for detecting the sound in the cochlea (*Figure 1.3A*), the linear accelerations in the utricle and saccule (*Figure 1.3B*), and the angular accelerations in the ampullae (*Figure 1.3C*). For an overview, refer to the textbook by Boron and Boulpaep [12].
In the cochlea, one row of inner hair cells and three rows of outer hair cells are arranged in parallel in a structure termed organ of Corti (*Figure 1.3A*). The hair cells on the basal turn of the cochlea are responsible for detecting high-frequency sound, while the hair

cells on the upper turn of the basilar membrane are responsible for detecting low-frequency sound. This spatial arrangement of hair cells for detecting distinct frequencies of sound is known as tonotopy. The distinct mechanical properties of the individual hair cells (the length and stiffness of hair bundles), as well as those of the basilar membrane (the thickness and width) confer functional requirements of tonotopy [13,14]. In the vestibular labyrinth, the vestibular hair cells are arranged in clusters in the maculae of the utricle and saccule as well as in the crista of the ampullae (*Figure 1.3B and C*). Two types of vestibular hair cells are present in the vestibular labyrinth. Type I cells have a flask shape with constricted neck; while type II cells have a cylindrical cell body [15].

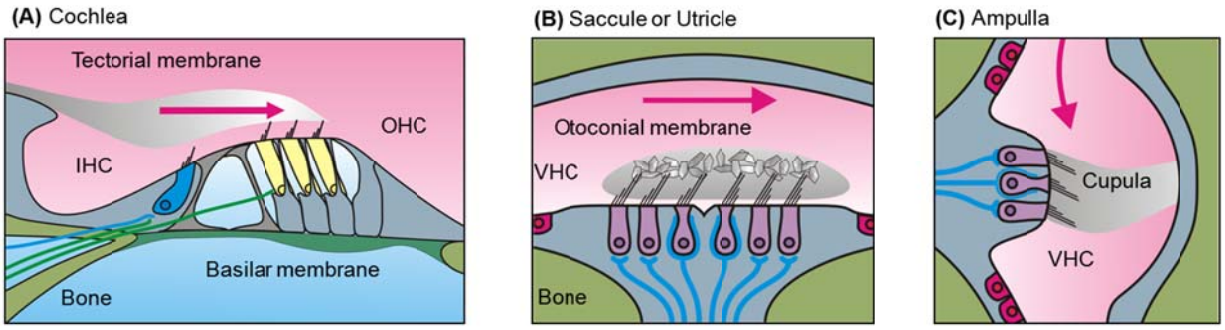

Figure 1.3: Mechanotransduction

Schematic diagram of the organ of Corti in the cochlea (A), the saccule or utricle (B), and an ampulla of vestibular labyrinth (C). The direction of hair bundle deflections that cause opening of MTC is marked (red arrows). Panels are adapted from Marcus and Wangemann 2010 [16]. IHC: Inner hair cell. OHC: Outer hair cells. VHC: Vestibular hair cells.

The hair cells have the mechanic sensitive organelle, the hair bundles, present on their apical surface. In the vestibular labyrinth, the hair bundles are comprised of one single kinocilium adjacent to multiple rows of stereocilia of descending heights. In contrast, hair bundles in the cochlea are comprised solely of stereocilia. Cochlea hair cells form a kinocilium during development but this kinocilium is lost with maturation of the hair bundle [17].

The stereocilia contain mechanosensitive transduction channels (MTCs), which are nonselective cation channels of unclear molecular identity [18]. The stereocilia are overlaid by extracellular matrices. In the cochlea, outer hair cells contact the tectorial membrane and in the ampullae, vestibular hair cells contact the cupulae (*Figure 1.3*). The tectorial membrane and the cupulae consist of non-mineralized protein matrices. In utricle and saccule, vestibular hair cells are covered by otoconial membranes, which consist of a protein matrix embedded with mineralized otoconia that provide inertia. Sound and acceleration induce relative movements between the extracellular matrices and the stereocilia and cause deflections of the hair bundles. The deflection of stereocilia towards the higher rows opens the MTCs, whereas the deflection of stereocilia towards the lower edges closes the MTCs [19]. MTC opening allows the influx of cations, primarily K^+, which depolarizes the membrane potential. This depolarization triggers the release of neurotransmitters from the basal pole of the hair cell into the synaptic cleft which modulates the action potential frequency of contacting neurons. For more detailed information of mechanotransduction, see reviews Holt & Corey, 2000 and Schwander et al., 2010 [17,20].

K^+ recycling

K^+ is the main current carrier for mechanotransduction, since K^+ is the major cation in endolymph. The high concentration of K^+ in cochlear and vestibular endolymph (~150 mM) originates from marginal cells in the cochlea and from dark cells in the vestibular labyrinth [21]. The physiological benefits for K^+ as the major current carrier are: 1) K^+ is the most abundant cytosolic cation, therefore the influx of K^+ minimally disturbs intracellular ion homeostasis; 2) the influx and extrusion of K^+ follow the electrochemical gradient, therefore, the mechanotransduction process is energetically inexpensive for the sensory cells [22].

The high K^+ concentration in cochlear endolymph originates from marginal cells of stria vascularis. Stria vascularis is a multi-layered sheet of vascularized non-sensory epithelial cells in the lateral wall of the cochlea that rest on the spiral ligament, which consist of specialized fibrocytes [23]. Stria vascularis is comprised of three cell layers,

basal cells, intermediate cells and marginal cells (*Figure 1.4*). The interstitial space between marginal cells and basal cells is filled with intrastrial fluid. The interstitial space between fibrocytes of the spiral ligament is continuous with perilymph. Spiral ligament fibrocytes take up K^+ and channel K^+ through gap junctions into the intermediate cells of stria vascularis from where it is released into the intrastrial space [6]. From the intrastrial fluid space, K^+ is taken up into the strial marginal cells. This uptake is mediated by a cooperation of the Na^+/K^+-ATPase and SLC12A2 ($Na^+/2Cl^-/K^+$ cotransporter) in the basolateral membrane. Marginal cells then secrete K^+ into endolymph via the K^+ channels KCNQ1/KCNE1 in the apical membrane.

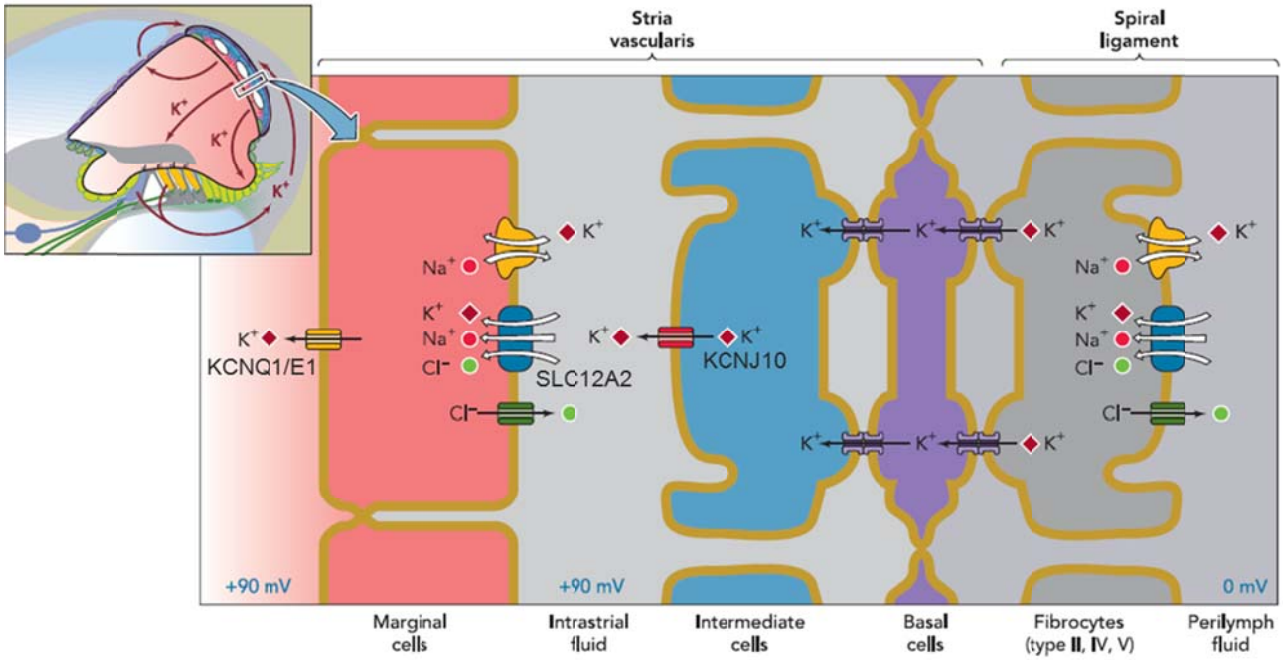

Figure 1.4: K^+ recycling and generation of endolymphatic potential in cochlea.

Schematic diagram of K^+ cycling in the cochlea and of K^+ transport and generation of the endocochlear potential in stria vascularis. Figure is reproduced from Zdebik et al. 2009 [24]

The high concentration of K^+ in endolymph is required for sensory transduction. K^+ that enters hair cells via the MTC is released into perilymph through K^+ channels in the basolateral membranes of hair cells. From perilymph K^+ is recycled back to endolymph. The recycling of K^+ may follow different pathways [24]: 1) K^+ released from the hair cells

may be buffered by supporting cells in the organ of Corti and ultimately diffuse via perilymph toward the fibrocytes in the spiral ligament. 2) K^+ may be taken up into supporting cells in the organ of Corti and reach fibrocytes in the spiral ligament through a network of gap junctions. K^+ leaves endolymph not only via hair cells but also via non-sensory epithelial cells, including those of the outer sulcus [25,26]. K^+ cycling is not limited to the cochlea. In the vestibular labyrinth, K^+ cycling consists of K^+ secretion in vestibular dark cells and K^+ efflux via hair cells and transitional cells [4].

Endocochlear potential

The driving force for mechanotransduction is primarily generated by K^+ channels in the basolateral membrane that generate a negative membrane potential in cochlear and vestibular hair cells. The endocochlear potential is a transepithelial potential that is generated by stria vascularis and that contributes to the driving force for mechanotransduction in the cochlea [27,28]. The endocochlear potential is specific to the cochlea. There is no equivalently large positive transepithelial potential in the vestibular labyrinth. To the contrary, the transepithelial potential in the vestibular labyrinth is negative [29]. The endocochlear potential depends on a serial arrangement of two epithelial barriers that exists in the cochlea but not in the vestibular labyrinth.

In cochlea, stria vascularis consist two epithelial barriers that are comprised of epithelial cells linked by tight junctions [4]. Tight junction-linked marginal cells form the barrier that separates intrastrial fluid from endolymph and tight junction-linked basal cells form the barrier that separates intrastrial fluid from perilymph (*Figure 1.4*). Intermediate cells are connected via gap junctions to the inner membrane of basal cells and fibrocytes of the spiral ligament are connected via gap junctions to the outer membrane of basal cells. The density of gap junctions is extremely high so that the membrane potential across the inner membrane of basal cells is defined by the K^+ channel KCNJ10 that is located in intermediate cells and that the membrane potential across the outer membrane of basal cells is defined by the channels that are located in fibrocytes. The endocochlear potential is a K^+ diffusion potential that is generated across the K^+ channel KCNJ10 located on intermediate cells [29]. The magnitude of the potential depends on the low

K^+ concentration in the intrastrial fluid and the high K^+ concentration in the cytosol of the intermediate cells [6].

Pendrin

Hearing loss associated with enlarged vestibular aqueduct (EVA)

The association between pendrin and hearing loss associated with EVA has been studied extensively and this literature has been reviewed by Ito et al 2011 and Griffith and Wangemann 2011 [30,31]. An excerpt assembled from these reviews is presented here.

Mutations of *SLC26A4* are a common cause for neurosensory hearing loss with enlarged vestibular aqueduct (EVA), which manifest in a non-syndromic and a syndromic form. The non-syndromic form is called DFNB4 (non-syndromic deafness, autosomal recessive 4; MIM # 600791) and the syndromic form is called Pendred syndrome (MIM #: 274600)[32–35]. Pendred syndrome consists of neurosensory hearing loss and deficiency in iodine organification in the thyroid. The degree of hearing loss in humans with DFNB4 or Pendred syndrome is highly variable ranging from mild to profound with a manifestation that can be unilateral or bilateral, stable, fluctuating and/or progressive in nature [36].

DFNB4 and Pendred syndrome are autosomal recessive conditions. If mutations of *SLC26A4* were the sole causes for DFNB4 or Pendred syndrome, it would be expected that carriers of bi-allelic mutations manifest disease and carriers of mono-allelic mutations do not manifest disease. However, in many patients with DFNB4 or Pendred syndrome, only one or even no mutant allele of *SLC26A4* was found [37]. This finding suggests that factors, other than the mutations of *SLC26A4* that were detected in screens can cause DFNB4 and Pendred syndrome. Factors may be environmental, epigenetic or genetic in nature [37]. For example, common screening methods do not cover the complete non-coding regions, including the entire promoter and introns, in which mutations could be hidden [38]. Further, genes other than *SLC26A4* may be responsible or contribute to disease manifestation. A digenic inheritance pattern has

been demonstrated in mice where double-heterozygous mouse *Foxi1*$^{+/-}$ / *Slc26a4*$^{\Delta/+}$ develop neurosensory hearing loss and EVA [39]. Analogous, a digenic inheritance pattern has been found in patients with neurosensory hearing loss and EVA, who carry mono-allelic mutations of *SLC26A4* and mono-allelic mutations of *FOXI1* or *KCNJ10* [39,40]. These digenic inheritance patterns, however, have been found only in a few families and appear to not represent a prevalent cause of neurosensory hearing loss with EVA [41,42]. Other candidates for digenic inheritance patterns are genes, such as *ATP6V1B1* and *ATP6V0A4* that are expressed in mitochondria-rich cells of the endolymphatic sac and contribute to ion transport similar to *SLC26A4*.

ATP6V1B1 and *ATP6V0A4* encode subunits of the vacuolar H^+-ATPase. In humans, bi-allelic mutations of *ATP6V1B1* are associated with early-onset profound neurosensory hearing loss and EVA [43–46]. Bi-allelic mutations of *ATP6V0A4* are associated with late-onset of neurosensory hearing loss with various degrees of severity [43,47].

Unlike human patients with bi-allelic mutations of *ATP6V1B1*, mice lacking functional expression of *ATP6V0B1* develop normal hearing [48], which is due to a compensatory mechanism mediated by the ATP6V0B2, the B2 subunit of vacuolar H^+-ATPase [49]. Unlike human patients with bi-allelic mutations of *ATP6V0A4,* mice lacking functional expression of ATP6V0A4 are profound deaf and develop an enlarged endolymphatic space and EVA [50–52].

Based on these studies in humans and animal models, it is plausible to speculate that double-heterozygous mouse *Atp6v0a4*$^{\Delta/+}$ / *Slc26a4*$^{\Delta/+}$ may develop neurosensory hearing loss and EVA and that a digenic inheritance pattern consisting of mono-allelic mutations of *ATP6V1B1* and mono-allelic mutations of *SLC26A4* may exists among patients presenting with neurosensory hearing loss and EVA.

Protein structure

Pendrin, encoded by *SLC26A4*, belongs to the solute carrier *26A* (*SLC26A*) family, which contains 11 members in human [53]. *SLC26A1* and *SLC26A2* encode sulfate transporters. *SLC26A3*, *SLC26A4* and *SLC26A6* encode Cl^-/HCO_3^- exchangers,

SLC26A7 and *SLC26A9* encode Cl^- channels and *SLC26A5* encodes the motor protein prestin, which is expressed in the basolateral membrane of the cochlear outer hair cells. The function of *SLC26A8* and *SLC26A11* is unknown and *SLC26A10* is a pseudogene that lacks protein-coding ability. Both human and murine pendrin has 780 amino acids, with a similarity of 88% (blastp, http://blast.ncbi.nlm.nih.gov/Blast.cgi?PROGRAM=blastp&PAGE_TYPE=BlastSearch&LINK_LOC=blasthome).

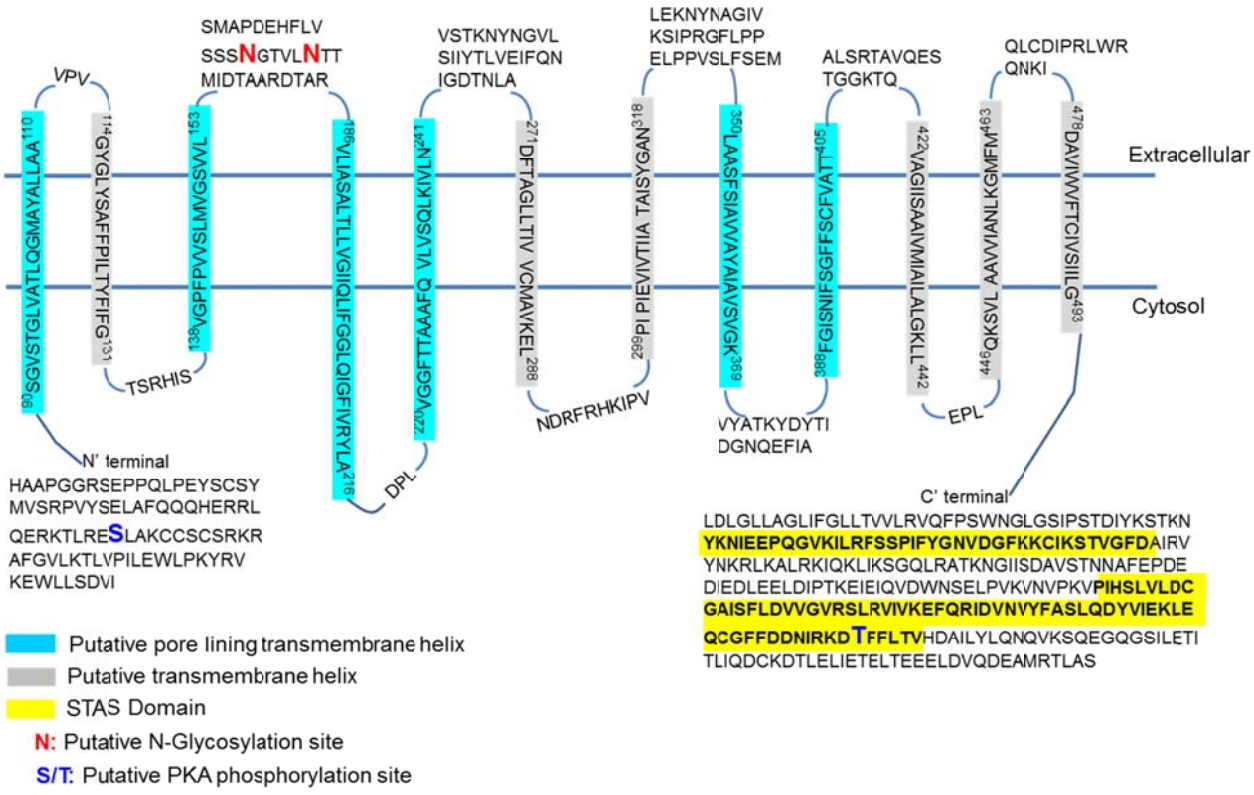

Figure 1.5: Putative structure of human pendrin

The sequence of human pendrin was acquired from NCBI (NP_000432.1). The topology of pendrin is predicted using web-based on-line software MEMSAT version3 http://bioinf.cs.ucl.ac.uk/psipred/?memsatsvm=1 .

The structure of pendrin is unknown, since crystallography and nuclear magnetic resonance data are lacking. Pendrin is predicted to have twelve transmembrane domains (*Figure 1.5*) with the N- and C-terminals located on the cytosolic side of the

plasma membrane [54]. Pendrin, and other members in SLC26 family, contain a STAS (Sulfate Transporter and Anti-Sigma factor antagonist) domain near their C-terminal position. The STAS domain in pendrin may regulate the interaction with CFTR that leads to a stimulation of ion transport [55,56]. Human pendrin contains two predicted protein kinase A (PKA) phosphorylation sites, whereas mouse pendrin contains only one PKA phosphorylation site. Phosphorylation sites may be involved in regulating the trafficking of pendrin to plasma membrane [57,58] (*see "*Posttranslational regulation"). In addition, human and mouse pendrin contains two predicted N-linked glycosylation sites at asparagine (N) 167 and 172. Glycosylation has been shown to confer pH sensitivity upon pendrin [59] (*see "*Posttranslational regulation").

Function

Pendrin is an electroneutral anion exchanger unlike SLC26A3 and SLC26A6, which are electrogenic ion exchangers [60,61]. Pendrin was initially thought to transport SO_4^{2-} based on membership in the SLC26A family, which contains the SO_4^{2-} transporters, SLC26A1 and SLC26A2 [33]. However, functional expression studies of pendrin in oocytes as well as insect and mammalian cell lines revealed that pendrin does not transport SO_4^{2-}, but other small anions such as Cl^- , I^- , OH^-, $CHOO^-$ and HCO_3^- [62–65]. Anion transport mediated by pendrin has been investigated in native tissues and cell lines from the kidney, thyroid, salivary gland and the airways. In the cortical collecting ducts of the kidney, pendrin mediates HCO_3^- secretion [66]. In thyroid cells, pendrin mediates iodide efflux [67,68,68,69]. In parotic ducts of the salivary gland, pendrin mediates I^- secretion [70] and in bronchial epithelial cells of the airways, pendrin mediates SCN^- secretion [71].

Transcriptional regulation

The transcriptional regulation of pendrin has been studied extensively and this literature has been reviewed by Rozenfeld et al., 2011 [64]. An excerpt assembled from this review is presented here.

The expression of pendrin is regulated at the mRNA level by transcriptional factors such as FOXI1 (Forkhead box transcription factor I 1) and TTF1 (thyroid transcriptional factor 1), hormones, such as aldosterone and uroguanylin, cytokines, such as IL4 and IL13, and pH. The localization of *cis*-elements on the *SLC26A4* promoter as well as the effects, either stimulation or inhibition, have been identified [64] (*Figure 1.6*).

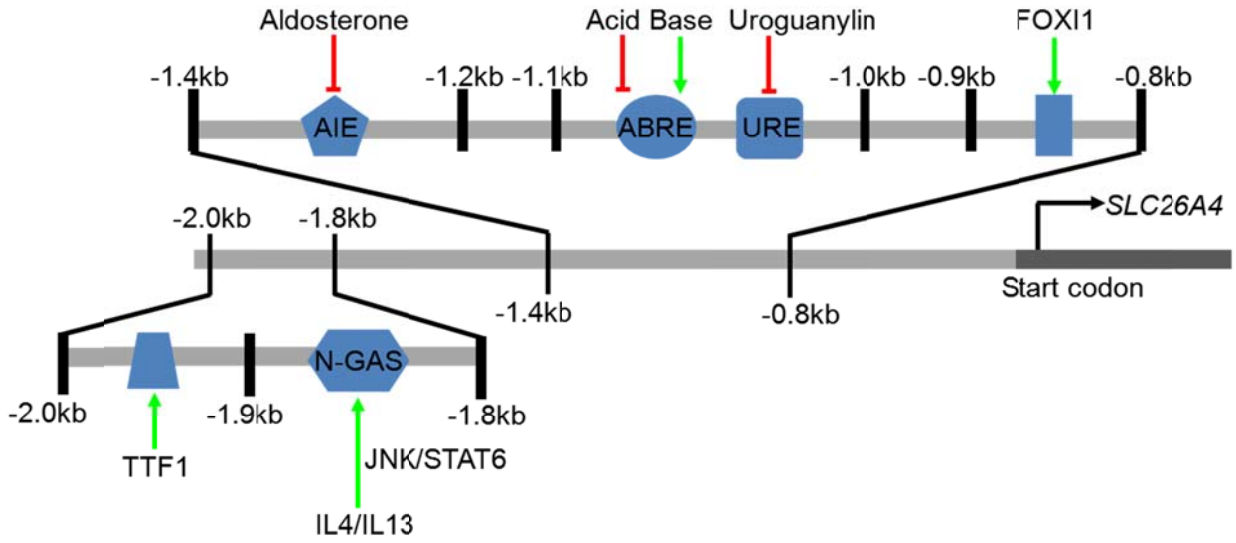

Figure 1.6: Regulatory elements on human SLC26A4 promoter.

*This diagram is adapted from Rozenfeld et al 2011 [64]. Trans-elements and corresponding cis-elements (**blue shapes**) are shown. Stimulatory and inhibitory effects are marked with **green arrows** and **red stop-bars**, respectively. Numbers in the diagram mark the distance from the start codon in kilobases (kb).*

Aldosterone-induced element (AIE): the AIE is located -1.4kb to -1.2kb upstream of the *SLC26A4* start codon (Adler et al., 2008 RM_6561). In the kidney, aldosterone inhibits pendrin mRNA expression *in vitro* (Adler et al., 2008 RM_6561); whereas analogs of aldosterone increase pendrin mRNA *in vivo* [72]. This aldosterone-induced effect on pendrin mRNA expression is kidney-specific and not observed in the thyroid or the inner ear (Adler et al., 2008 RM_6561). The discrepancy between *in vitro* and *in vivo* conditions may be because the administration of aldosterone *in vivo* controls the expression of a number of transporters and channels besides pendrin, such as epithelial sodium channel, sodium chloride symporter and chloride channels [73]. These may subsequently affect the expression of pendrin through feedback mechanisms. The *in*

vivo stimulatory effect of aldosterone on pendrin mRNA expression modulates the activity of NaCl absorption in kidney and consequently regulates the volume of extracellular fluid.

Uroguanylin response element (URE): the URE is located -1.1 kb to -1.0 kb upstream of the*SLC26A4* start codon [74]. Heat shock factor 1 has been suggested to function as the *trans*-element of URE [74]. In the kidney, applications of uroguanylin, a natriuretic peptide that is mainly secreted by the intestine [75], inhibit pendrin mRNA expression [74]. This inhibitory effect of uroguanylin on pendrin mRNA expression increases renal natriuresis under the condition of high salt diet.

Acid-base response element (ABRE): the ABRE is located -1.1kb to -1.0kb upstream of the *SLC26A4* start codon, which overlaps the URE (Adler et al., 2008 RM_6561). The effect of pH on pendrin mRNA expression is tissue-specific. In the kidney and inner ear, acidic pH inhibits pendrin mRNA expression and basic pH stimulates pendrin expression [76,77]. In the liver, acidic pH increases pendrin mRNA expression, whereas basic pH does not affect its expression [78]. In the thyroid, pH has no effect on pendrin mRNA expression [76]. The regulatory effect of pH on pendrin mRNA expression in the kidney and the liver may help maintain the systemic acid-base balance [77,79,80]. In the inner ear, the regulatory effect of pH on pendrin mRNA expression may help maintain the acid-base balance of inner ear fluids [81].

N-GAS motif: the N-GAS motif is the response element for the cytokines IL4 and IL13 that is located -1.9kb to -1.8kb upstream of the *SLC26A4* start codon [82]. IL4 and IL13 stimulate pendrin mRNA expression in the airways [83–85]. This effect is mediated via the JNK/STAT pathway, which activates nuclear translocation and binding of the *trans*-element STAT6 to the N-GAS motif [82]. The stimulatory effects of IL4 and IL13 on pendrin mRNA expression mediate the innate defense, which may play a role in pathologic immune responses seen in asthma and chronic obstructive pulmonary disease [71,82].

FOXI 1 (Forkhead box transcription factor I 1): the *cis*-element of FOXI1 is located -1.9kb to -0.8kb upstream of the *SLC26A4* start codon [39,64]. FOXI1 is a master transcriptional factor that is expressed in FORE (forkhead related) cells that are present

in the kidney, the inner ear, and the male reproductive duct [86,87] [88]. FOXI1 controls the expression of multiple genes that are involved in pH homeostasis. These genes encode the apically expressed Cl^-/HCO_3^- exchanger pendrin [87], the basolaterally expressed Cl^-/HCO_3^- exchangers SLC4A1 and SLC4A9 [89], multiple subunits of the vacuolar H^+-ATPase including ATP6V1B1, ATP6V0A1, ATP6V0A4 and ATP6V0E2 [90], as well as the carbonic anhydrase CAR2 [88].

Thyroid transcription factor *1 (TTF1)*: the *cis*-element of TTF1 is located -2.0kb to -1.9kb upstream of the *SLC26A4* start codon [91]. TTF1 is a master transcriptional factor expressed in the thyroid [91,92]. TTF1 controls the expression of genes involved in the thyroid hormone synthesis. These genes encode the thyrotropin receptor [93], the Na^+-I^- symporter SLC5A5 for iodide uptake [94], the Cl^-/I^- exchanger pendrin for iodide efflux, the enzyme thyroid peroxidase for iodide oxidation [95], as well as the protein thyroglobulin for iodine organification [96].

Post-translational regulation

Pendrin can be regulated by post-translational modifications, including phosphorylation and glycosylation, that influence plasma membrane abundance and function. Furthermore, the activity of pendrin may be modulated through interactions with CFTR.

PKA phosphorylations associated with the membrane abundance of pendrin.

Human pendrin is predicted to contain two PKA dependent phosphorylation sites, serine 49 and threonine 717, which are located in the C- and N-terminal cytosolic regions, respectively (*Figure 1.5*). Mouse pendrin is predicted to contain only one PKA dependent phosphorylation sites, serine 49, which is located in the N-terminal cytosolic region. The phosphorylation and trafficking of pendrin to plasma membrane can be regulated via the cAMP/PKA signaling pathway [57,58]. Upon elevated intracellular cAMP levels, the phosphorylation of pendrin increased in conjunction with an increased membrane abundance. Mutations of serine 49 and threonine 717 to alanine mitigate this response [57,58].

N-glycosylation may confer pH sensitivity upon pendrin

Acidification of the extracellular pH increases the binding affinity of anions as well as the rate of anion exchange in pendrin [59]. This pH sensitivity has been found to depend on the predicted N-glycosylation sites at asparagine (N) 167 and 172 (Figure 1.5) based on the finding that the pH sensitivity and glycosylation were lost in pendrin with alanine-substitutions of asparagine 167 and 172 (N167A/N172A). These substitutions abolished pH sensitivity but did not affect surface expression or basal anion exchange activity of pendrin.

Regulation of pendrin activity through the interaction of STAS domain with CFTR.

Members of the SLC26 family of proteins contain a STAS domain that is comprised of two regions in the C-terminal. In pendrin these span amino acid residues 536-573 and 654-722 (Figure 1.5). Studies in SLC26A3 and SLC26A6 demonstrate that the STAS domain interacts with the regulatory domain of CFTR and that this interaction stimulates the activity of both, the SLC26A member and CFTR [55,97,98]. Evidence for a similar interaction between pendrin and CFTR has been provided [55,56].

Physiological role

Pendrin is expressed in a variety of tissues, including the inner ear, the thyroid gland, the kidney, the male and female reproductive system as well as the airways [33,71,88,99]. The role of pendrin in the inner ear is essential, as the loss of pendrin expression leads to organ failure. This section focuses on the physiologic role of pendrin in the inner ear.

Location and onset of expression

In the murine inner ear, pendrin is expressed in the mitochondria-rich cells of the endolymphatic sac, the spiral prominence, root cells, and the spindle-shaped cells in the cochlea, and the transitional cells in the utricle, saccule and ampullae of the vestibular labyrinth (*Figure 3.1*) [100–102]. Pendrin expression in the inner ear begins in the endolymphatic sac at E11.5, in the cochlea at E14.5, and in the utricle, saccule and ampullae of the vestibular labyrinth at E16.5 [102].

Mouse models for hearing loss associated with EVA

Mutations of pendrin are the most prevalent causes for hearing loss associated with EVA. A number of mouse models in which *Slc26a4* expression is genetically modified were created and used to elucidate the etiology of this form of hearing loss:

Slc26a4$^{\Delta/\Delta}$ *mice*: *Slc26a4*$^{\Delta/\Delta}$ mice bear a deletion of exon 8 of *Slc26a4* , which introduce a frame-shift [103]. This frame-shift creates a stop codon which can be expected to cause a truncation of pendrin after the translation of 347 amino acids, which is ~44% of the normal pendrin protein. *Slc26a4*$^{\Delta/\Delta}$ mice lack pendrin expression, fail to develop hearing and balance, and develop enlarged endolymphatic compartments and giant otoconia.

Foxi1$^{-/-}$ *mice*: *Foxi1*$^{-/-}$ mice bear a complete deletion of the *Foxi1* coding sequence [104]. *Foxi1* controls *Slc26a4* expression in mitochondria-rich cells of the endolymphatic sac but *Foxi1* does not affect *Slc26a4* expression in the cochlea or the vestibular labyrinth. *Foxi1* ablation results in the absence of detectable *Slc26a4* in endolymphatic sac. *Foxi1*$^{-/-}$ mice are deaf and developed an enlarged endolymphatic space.

Slc26a4$^{loop/loop}$ *mice*: *Slc26a4*$^{loop/loop}$ mice were identified in a screen of mice in which mutations were induced by N-ethyl-N-nitroso-urea (ENU) [105,106]. *Slc26a4*$^{loop/loop}$ mice bear a missense mutation (C to T transition), that results in a serine to phenylalanine substitution at position 408 (S408F) and in a reduction of ion transport activity. *Slc26a4*$^{loop/loop}$ mice maintain pendrin expression in the inner ear, however, fail to develop hearing and balance, and develop enlarged endolymphatic compartments and giant otoconia.

Slc26a4$^{tm1Dontuh/tm1Dontuh}$ *mice*: *Slc26a4*$^{tm1Dontuh/tm1Dontuh}$ mice bear a point-mutation (c.919-2A>G) at the splicing site of exon 8 of *Slc26a4* [107]. This mutation mimics a common mutation observed in Asian populations [108]. In humans, the c.919-2A>G mutation reduces the fidelity of splicing leading to the coexistence of correctly splice mRNA that contains exon 8 and mRNA that lacks exon 8 [109]. The reduced fidelity of splicing is likely leading to a reduced level of protein expression. *Slc26a4*$^{tm1Dontuh/tm1Dontuh}$ mice maintain pendrin expression in the adult cochlea, however, pendrin expression levels appear to not be sufficient during the development of the

inner ear. Consequently, *Slc26a4*$^{tm1Dontuh/tm1Dontuh}$ fail to develop hearing and balance, and develop enlarged endolymphatic compartments and giant otoconia.

Slc26a4$^{tm2Dontuh/tm2Dontuh}$ *mice*: *Slc26a4*$^{tm2Dontuh/tm2Dontuh}$ mice bear a point-mutation (c.2168-A>G) in *Slc26a4* that results in a substitution of histidine 723 for arginine (H723R) [110]. This mutation mimics a common mutation observed in Asian populations [108]. In humans, the H723R mutation leads to a trafficking defect that reduces surface expression and eliminates function. *In vitro* studies have shown that this trafficking defect can be rescued by low temperature or the admission of chemical chaperones that restored surface expression and pendrin function [111,112]. Unlike humans, mice carrying the H723R mutation develop normal hearing [110]. It is conceivable that the H723R mutation in the context of the murine pendrin protein has a lesser effect on trafficking so that sufficient levels of pendrin protein are in the inner ear, in particular during development.

Atp6v0a4$^{\Delta/\Delta}$ *mice*: Two strains of *Atp6v0a4*$^{\Delta/\Delta}$ mice were generated [50,52]. One strain bears a deletion of exons 2-4 and the other a deletion of exon 11 of *Atp6v0a4.* *Atp6v0a4* encodes a subunit of the H^+ ATPase, which is expressed in the cochlea, the vestibular labyrinth and the endolymphatic sac of the inner ear. In the endolymphatic sac, Atp6v0a4 is expressed in the apical membrane of mitochondria-rich cells together with pendrin [113]. *Atp6v0a4*$^{\Delta/\Delta}$ mice fail to develop hearing, develop enlarged endolymphatic compartments and lack otoconia [50–52].

Tg(E);Tg(R);Slc26a4$^{\Delta/\Delta}$ *mice*: Pendrin expression in *Tg(E);Tg(R);Slc26a4*$^{\Delta/\Delta}$ mice is controlled by the bi-transgenic doxycycline-inducible expression system which permits control of the time and duration of pendrin expression [114]. This mouse model has been used to define the critical time period during which pendrin needs be present for the development of a hearing phenotype, *see* “Pendrin is temporally required for hearing acquisition”.

Tg(+);Slc26a4$^{\Delta/\Delta}$ *mice:* Pendrin expression in *Tg(+);Slc26a4*$^{\Delta/\Delta}$ mice is limited in the inner ear to the endolymphatic sac [115]. This mouse model does not express murine pendrin but human pendrin in the endolymphatic sac and lacks the expression of pendrin in the cochlea or the vestibular labyrinth. This mouse model has been used to

define the spatial requirement of pendrin expression for the development of a hearing phenotype, *see* “Pendrin is spatially required for hearing acquisition”.

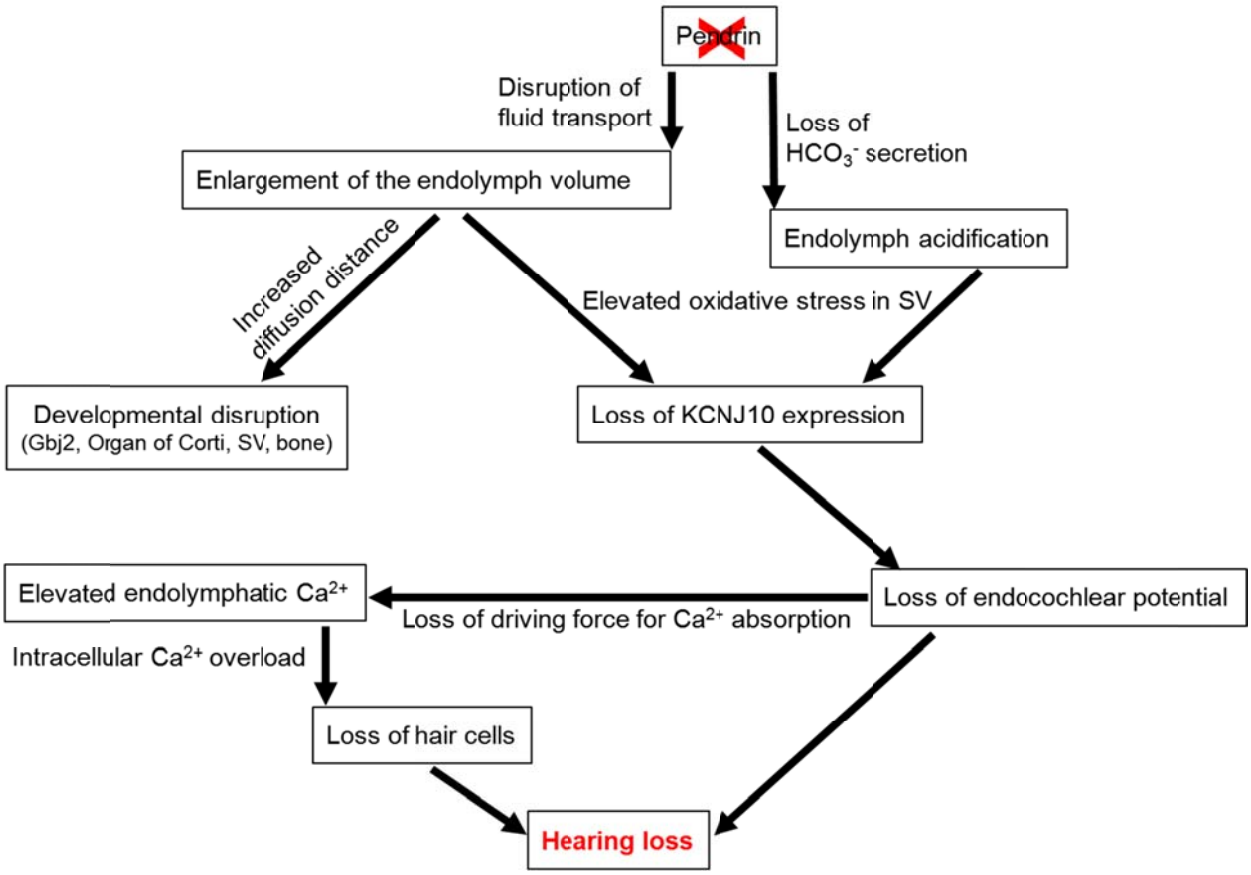

Figure 1.7: Pathological events leading to hearing loss in the absence of pendrin.

Schematic diagram of the major events that relate absence of pendrin to hearing loss.

Inner ear development in the absence of pendrin

The association between pendrin and hearing loss associated with EVA has been studied in mouse models and this literature has been reviewed by Wangemann 2011 and Griffith and Wangemann 2011 [7,30,31]. An excerpt assembled from these reviews is presented here.

Studies in mouse models have revealed that four major events lead to the failure to develop hearing in the absence of functional pendrin expression (*Figure 1.7*): a) enlargement of the endolymph volume, b) endolymph acidification, c) loss of the

endocochlear potential, and d) elevation of endolymphatic Ca^{2+} and loss of hair cells. These events are described in the following paragraphs.

Enlargement of the endolymph volume: A ~10-fold enlargement of endolymph volume develops in *Slc26a4*$^{\Delta/\Delta}$ mice at E14.5, the time when *Slc26a4*$^{\Delta/+}$ mice develop a surge in *Slc26a4* expression in the endolymphatic sac [3]. This enlargement persists throughout life [116]. Experiments ablating the endolymphatic sac from cultured otocysts have demonstrated that the endolymphatic sac regulates fluid absorption at the early phase of cochlear luminal growth [3]. These studies suggest that the enlargement is a consequence of a failure to absorb fluid. Measurements of the endolymphatic Na^+ and K^+ concentrations have revealed that endolymph consists of a NaCl-rich solution during the phase of cochlear growth and luminal enlargement [117]. These experiments suggest that enlargement of the endolymphatic volume may be a consequence of disrupted Na^+ absorption by the endolymphatic sac. The study that contains measurements of ion concentrations in embryonic endolymph is presented in Chapter 2.

The enlargement of endolymph volume stretches the surrounding epithelia and likely leads to an increase in diffusional distances for developmental factors, which leads to a disruption of inner ear development [116]. Disruption of inner ear development consists of events that occur premature or delayed. For example, Connexin 26, encoded by *Gjb2*, is expressed prematurely in *Slc26a4*$^{\Delta/\Delta}$ mice, whereas the development of stria vascularis, the organ of Corti, and bone is delayed [102,116].

Endolymph acidification: Lack of pendrin expression in *Slc26a4*$^{\Delta/\Delta}$ mice leads to an acidification of endolymph, which is a direct consequence of the loss of pendrin-mediated HCO_3^- secretion [81,118]. Acidification begins in the cochlea at E15.5 and in the endolymphatic sac at E17.5 [102]. The later onset of endolymph acidification in the endolymphatic sac may be due to a stronger buffering capacity of endolymph in the endolymphatic sac compared to endolymph in the cochlea. In addition, it is conceivable that lack of pendrin expression reduces surface expression of the H^+-ATPase, which limits the acid secretion.

Consequence of the acidification of endolymph include an elevation of the endolymphatic Ca^{2+} concentrations in the cochlea and the vestibular labyrinth [81,118].

In addition, the acidification may increase activity of the K^+ channel Kcnq1/Kcne1 in the apical membrane of stria marginal cells [119].

Loss of the endocochlear potential: Loss of the endolymphatic potential in *Slc26a4*$^{\Delta/\Delta}$ mice is a consequence of the degeneration of KCNJ10 beginning between P10 and P15, which coincides with the onset of expression of KCNJ10 and the development of a mature endocochlear potential [120,121]. Loss of KCNJ10 is due to an elevated level of oxidative and nitrative stress in stria vascularis [122]. Oxidative and nitrative stress in stria vascularis may be a consequence of delayed development of anti-oxidant defence mechanisms or a consequence of higher metabolic rates associated with higher rates of K^+ secretion.

Elevation of endolymphatic Ca^{2+} and loss of hair cells: Loss of hair cells in *Slc26a4*$^{\Delta/\Delta}$ mice begins at P15, the time at which hearing in *Slc26a4*$^{\Delta/+}$ mice matures [103]. The mechanism that leads to the loss of hair cells is not completely understood. It is conceivable that the elevated endolymphatic Ca^{2+} concentration leads to a cellular Ca^{2+} overload in the hair cells which triggers apoptosis-mediated cell death [81].

Pendrin is temporally required for hearing acquisition

Loss of pendrin expression in the inner ear of *Slc26a4*$^{\Delta/\Delta}$ mice leads to a severe expansion of the endolymphatic space and to a failure to acquire hearing [81,103]. This raises the question of whether pendrin is required to maintain hearing throughout life or whether pendrin is required only for the acquisition of hearing during development. The latter would define a time-window for a therapeutic intervention. This question has been addressed by investigations that used a model, Tg(E);Tg(R);*Slc26a4*$^{\Delta/\Delta}$ mice, in which the expression of pendrin could be controlled by a drug administered in the drinking water. Tg(E);Tg(R);*Slc26a4*$^{\Delta/\Delta}$ mice are a bi-transgenic model, in which the expression of *SLC26A4* is controlled by a doxycycline-inducible expression system [114]. Two sets of experiments were conducted. In the first set, the onset of doxycycline administration was varied during development. Induction of pendrin expression at E13.5 but no later than E16.5 led to the acquisition of normal hearing. Induction of pendrin after E16.5 led to hearing loss. In the second set of experiments, doxycycline was present during

conception and administration was discontinued at different times of development. Discontinuation of pendrin not earlier than P2, yielded normal hearing. This study establishes E16.5 to P2 as a critical period of development during which sufficient pendrin expression is required for the acquiring of normal hearing.

Pendrin is spatially required for hearing acquisition

The restoration of pendrin expression in the inner ear may be the most direct way for rescuing the hearing. Restoration of pendrin expression, however, may not be feasible since pendrin is expressed in many different epithelial cells in the inner ear including epithelial cells in the cochlea, the vestibular labyrinth and the endolymphatic sac [100–102]. Mitochondria-rich cells in endolymphatic sac are the first site where the expression of pendrin begins in the inner ear [102]. At the time in development at which the enlargement begins in *Slc26a4*$^{\Delta/\Delta}$ mice, the endolymphatic sac is the only site with appreciable pendrin expression in *Slc26a4*$^{\Delta/+}$ mice [102]. This finding suggested that restoring pendrin in the endolymphatic sac would prevent or at least postpone the enlargement of endolymph volume. Consistently, studies in *Foxi1*$^{-/-}$ mice revealed that pendrin expression in the cochlea and the vestibular labyrinth without expression in the endolymphatic sac is not sufficient for prevention of enlargement of endolymph volume and development of normal hearing [123]. Based on these findings, the hypothesis arose that pendrin expression in the endolymphatic sac may be more important than the expression in the cochlea or the vestibular labyrinth. This hypothesis was tested in Tg(+);*Slc26a4*$^{\Delta/\Delta}$ mice, a transgenic mouse model that expresses pendrin in the endolymphatic sac and lacks pendrin expression in the cochlea and the vestibular labyrinth [115]. Tg(+);*Slc26a4*$^{\Delta/\Delta}$ mice never develop an enlargement of endolymph volume and acquire normal hearing and balance function. These findings suggest that a spatial limited expression of pendrin in the endolymphatic sac is sufficient to restore normal inner ear function. The complete study of Tg(+);*Slc26a4*$^{\Delta/\Delta}$ mice is presented in Chapter 3.

Chapter 2 Endolymphatic Na^+ and K^+ concentrations during development

These data have been published in the following refereed journal article:

Xiangming Li, Fei Zhou, Daniel C. Marcus, Philine Wangemann
Endolymphatic Na^+ and K^+ concentrations during cochlear growth and enlargement in mice lacking *Slc26a4*/pendrin
PLoS ONE 8(5): e65977. doi:10.1371/journal.pone.0065977

Author Contributions

XL PW	Conceived and designed the experiments
XL FZ	Performed the experiments
XL FZ PW DCM	Analyzed the data
PW	Contributed reagents/materials/analysis tools
XL PW	Wrote the paper

Abstract

Slc26a4$^{\Delta/\Delta}$ mice are deaf, develop an enlarged membranous labyrinth, and thereby largely resemble the human phenotype where mutations of *SLC26A4* cause an enlarged vestibular aqueduct and sensorineural hearing loss. The enlargement is likely caused by abnormal ion and fluid transport during the time of embryonic development, however, neither the mechanisms of ion transport nor the ionic composition of the luminal fluid during this time of development are known. Here we determine the ionic composition of inner ear fluids at the time at which the enlargement develops and the onset of expression of selected ion transporters. Concentrations of Na^+ and K^+ were measured with double-barreled ion-selective electrodes in the cochlea and the endolymphatic sac of *Slc26a4*$^{\Delta/+}$, which develop normal hearing, and of *Slc26a4*$^{\Delta/\Delta}$ mice, which fail to develop hearing. The expression of specific ion transporters was examined by quantitative RT-PCR and immunohistochemistry. High Na^+ (~141 mM) and low K^+ concentrations (~11 mM) were found at embryonic day (E) 16.5 in cochlear endolymph of *Slc26a4*$^{\Delta/+}$ and *Slc26a4*$^{\Delta/\Delta}$ mice. Shortly before birth the K^+ concentration began to rise. Immediately after birth (postnatal day 0), the Na^+ and K^+ concentrations in cochlear endolymph were each ~80 mM. In *Slc26a4*$^{\Delta/\Delta}$ mice, the rise in the K^+ concentration occurred with a ~3 day delay. K^+ concentrations were also found to be low (~15 mM) in the embryonic endolymphatic sac. The onset of expression of the K^+ channel KCNQ1 and the $Na^+/2Cl^-/K^+$ cotransporter SLC12A2 occurred in the cochlea at E19.5 in *Slc26a4*$^{\Delta/+}$ and *Slc26a4*$^{\Delta/\Delta}$ mice. These data demonstrate that endolymph, at the time at which the enlargement develops, is a Na^+-rich fluid, which transitions into a K^+-rich fluid before birth. The data suggest that the endolymphatic enlargement caused by a loss of *Slc26a4* is a consequence of disrupted Na^+ transport.

(293 words)

Key words: Enlarged vestibular aqueduct; Pendred syndrome; ion-selective electrodes; endolymphatic sac; transepithelial potential; endocochlear potential;

Introduction

Enlargement of vestibular aqueduct (EVA) is a common inner ear malformation found in children with non-syndromic sensorineural hearing loss and hearing loss associated with Pendred syndrome [31]. Mutations of *SLC26A4* are a prevalent cause of EVA and of progressive and often fluctuating hearing loss with an onset before or around speech acquisition [108,124–127]. *SLC26A4* codes for pendrin, an anion exchanger that functions as a Cl^-/HCO_3^- exchanger in the inner ear [81]. In some populations, mutations in *SLC26A4* occur in 13-14% of deaf subjects [128,129].

Slc26a4$^{\Delta/\Delta}$ mice closely resemble the human phenotype, since *Slc26a4*$^{\Delta/\Delta}$ mice acquire an enlargement of the vestibular aqueduct during embryonic development. The vestibular aqueduct is a bony tunnel that forms around the epithelia-lined endolymphatic duct. Swelling of the fluid-filled epithelium of inner ear in *Slc26a4*$^{\Delta/\Delta}$ mice leads to an enlargement of the vestibular aqueduct. *Slc26a4*$^{\Delta/\Delta}$ mice fail to acquire hearing during the postnatal phase of development [81,103]. Studies on *Slc26a4*$^{\Delta/\Delta}$ mice suggest that the endolymphatic enlargement entails a ~10-fold larger luminal volume in the cochlea, that the endolymphatic acidification entails a ~2-fold higher H^+ ion concentration, and that the enlargement and acidification are key events that mark the onset of the pathology [102,116].

The development of the murine inner ear begins with an ectodermal invagination that forms an otocyst at embryonic day (E) 9.5. The otocyst is filled with amniotic fluid, which is a NaCl-rich fluid [130]. The otocyst extends two protrusions: one to form scala media of the cochlea and the other to form the endolymphatic duct and sac, while the middle of the otocyst is reorganized into the vestibular labyrinth [8]. The lumen of the endolymphatic sac opens at E10.5 and the lumen of the cochlea begins to open at E14.5. The fluid inside the lumen is called endolymph and the fluid surrounding the epithelium is called perilymph. In *Slc26a4*$^{\Delta/\Delta}$ mice, the enlargement of the endolymphatic lumen begins at E14.5, which coincides with cochlear growth and lumen formation between E14.5 and E18.5 [3,31].

The mesenchymal tissue surrounding the cochlea, the vestibular labyrinth and the endolymphatic duct forms cartilage during embryonic development that is later

converted into bone (*Figure 2.1A*). In addition, the cochlea and the vestibular labyrinth are enclosed in the temporal bone. Access to scala media of the cochlea is available via the round window that is located near the base of the cochlea. The endolymphatic sac is the only part of the inner ear that is not enclosed in cartilage or bone.

The mechanisms that lead to cochlear enlargement in *Slc26a4*$^{\Delta/\Delta}$ mice are not known. It is conceivable that fluid accumulation leading to the enlargement occurs in the wake of an abnormally low rate of ion absorption or an abnormally high rate of ion secretion. Ion transport in the inner ear has so far mainly been studied in adult animals, when endolymph consists of a K^+-rich fluid [6]. The enlargement of the endolymphatic lumen in *Slc26a4*$^{\Delta/\Delta}$ mice, however, occurs during embryonic development. Thus, it is of great interest to determine whether endolymph in *Slc26a4*$^{\Delta/\Delta}$ and *Slc26a4*$^{\Delta/+}$ mice at the time of enlargement is a K^+-rich fluid, as observed in the adult inner ear, or whether endolymph at this time is a Na^+-rich fluid similar in composition to amniotic fluid. The determination of the ion composition during the phase of enlargement is the very first step for understanding how the enlargement occurs. Thus the main goal of the present study was to determine the Na^+ and K^+ concentrations in cochlear endolymph during embryonic development.

Methods

Ethics Statement

All procedures involving animals were approved by the Institutional Animal Care and Use Committee at Kansas State University (IACUC#: 2961, 2925 and 3245).

Animals

A colony of *Slc26a4*$^{\Delta/+}$ and *Slc26a4*$^{\Delta/\Delta}$ mice was maintained at Kansas State University. *Slc26a4*$^{\Delta/+}$ dams and *Slc26a4*$^{\Delta/\Delta}$ sires were housed in monogamous pairs. Litter sizes averaged 4.3 pups with *Slc26a4*$^{\Delta/+}$ and *Slc26a4*$^{\Delta/\Delta}$ offspring in the near Mendelian ratio of 50.1 to 49.9. The average gestational period was 21 days. Gestational age was counted from the day when a vaginal plug was detected. This day was set to embryonic (E) day 0.5 (E0.5). Pregnancies were verified by ultrasound (Terason t3000, Universal Medical Systems, Bedford Hills, NY).

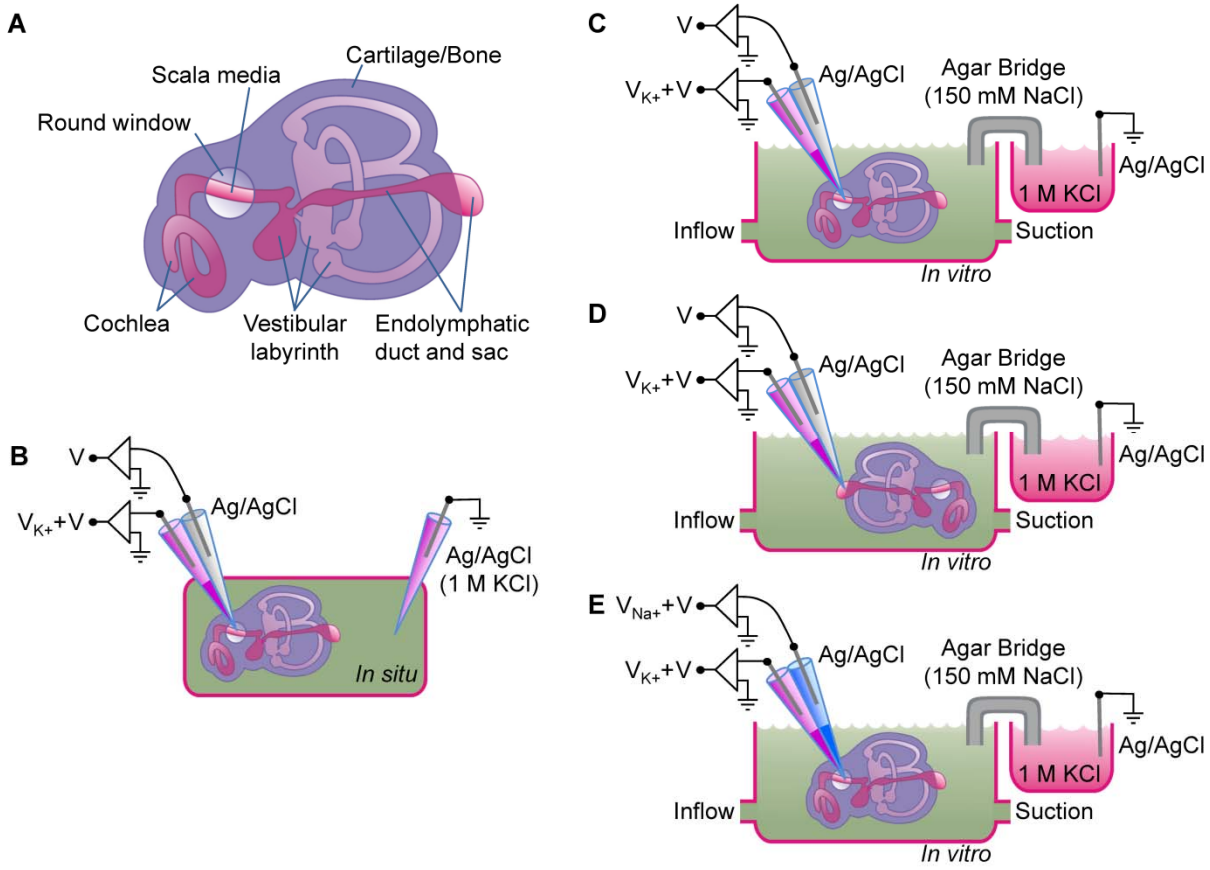

Figure 2.1:Experimental configurations.

Schematic diagrams of the inner ear and of experimental configurations. ***A)*** *Diagram of the bone-enclosed inner ear consisting of the cochlea, the vestibular labyrinth and the endolymphatic duct and sac. Note, that scala media of the cochlea is accessible via the round window and that the endolymphatic sac is the only structure not enclosed in bone.* ***B-E)*** *Experimental configurations for the measurement of voltages and of Na^+ and K^+ concentrations. Voltage electrodes were used to record the voltage (V) and ion-selective electrodes, which were filled at the tip with liquid ion exchanger, recorded a signal that consisted of the sum of the voltage (V) and the ion-voltage (V_{K+} or V_{Na+}).* ***B)*** *Configuration for in situ measurements of voltage and K^+ concentrations in the cochlea.* ***C-E)*** *Configuration for in vitro measurements. Temporal bones were isolated and superfused in a bath chamber that was outfitted with an inflow and a suction outlet.* ***C)*** *Configuration for in vitro measurements of voltage and K^+ concentrations in the cochlea.* ***D)*** *Configuration for in vitro measurements of voltage and K^+ concentrations in the endolymphatic sac.* ***E)*** *Configuration for in vitro measurements of Na^+ and K^+ concentrations in the cochlea.*

The colony was maintained free of known and suspected murine pathogens, as reported earlier [3]. *Slc26a4*$^{\Delta/+}$ and *Slc26a4*$^{\Delta/\Delta}$ mice ranging in age from E14.5 to P72 were used in the present study. Time-pregnant dams were deeply anesthetized with 4% tri-bromo-ethanol and sacrificed by decapitation after harvesting embryos by sterile laparotomy. Embryos were sacrificed by decapitation. Neonatal mice (P0) were anesthetized by a combination of intraperitoneal (i.p.) injection of 0.014 ml/g body weight of 4% tri-bromo-ethanol and rapid cooling on a slush of ice. Older mice (>P3) were anesthetized solely by i.p. injection of 0.014 ml/g body weight of 4% tri-bromo-ethanol. Neonatal and older mice were sacrificed by decapitation under deep anesthesia.

Measurement of voltage, Na^+ and K^+ concentrations

Voltage, Na^+ and K^+ concentrations were measured with double-barreled ion-selective electrodes. Measurements in prenatal and neonatal mice were carried out using a novel *in vitro* approach. This novel approach was developed since the well-established *in situ* approach is not suitable for measurements in prenatal mice. Limitations of the *in vitro* approach were established by comparing results from postnatal mice obtained *in vitro* to data obtained *in situ*.

For *in situ* measurements of K^+ concentrations, one barrel of the double-barreled electrode was used to measure the K^+ concentration and the other barrel was used to measure the transepithelial voltage (*Figure 2.1B*). Electrodes were manufactured using established protocols [29]. Briefly, the K^+ selective barrel was silanized prior to being filled at the tip with liquid ion exchanger (Ionophore I - cocktail B, Cat# 60398, Sigma-Aldrich) and backfilled with 1 M KCl solution. The voltage barrel was filled with 500 mM NaCl solution. Each barrel was connected via a Ag/AgCl electrode to a dual electrometer with high input-resistance (FD223, World Precision Instruments, Sarasota, FL).

Mice between ages P62 and P72 were deeply anesthetized and maintained at 37°C body temperature using a heated platform. Surgery consisted of a tracheotomy to maintain unobstructed ventilation, the subdermal installation of a flowing 1 M KCl

reference electrode in the chest region, and of a ventral approach to the temporal bone, using established methods [29]. Briefly, a small opening in the temporal bone was made and measurements were obtained by guiding the electrode through the round window into the perilymph-filled scala tympani and then into the endolymph-filled scala media. Anoxia was induced by i.p. injection of succinylcholine chloride (1 mg/g body weight) after obtaining stable readings of the K^+ concentration and the endocochlear potential.

For *in vitro* measurements of K^+ and Na^+ concentrations, temporal bones were isolated from pre- and postnatal mice and placed into a bath chamber superfused with warm (37°C) artificial perilymph (in-line heater SHM-8 and controller TC-344B, Warner instruments, Hamden, CT). Artificial perilymph contained (in mM): 135 NaCl, 25 $NaHCO_3$, 4 KCl, 1.5 $CaCl_2$, 1 $MgCl_2$ and 5 glucose and was bubbled with a humidified gas mixture consisting of 5% CO_2 and 95% O_2 to set the pH to pH 7.3 - pH 7.4. The bath chamber was grounded via a Ag/AgCl electrode that was bathed in a vial filled with 1 M KCl solution and connected to the bath chamber via an agar-bridge made from 150 mM NaCl solution (*Figure 2.1C-E*). For measurements in the cochlea, an approach via the round-window was used. For *in vitro* measurements of K^+ concentrations, one barrel of the double-barreled electrode was used to measure the K^+ concentration and the other barrel was used to measure the transepithelial voltage (*Figure 2.1C*). For *in vitro* measurement of Na^+ concentrations, one barrel of the double-barreled electrode was used to measure the Na^+ concentration and the other barrel was used to measure the K^+ concentration as an indicator for successful penetration into the endolymph-filled scala media (*Figure 2.1E*). This unusual configuration was found necessary, since at the ages of interest, the transepithelial voltage was found to be near zero and the Na^+ concentration in endolymph was found to be similar to the concentration in perilymph, such that neither the recording of the voltage nor the recording of the Na^+ concentration could serve as an indicator for successful penetration into the endolymph-filled scala media.

Dual ion selective electrodes were manufactured using a modified protocol. Both barrels were silanized by a 20 s exposure to silane vapors generated by injecting 10 µl di-methyl-di-chloro-silane into a 150 ml beaker sitting on a hot-plate heated to 210 °C.

Silanized electrodes were baked for 2 hr at 180 °C. Tips were broken to an outer diameter of 10-12 µm. The Na^+ electrodes were filled at the tip with a calixarene-based liquid ion exchanger (Cocktail 2 consisting of (%w/w) 3.5% Na^+ ionophore X (Cat# 71747, Sigma-Aldrich), 95.9% 2-nitrophenyl-octyl-ether (Cat# 73732, Sigma-Aldrich), 0.6% potassium-tetrakis-(4-chlorophenyl)-borate (Cat# 60591, Sigma-Aldrich) and backfilled of 1 M NaCl [131]. Electrodes were stored in 500 mM KCl solution for 2-4 hr prior to experiments.

Calibration of ion selective electrodes in warm (37°C) solutions was performed immediately after withdrawal of the electrodes from the temporal bone. All measurements were corrected for calculated liquid junction potentials (JPCalc in Clampex, Molecular Devices, Silicon Valley, CA [132]).

Data were recorded via a flat-bed chart recorder (BD12E, Kipp & Zonen, The Netherlands) for easy annotation and also were recorded digitally (Digidata 1322A and AxoScope 9, Molecular Devices) for easy analysis using custom software written by P.W. (Origin 6.0, The Origin Company, Northhampton, MA).

Quantitative RT-PCR

Total RNA was isolated from the cochlea of *Slc26a4*$^{\Delta/+}$ and *Slc26a4*$^{\Delta/\Delta}$ mice between E14.5 and P8 (RNeasy micro, Qiagen, Valencia, CA). Quantity and quality of total RNA were evaluated by microfluidic electrophoresis (BioAnalyzer, Agilent, Santa Clara, CA) and by microliter absorption photometry (Nanodrop, Wilmington, DE). RNA samples were accepted only when they were free of contamination and when RIN was >7.0, which indicates excellent quality. RIN is a quality indicator on a scale from 0 (worst) to 10 (best) that is computed from microfluidic electrophoresis runs (BioAnalyzer, Agilent).

Total RNA, primers, enzymes and buffers necessary for quantitative RT-PCR reactions were assembled with the assistance of an automatic pipetting station (Biomek NX^P, Beckman Coulter, Fullerton, CA) with hardware modifications and software programming by P.W. Reactions were carried out in 96-well plates with each well containing ~10 ng of total RNA, gene specific primers, SYBR-green, and an enzyme mix containing reverse transcriptase and DNA polymerase (iScript, BioRad, Hercules, CA) in a total volume of 25 µl. Reverse transcription was performed for 10 min at 50 °C and

terminated by heating to 95 °C for 5 min (OneStepPlus, Applied Biosystems, Foster City, CA). PCR consisted of 40 cycles of 10 s melting at 95 °C, 30 s annealing and elongation at 58 °C, and 15 s fluorescence detection at 78 °C (OneStepPlus, Applied Biosystems).

Gene specific primers were designed using software (Primer 3.0 [133]). Primer pairs spanned introns to discourage amplification of genomic DNA (*Table 1*). Amplification of a single product of the appropriate size was verified by microfluidic electrophoresis (BioAnalyzer, Agilent).

The number of template molecules ($cDNA_{templates}$) was estimated according to

$$cDNA_{templates}\left[\text{molecules}\right] = \frac{6.02 \times 10^{23}\left[\text{molecules}\right] \times Product_{threshhold}\ [\text{g}] \times [\text{mol}] \times [\text{bp}]}{[\text{mol}] \times Product_{size}\,[\text{bp}] \times Weight_{bp}\,[\text{g}] \times [\text{mol}] \times Efficiency\ \hat{}\ C_t}$$

where 6.02×10^{23} molecules/mol represents Avogadro's number, $Product_{threshold}$ is the weight of the PCR-product at threshold (0.49×10^{-9} g) that was obtained from calibration experiments, $Product_{size}$ is the size of the product in base pairs (bp), $Weight_{bp}$ is average weight of one bp (660 g/mol), *Efficiency* is the PCR-efficiency obtained from the slope of the log-linear phase of the growth curve [134] and C_t is the cycle at which the fluorescence of the product molecules reaches a common threshold chosen in the middle of the log-linear part of the growth curve.

Confocal immunohistochemistry

Temporal bones were isolated from *Slc26a4*$^{\Delta/+}$ and *Slc26a4*$^{\Delta/\Delta}$ mice and fixed at 4 °C in PBS-solution to which 4% paraformaldehyde (Cat# 15714, Electron Microscopy Sciences, Hatfield, PA) had been added. PBS-solution contained (mM): 137 NaCl, 2.7 KCl, 10.1 Na_2HPO_4, and 1.8 KH_2PO_4, pH 7.4. Fixed tissues were processed through a sucrose gradient (10% and 20%, each 30 min, followed by 30% overnight, all solutions in PBS at 4 °C), infiltrated with polyethylene glycol (Cat# 72592-B, Electron Microscopy Sciences) and cryo-sectioned (12 µm, CM3050S, Leica, Germany). Mid-modiolar

sections of the cochlea were mounted on charged slides (Cat# 22-230-900, Fisher) and blocked for 1 hr with 5% bovine serum albumin (BSA) in PBS-solution containing 0.2% TritonX-100 (PBS-TX solution).

Sections were incubated at 4°C overnight with primary antibodies, goat anti-KCNQ1 (1:200, Cat# SC-10646, Santa Cruz, Dallas, TX) or rabbit anti-SLC12A2 (1:200, Cat# AB3560P, Chemicon, Temecula, CA). Sections were washed 3 times for 1 min each with PBS-TX solution and incubated at room temperature for 1 hr with diluted secondary antibodies, Alexa Fluor 594 chicken-anti-goat (1:1000, Cat# A21468, Invitrogen, Grand Island, NY) or Alexa Fluor 594 goat-anti-rabbit (1:1000, Cat# A11037, Invitrogen). Primary and secondary antibodies were diluted in PBS-TX solution containing 2.5% BSA. After washing three times in PBS-TX, sections were stained with phalloidin 488 (1:40, Cat# A-12379, Invitrogen) and DAPI (1:1000; Cat# D-3571, Invitrogen). Stains were diluted in PBS-TX solution without BSA. After staining, sections were washed another 3 times in PBS-TX solution and cover-slipped with mounting medium (Cat# H-1400, Vector laboratories, Burlingame, CA) and examined by confocal laser scanning microscopy (LSM 510 Meta, Carl Zeiss, Göttingen, Germany).

Gene	Genbank	Genbank	Genbank	Location
18S	NR_003278	Left: gag gtt cga aga cga tca ga	316 bp	
		Right: tcg ctc cac caa cta aga ac		
Kcnq1	NM_008434	Left: ttc tcc tcc tac ttt gtc tac ttg g	262 bp	Exon 6
		Right: tct gcc tct gct tct gct		Exon 8
Slc12a2	NM_009194	Left: gga agc aaa ggc tca gat tg	345 bp	Exon 7–8
		Right: aca aca cac gaa ccc aca ga		Exon 8–9
Atp1a1	NM_144900	Left: tgc ccg cct caa cat tcc	291 bp	Exon 14
		Right: gac aca tca gag cca aca atc c		Exon 16
Scnn1a	NM_011324	Left: agg aag gac tgg aaa atc g	248 bp	Exon 2
		Right: atg ggg tgg tgg aac tga		Exon 4
Scnn1b	NM_011325	Left: ctt cac gcc tat ctt cta ccc	268 bp	Exon 5
		Right: gtc cac cag cac ccc aat		Exon 7
Scnn1g	NM_011326	Left: ggt ggg att tca gtt gtg ct	282 bp	Exon 3–4
		Right: agg atg gtg gcg ttt tct ct		Exon 5

Table 2.1: Primers

Statistics

Numerical data were presented as average ± sem with n being the number of replicates. Statistical significance was determined based on unpaired t-tests. Significance was assumed at $p<0.05$.

Results

Selectivity and sensitivity of K^+- and Na^+-selective electrodes

The sensitivity and selectivity of K^+ electrodes was evaluated by making recordings in solutions containing various concentrations of KCl and NaCl. Recordings were corrected for calculated liquid junction potentials and corrected measurements were subjected to a three-dimensional fit to the Nicolski equation:

$$V = V_i + S_{K+} \times \log_{10}\left(\left[K^+\right] + A \times \left[Na^+\right]\right)$$

where V represents the measured voltage, V_i is an offset term, S_{K+} is the slope representing the sensitivity for K^+, $[K^+]$ and $[Na^+]$ represent the K^+ and Na^+ concentrations, and A is the selectivity coefficient. K^+ electrodes were found to be highly sensitive with S_{K+} near the theoretical value of 60 (52.9 ± 0.5 mV/decade, n=4) and highly selective with A close the ideal value of zero (0.028 ± 0.005, n=4). Accordingly, steep voltage changes were recorded when the KCl concentration was changed in the presence of a constant NaCl concentration of 10 mM and nearly no voltage changes were observed when the NaCl concentration was altered at constant KCl concentrations of 3, 35 or 68 mM (*Figure 2.2A*).

The sensitivity and selectivity of Na^+ electrodes was evaluated in a similar fashion using solutions containing various concentrations of NaCl and KCl. Recorded voltages were corrected for calculated liquid junction potentials and corrected voltages were subjected to a three-dimensional fit to the Nicolski equation:

$$V = V_i + S_{Na+} \times \log_{10}\left(0.8 \times \left[Na^+\right] + A \times \left[K^+\right]\right)$$

where S_{Na+} is the slope representing the sensitivity for Na^+ and all other symbols have the same meaning as above. Na^+ electrodes were found to be highly sensitive with S_{Na+} near the theoretical value of 60 (57.8 ± 0.9 mV/decade, n=12) and moderately selective with A being different from zero (0.13 ± 0.03, n=12). Accordingly, steep voltage changes were recorded when the NaCl concentration was changed at constant KCl concentration of 3 or 13 mM and less steep changes were observed when the KCl concentration was altered in the presence of a constant NaCl concentration of 10 mM (*Figure 2.2B*).

Simplified calibration procedure for K^+-selective electrodes

The high selectivity of K^+ electrodes encouraged us to simplify the calibration process for K^+ electrodes by using solutions composed of KCl and NaCl, where the total cation concentration was kept constant at 150 mM. Recorded voltages were corrected for calculated liquid junction potentials and corrected voltages were subjected to a two-dimensional fit to a simplified Nicolski equation:

$$V = V_i + S_{K+} \times \log_{10}\left(\left[K^+\right] + A \times \left(150 - \left[K^+\right]\right)\right)$$

where symbols have the same meaning as above. Again, K^+ electrodes were found to be highly sensitive with S_{K+} near the theoretical value of 60 (54.9 ± 0.4, n=137) and highly selective with A near the ideal value of zero (0.018 ± 0.001, n=137). Accordingly, the relationship between voltage and K^+ was found to be non-linear (*Figure 2.2C*).

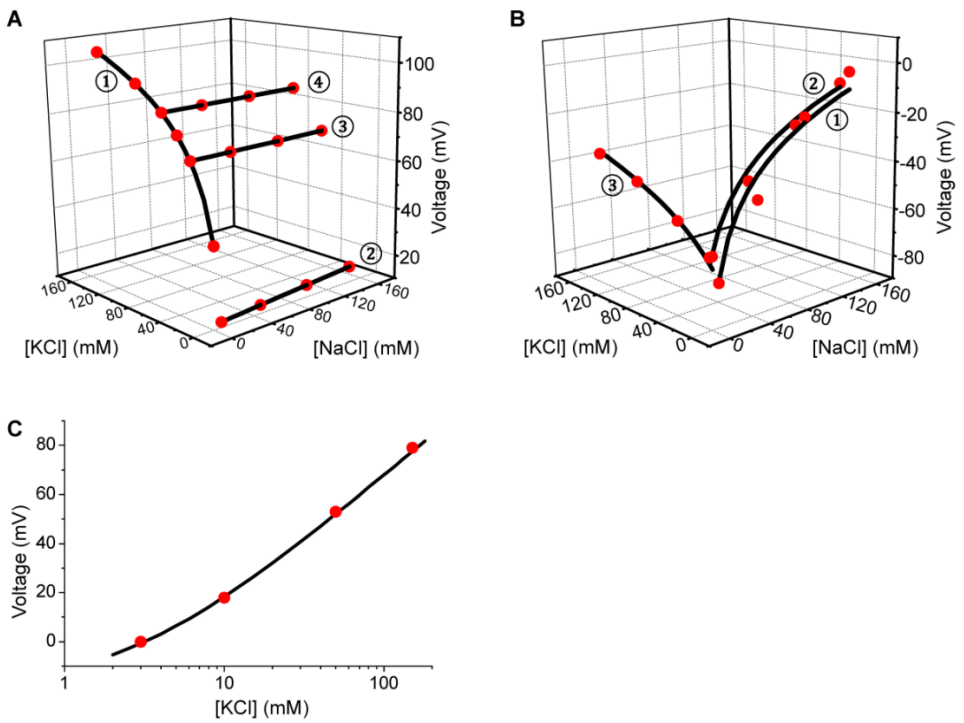

Figure 2.2: Selectivity and sensitivity of Na^+ and K^+-selective electrodes.

Electrodes were calibrated using mixtures of NaCl and KCl and the resulting two- or three-dimensional data (red dots) were fitted to the Nicolski equation (black lines). ***A)*** *Three-dimensional calibration of K^+ selective electrodes. Curve 1: The KCl concentration was varied between 10 and 150 mM in the presence of a constant NaCl concentration of 10 mM. Curve 2: The NaCl concentration was varied between 10 to 150 mM in the presence of a constant KCl concentration of 3 mM. Curve 3: The NaCl concentration was varied between 10 to 150 mM in the presence of a constant KCl concentration of 35 mM. Curve 4: The NaCl concentration was varied between 10 to 150 mM in the presence of a constant KCl concentration of 68 mM. Note, that K^+ selective electrodes were highly selective for K^+ which is evident from the steep relationship between the Voltage and the KCl concentration (Curve 1) and the flat relationships between the voltage and the NaCl concentration (Curves 2-4).* ***B)*** *Three-dimensional calibration of Na^+ selective electrodes. Curve 1: The NaCl concentration was varied between 10 and 150 mM in the presence of a constant KCl concentration of 3 mM. Curve 2: The NaCl concentration was varied between 10 to 150 mM in the presence of a constant KCl concentration of 13 mM. Curve 3: The KCl concentration was varied between 10 to 150 mM in the presence of a constant NaCl concentration of 10 mM. Note, that Na^+ selective electrodes were highly selective for Na^+ but, although to a lesser degree, also detected K^+, which is evident from the steep relationships between the Voltage and the NaCl concentration (Curve 1 and 2) and the less steep relationship between the voltage and the KCl concentration (Curve 3).* ***C)*** *Two-dimensional calibration of K^+ selective electrodes. Calibration procedures were simplified by using solutions in which the sum of NaCl and KCl was maintained constant at 150 mM.*

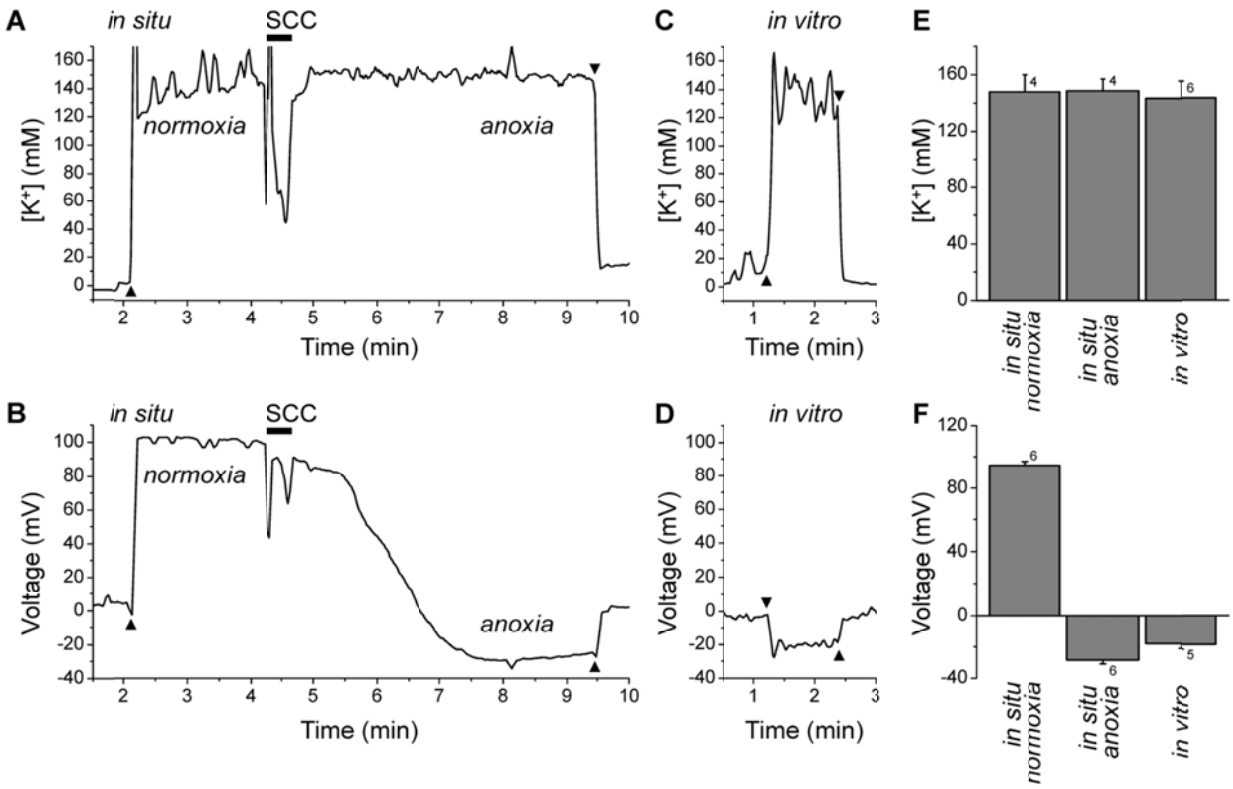

Figure 2.3: K^+ concentration and endocochlear potential in situ and in vitro

Measurements of the cochlear K^+ concentration and the endocochlear potential in situ and in vitro in adult Slc26a4$^{\Delta/+}$ mice. ***A-B****) Representative traces of in situ measurements. Penetration and withdrawal from the epithelium are marked (filled triangles). Upon establishment of a stable voltage recording, the paralytic agent succinyl-choline chloride (SCC) was injected to induced anoxia. Note that the endocochlear potential, which is positive under normoxic conditions, declined under anoxic conditions within 3 min to negative values. The K^+ concentration, however, was maintained constant during the recording time.* ***C-D)*** *Representative traces of in vitro measurements. Penetration and withdrawal from the epithelium are marked (filled triangles).* ***E-F)*** *Data summary. Note that the K^+ concentrations recorded in vitro were similar to measurements made in situ and that the endocochlear potential in vitro was negative similar to in situ measurements under anoxic conditions. Numbers next to bars represents the number of animals.*

K^+ concentration & voltage measurements in situ & in vitro in the adult cochlea

Measurements of the endocochlear potential and of ion concentrations in cochlear endolymph are usually performed *in situ* using adult animals, although some investigators have succeeded to obtain measurements in pre-weaning and even neonatal mice [81,135]. The *in situ* technique, however, cannot be extended to the

prenatal phase of development. Therefore, we established an *in vitro* method where measurements of the transepithelial voltage and of endolymphatic ion concentrations are conducted in isolated superfused temporal bones. This method was evaluated by comparing data from adult *Slc26a4*$^{\Delta/+}$ mice (P62-P72) that were obtained with the *in situ* technique and with the *in vitro* method (*Figure 2.3*). Measurements *in situ* yielded an endolymphatic K^+ concentration of 157 ± 14 (n=4) mM and an endocochlear potential at normoxic conditions of 95 ± 2 (n=6) mV. Upon induction of anoxia by injection of succinylcholine, the endocochlear potential declined within 2-3 min to -29 ± 2 (n=6) mV, while the endolymphatic K^+ concentration remained stable (153 ± 9 mM, n=4). Measurements *in vitro* were obtained within 10-15 min after sacrifice and yielded an endolymphatic K^+ concentration of 144 ± 12 (n=6) mM, which is similar to results obtained *in situ*, and an endocochlear potential of -16 ± 3 (n=6) mV, which is similar to the anoxia potential found *in situ*. These data suggest that the *in vitro* method is suitable to evaluate the K^+ concentration, and presumably the Na^+ concentration, and that *in vitro* measurements of the transepithelial potential more closely approximate anoxic rather than normoxic conditions.

K^+ concentration & voltage measurements in the cochlea & endolymphatic sac

The *in vitro* method was used to determine the endolymphatic K^+ concentration and the transepithelial potential in the cochlea and the endolymphatic sac during development. Measurements were made with double-barreled K^+ selective electrodes in prenatal and neonatal *Slc26a4*$^{\Delta/+}$ and *Slc26a4*$^{\Delta/\Delta}$ mice (*Figure 2.4*).

In the cochlea, the endolymphatic K^+ concentration between age E14.5 and E17.5 was 10.7 ± 0.7 (n=20) mM with no differences between *Slc26a4*$^{\Delta/+}$ and *Slc26a4*$^{\Delta/\Delta}$ mice (*Figure 2.4A*). At E19.5, the endolymphatic K^+ concentration began to rise in both genotypes. At P0 and P3, the endolymphatic K^+ concentrations in the cochlea of *Slc26a4*$^{\Delta/\Delta}$ mice was significantly lower compared to in *Slc26a4*$^{\Delta/+}$ mice, however, this difference disappeared with further development. The perilymphatic K^+ concentration was 3.29 ± 0.07 (n=72) mM and did not change with age and displayed no differences between genotypes. *Slc26a4*$^{\Delta/+}$ mice developed a positive transepithelial voltage of 4.4 ± 1.7 (n=6) mV at E19.5 (*Figure 2.4B*). With further development, the transepithelial

voltage became negative. Transepithelial voltages in *Slc26a4*$^{\Delta/\Delta}$ mice remained close to zero till age P5, but was found to be negative in adult mice (-3.9 ± 0.5 mV, n=5).

In the endolymphatic sac, the endolymphatic K^+ concentration between ages E14.5 and E17.5 was 15.4 ± 1.6 (n=21) mM with no differences between *Slc26a4*$^{\Delta/+}$ and *Slc26a4*$^{\Delta/\Delta}$ mice (*Figure 2.4C*) and the transepithelial potential was -5.1 ± 0.7 (n=21) mM, again with no differences between *Slc26a4*$^{\Delta/+}$ and *Slc26a4*$^{\Delta/\Delta}$ mice (*Figure 2.4D*). Between ages E14.5 and E17.5, no difference was found between the endolymphatic K^+ concentration in the cochlea and the endolymphatic sac.

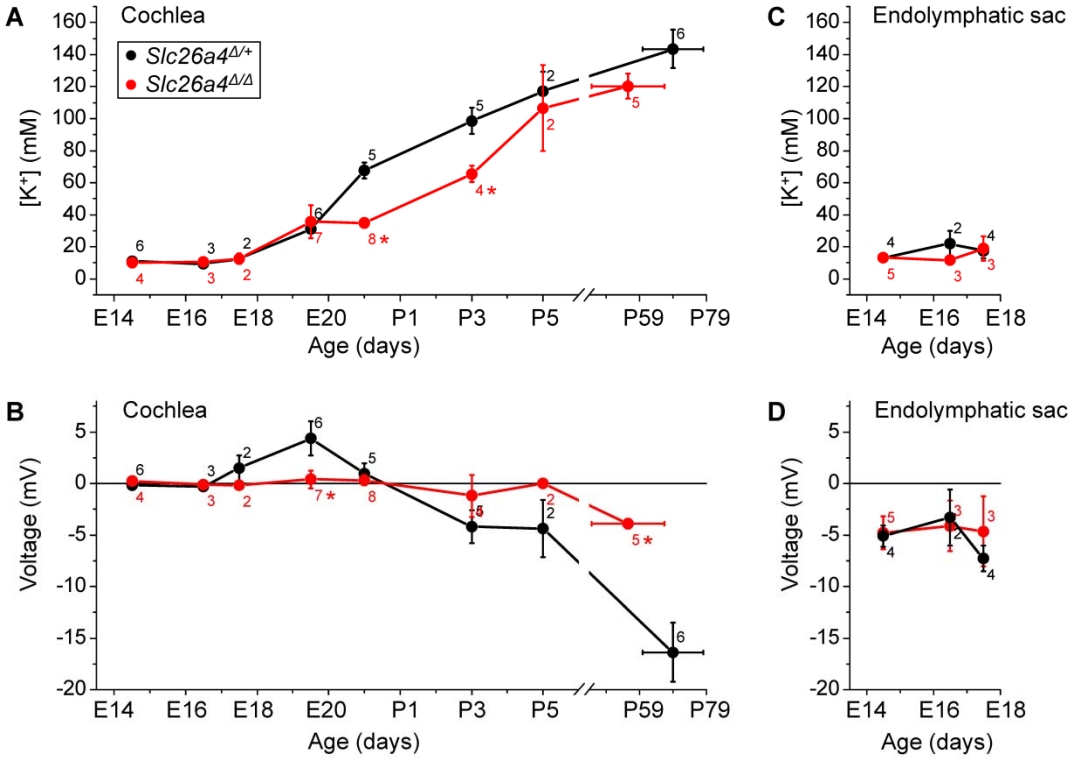

Figure 2.4: K^+ concentration and voltage in the cochlea & the endolymphatic sac

Summary of measurements of the endolymphatic K+ concentration and transepithelial voltage in vitro in the cochlea and the endolymphatic sac of Slc26a4Δ/+ (black symbols) and Slc26a4Δ/Δ mice (red symbols).. A-B) Measurements in the cochlea. C-D) Measurements in the endolymphatic sac. Measurements in Slc26a4Δ/Δ mice that differed significantly from measurements in Slc26a4Δ/+ mice are marked (*).

Na^+ and K^+ concentration measurements in the cochlea

The *in vitro* method was further used to determine the endolymphatic Na^+ and K^+ concentrations in the cochlea of *Slc26a4*$^{\Delta/+}$ and *Slc26a4*$^{\Delta/\Delta}$ mice at ages E16.5 and P0 (*Figure 2.5*). At both ages the endolymphatic K^+ concentration had been found in both genotypes to be significantly higher than the perilymphatic K^+ concentration and the transepithelial voltage had been found to be zero, *see above*. Measurements were made with double-barreled Na^+ and K^+ selective electrodes. Recordings with the K^+ electrode were used as indicator of a successful penetration into scala media (*Figure 2.5A and B*).

At age E16.5, the endolymphatic Na^+ and K^+ concentrations in the cochlea were 141 ± 3 (n=8) mM and 9.6 ± 0.3 (n=8) mM, respectively. No differences were detected between *Slc26a4*$^{\Delta/+}$ and *Slc26a4*$^{\Delta/\Delta}$ mice. At age P0, the endolymphatic Na^+ dropped in *Slc26a4*$^{\Delta/+}$ mice to 80 ± 12 (n=3) mM and the endolymphatic K^+ concentrations rose to 80 ± 14 mM (n=3). Smaller changes were observed in *Slc26a4*$^{\Delta/\Delta}$ mice where the endolymphatic Na^+ concentration dropped to 131 ± 4 (n=3) mM and the K^+ concentration rose to 31 ± 2 (n=3) mM. No difference was found between the genotypes in the sum of the Na^+ and the K^+ concentration (*Figure 2.5C and D*). At E16.5 the sum was 151 ± 3 (n=8) and at P0 the sum was 160 ± 5 (n=6). The perilymphatic Na^+ and K^+ concentrations did not vary with genotypes or age and were 147 ± 3 (n=14) mM and 4.2 ± 0.3 (n=14) mM, respectively. The sum of the perilymphatic Na^+ and K^+ concentrations was 151 ± 3 mM (n=14).

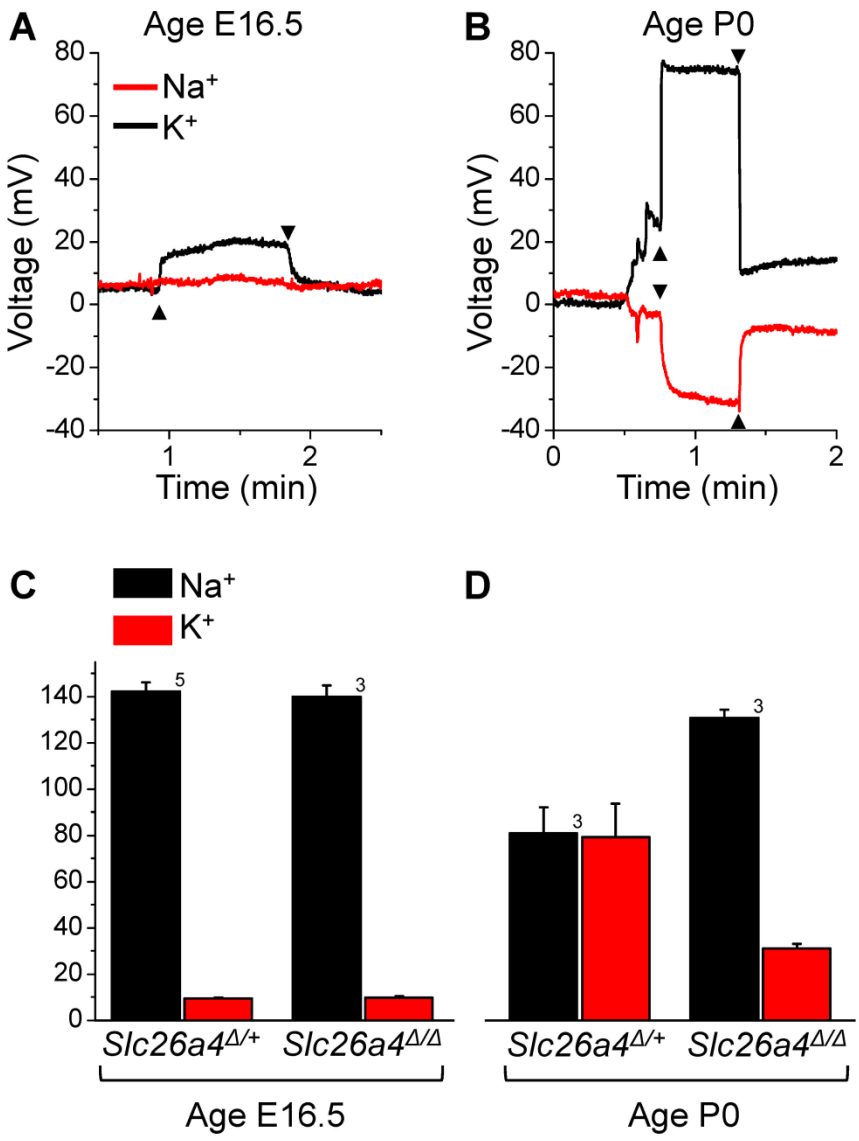

Figure 2.5: Endolymphatic Na^+ and K^+ concentrations in vitro.

Measurements of the endolymphatic Na+ and K+ concentrations in vitro. A) Representative traces of the Na^+ (red) and K^+ (black) concentration in the cochlea of an $Slc26a4^{\Delta/+}$ mouse at age E16.5. B) Representative traces of the Na^+ (red) and K^+ (black) concentration in the cochlea of an $Slc26a4^{\Delta/+}$ mouse at age P0. C-D) Summary of Na^+ and K^+ concentration measurements in cochlear endolymph in $Slc26a4^{\Delta/+}$ and $Slc26a4^{\Delta/\Delta}$ mice at age E16.5 and P0. Numbers next to bars represent the number of animals.

HCO_3^- and Cl^- concentration estimations in the cochlea

The HCO_3^- concentrations in cochlear endolymph were estimated under the assumptions that CO_2, HCO_3^- and pH are in equilibrium such that the HCO_3^- concentration can be calculated based on measurements of the endolymphatic pH. In the cochlea at age ~E16.5, the endolymphatic pH had been reported to be pH ~7.44 in *Slc26a4*$^{\Delta/+}$ mice and pH ~7.11 in *Slc26a4*$^{\Delta/\Delta}$ mice and the perilymphatic pH had been reported to be pH 7.30 in both genotypes [102]. According to the Henderson-Hasselbalch equation,

$$pK = pK_a + \log_{10}\left(\frac{\left[HCO_3^-\right]}{0.03 \times P_{CO2}}\right)$$

where pK_a is the logarithmic acid dissociation constant (pK_a = 6.1), '0.03' is the solubility of CO_2 in water and P_{CO2} is the partial pressure of CO_2 (P_{CO2} = 5%), the endolymphatic HCO_3^- concentration was calculated to be 25 mM in *Slc26a4*$^{\Delta/+}$ mice and 11.7 mM in *Slc26a4*$^{\Delta/\Delta}$ mice and 18 mM in perilymph of both genotypes. With further development, based on endolymphatic pH measurements at P10, the endolymphatic HCO_3^- concentration was calculated to be 35 mM in *Slc26a4*$^{\Delta/+}$ mice and 10.5 mM in *Slc26a4*$^{\Delta/\Delta}$ mice [81].

The Cl^- concentration in cochlear endolymph was estimated under the assumptions that Na^+, K^+, Cl^- and HCO_3^- are the major ions in cochlear endolymph, and that the sum of anions matches the sum of cations. Accordingly, the endolymphatic Cl^- concentration at age ~E16.5 was estimated to be 126 mM (=151-25) in *Slc26a4*$^{\Delta/+}$ and 139 mM (=151-11.7) in *Slc26a4*$^{\Delta/\Delta}$ mice and the perilymphatic Cl^- concentration was estimated to be 133 mM (=151-18) in both genotypes.

Cochlear expression of Atp1a1, Slc12a2, Kcnq1, Scnn1a, Scnn1b & Scnn1g

The molecular mechanism for K^+ secretion into endolymph has been established in the adult cochlea where K^+ is taken up across the basolateral membrane of stria marginal cells via the Na^+/K^+ ATPase that contains the α-subunit ATP1A1 and the $Na^+/2Cl^-/K^+$

cotransporter SLC12A2. K^+ is then secreted into endolymph via the apical K^+ channel KCNQ1 [21,23]. Whether this mechanism is responsible for the prenatal rise in the endolymphatic K^+ concentration is not unknown.

Cochlear mRNA expression of *Atp1a1*, *Slc12a2* and *Kcnq1* was quantified between ages E14.5 and P8 and the onset and localization of SLC12A2 and KCNQ1 protein expression was determined in the cochlea of *Slc26a4*$^{\Delta/+}$ and *Slc26a4*$^{\Delta/\Delta}$ mice. Expression levels of *Atp1a1* mRNA rose nearly in parallel between age E14.5 and P8 in *Slc26a4*$^{\Delta/+}$ and *Slc26a4*$^{\Delta/\Delta}$ mice (*Figure 2.6A*) with the exception that between E17.5 and P0 a steeper rise was observed in *Slc26a4*$^{\Delta/\Delta}$ mice compared to *Slc26a4*$^{\Delta/+}$ mice. In contrast, expression levels of *Slc12a2* and *Kcnq1* were stable between E14.5 and E17.5, increased between E17.5 and P0, where stable between P0 and P4 and then increased between P4 and P8 with no differences between genotypes (*Figure 2.6B and C*).

Cryosections were prepared from the cochlea of *Slc26a4*$^{\Delta/+}$ and *Slc26a4*$^{\Delta/\Delta}$ mice and revealed in *Slc26a4*$^{\Delta/\Delta}$ mice the dramatic enlargement of scala media (*Figure 2.7*). At E17.5, no protein expression of SLC12A2 or KCNQ1 was detected, however, expression of both proteins was found at E19.5 in *Slc26a4*$^{\Delta/+}$ and *Slc26a4*$^{\Delta/\Delta}$ mice. Expression of SLC12A2 was detected in the basolateral membrane of strial marginal cells and in the basolateral membranes of epithelial cells in Kölliker's organ and expression of KCNQ1 was found in the apical membrane of strial marginal cells. No difference in the location of expression was detected between *Slc26a4*$^{\Delta/+}$ and *Slc26a4*$^{\Delta/\Delta}$ mice. These results are based on the evaluation of 2-3 pairs of *Slc26a4*$^{\Delta/+}$ and *Slc26a4*$^{\Delta/\Delta}$ littermates that were collected from two timed-pregnant dams per gestational age.

The molecular mechanism for Na^+ absorption has been established for the adult cochlea in Reissner's membrane epithelial cells as well as in outer sulcus epithelial cells and Claudius' cells [25,136,137]. Outer sulcus epithelial cells absorb cations from endolymph including Na^+ and K^+, however, Reissner's membrane and Claudius' epithelial cells selectively absorb Na^+ across the apical membrane via the Na^+ channel ENaC which consists of the subunits *Scnn1a*, *Scnn1b* and *Scnn1g*. Cochlear mRNA

expression of the three ENaC subunits was quantified in *Slc26a4*$^{\Delta/+}$ and *Slc26a4*$^{\Delta/\Delta}$ mice between the ages E14.5 and P8.

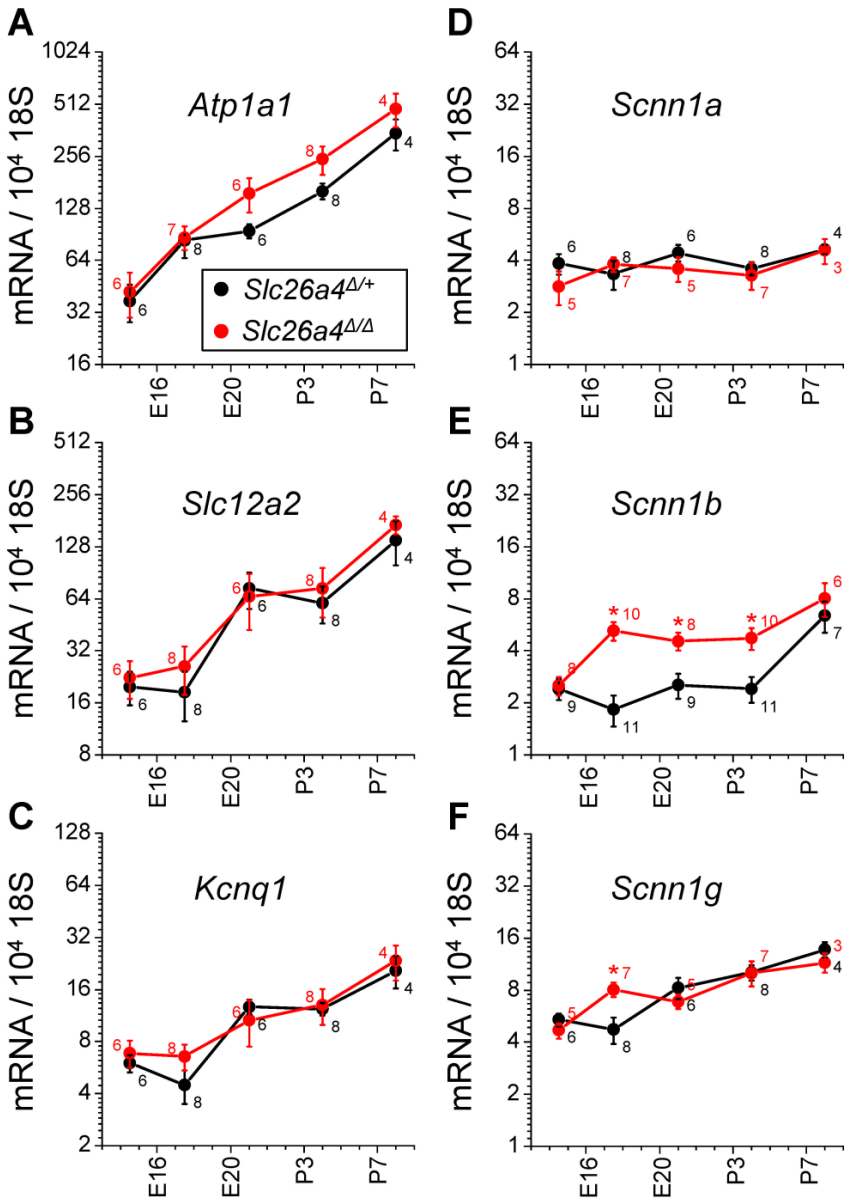

Figure 2.6: mRNAs encode selected Na$^+$ and K$^+$ channels and transporters

Expression of mRNAs that code for selected Na+ and K+ channels and transporters in the cochlea of Slc26a4Δ/+ and Slc26a4Δ/Δ mice. A) The α-subunit of the Na$^+$/K$^+$ ATPase Atp1a1. B) The Na$^+$/2Cl$^-$/K$^+$ cotransporter Slc12a2. C) The α-subunit of the K$^+$ channel Kcnq1. D-F) The α-, β- and γ-subunit of the Na$^+$ channel ENaC. Measurements in Slc26a4$^{\Delta/\Delta}$ mice that differed significantly from measurements in Slc26a4$^{\Delta/+}$ mice are marked (*).

Expression levels of *Scnn1a* were stable during the time of observation and did not differ between *Slc26a4*$^{\Delta/+}$ and *Slc26a4*$^{\Delta/\Delta}$ mice (*Figure 2.6D*). In contrast, expression levels of *Scnn1b* rose in *Slc26a4*$^{\Delta/+}$ mice between P4 and P8 and in *Slc26a4*$^{\Delta/\Delta}$ mice between E14.5 and E17.5, which is 9-15 days earlier (*Figure 2.6E*). Similarly, expression levels of *Scnn1g* rose between E17.5 and P0 in *Slc26a4*$^{\Delta/+}$ mice and between E14.5 and E17.5 in *Slc26a4*$^{\Delta/\Delta}$ mice, which is 1-5 days earlier (*Figure 2.6F*). With the exception of the measurement at E17.5, no difference in expression levels of *Scnn1g* were observed between *Slc26a4*$^{\Delta/+}$ and *Slc26a4*$^{\Delta/\Delta}$ mice.

Discussion

The most salient findings of the present study are that endolymph in the cochlea and the endolymphatic sac of *Slc26a4*$^{\Delta/+}$ and *Slc26a4*$^{\Delta/\Delta}$ mice is a NaCl rich fluid during the phase of cochlear growth and enlargement (*Figure 2.4 and 2.5*), that the onset of the rise in the K^+ concentration in the cochlea occurs prenatally and coincides with a decline in the Na^+ concentration (*Figure 2.5*), and that the rise in the K^+ concentration in the cochlea coincides with the onset of expression of the $Na^+/2Cl^-/K^+$ cotransporter SLC12A2 and the K^+ channel KCNQ1 (*Figure 2.7*).

The molecular mechanisms for K^+ secretion into endolymph have been well established in the adult cochlea, where K^+ secretion is mediated by marginal cells of stria vascularis [6,23]. Marginal cells take up K^+ across the basolateral membrane via the Na^+/K^+-ATPase and the $Na^+/2Cl^-/K^+$-cotransporter SLC12A2 and secrete K^+ into endolymph across the apical membrane via the K^+ channel KCNQ1/KCNE1 (formerly called IsK and MinK). The presented data suggest that this mechanism becomes operational with the onset of expression of SLC12A2 and KCNQ1 between E17.5 and E19.5 resulting in a rise of endolymphatic K^+ concentration in *Slc26a4*$^{\Delta/+}$ and *Slc26a4*$^{\Delta/\Delta}$ mice (*Figures 2.4 and 2.7*). Notably, the onset of the rise in the endolymphatic K^+ concentration was found to occur prenatally, at E19.5 (*Figure 2.4A*), which is ~5 days earlier than the previously reported onset at P3 that was based on serially-sectioned freeze-dried labyrinths and X-ray analysis of elemental composition [138,139]. The expression of SLC12A2 in the cochlea, however, was not limited to strial marginal cells but was also

found in the basolateral membrane of epithelial cells in Köllikers organ (*Figure 2.7*). These cells, which are lost during early postnatal development, have previously been shown to express Na^+/K^+-ATPase, which suggest they may be engaged in ion secretion [3]. Whether and what ions are transported across the apical membrane is not known.

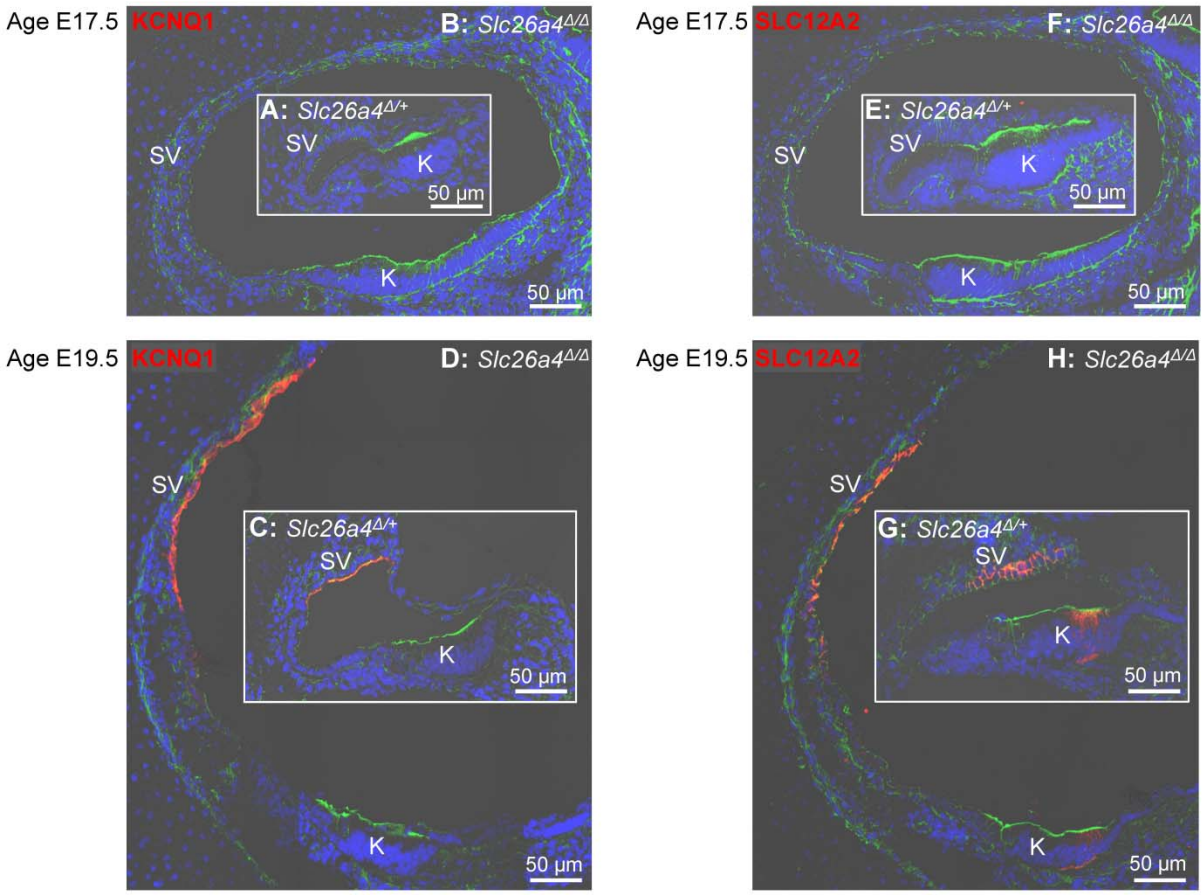

Figure 2.7: Protein of KCNQ1 and SLC12A2 in the cochlea.

Expression of protein of the K^+ channel KCNQ1 and the $Na^+/2Cl^-/K^+$ cotransporter SLC12A2 in the cochlea. ***A-D****) Expression of KCNQ1 (red) in the cochlea of $Slc26a4^{\Delta/+}$ and $Slc26a4^{\Delta/\Delta}$ mice at ages E17.5 and E19.5.* ***E-H****) Expression of SLC12A2 (red) in the cochlea of $Slc26a4^{\Delta/+}$ and $Slc26a4^{\Delta/\Delta}$ mice at ages E17.5 and E19.5. Note that the onset of expression of KCNQ1 and SLC12A2 occurred in $Slc26a4^{\Delta/+}$ and $Slc26a4^{\Delta/\Delta}$ mice between E17.5 and E19.5. Further, note that images of $Slc26a4^{\Delta/+}$ and $Slc26a4^{\Delta/\Delta}$ mice are reproduced at the same magnification to illustrate the dramatic enlargement in $Slc26a4^{\Delta/\Delta}$ mice. Stains included DAPI for nuclei (blue) and phalloidin for F-actin (green). Abbreviations: SV, Stria vascularis; K, Köllikers organ.*

The molecular mechanism for Na^+ absorption is well established in Reissner's membrane and Claudius' epithelial cells of the adult cochlea, where Na^+ absorption from endolymph in mediated via the Na^+ selective channel ENaC and Na^+ is extruded across the basolateral membrane via the Na^+/K^+-ATPase [136,137] . Other epithelial cells, such as outer sulcus cells and sensory hair cells, also absorb Na^+ but do not distinguish between Na^+ and K^+ absorption since their major apical cation channel is a cation non-selective channel [26,140]. The presented quantification of mRNA expression suggest that regulation of Na^+ absorption, if present, does not occur at the transcriptional level of the channel-forming α-subunit *Scnn1a* or the accessory γ-subunit *Scnn1g*, but occurs possibly at the transcriptional level of the β-subunit *Scnn1b* and at translational or regulatory levels. Interestingly, our observation of upregulation of the β-subunit between P4 and P8 coincides with the onset of amiloride-sensitive Na^+ transport in Reissner's membrane [141].

The onset of the rise in the K^+ concentration coincided with the observation of a positive transepithelial potential at E19.5 in *Slc26a4*$^{\Delta/+}$ mice (*Figure 2.4B*). This transepithelial potential may be generated by marginal cells of stria vascularis, which have been shown to generate a positive transepithelial potential when bathed at the apical membrane with a Na^+-rich solution [23]. This positive potential, however, is different from the endocochlear potential that is generated across the basal cell barrier of stria vascularis, begins to rise at P5, develops within ~10 days to levels of 90 -100 mV (*Figure 2.3*), and is exquisitely sensitive to anoxia [135]. The positive endocochlear potential is essentially a K^+ diffusion potential that is generated by the K^+ channel KCNJ10 that is located in intermediate cells of stria vascularis, which are part of the basal cell barrier [6].

From P3 onward, a negative transepithelial potential was found in the cochlea (*Figure 2.4B*). Negative potentials of similar magnitude have been recorded *in situ* under anoxic conditions [135]. The negative potentials recorded *in vitro* are most likely anoxia potentials that were recorded since our experimental conditions did not maintain normoxic conditions, which are necessary for the positive endocochlear potential. This shortcoming, however, has been shown to not affect the outcome of the ion measurements (*Figure 2.3C*). The negative endocochlear potential found under anoxic

conditions (*Figure 2.3D*) is a K^+ diffusion potential that is thought to be generated by K^+ channels in the basolateral membrane of the sensory hair cells and that depends on the openness of the non-selective transduction channel in the apical membrane of the sensory cells. Since the present measurements of the transepithelial potential were conducted *in vitro*, which mimics anoxic conditions, the presence of the negative transepithelial potential observed from P3 onward indicates the presence of mature sensory hair cells. This observation is consistent with previous findings on the opening of the transduction channels in murine cochlear hair cells at neonatal stage [142]. The observation that up to P5 neither a positive nor a negative potential was observed in the cochlea of *Slc26a4*$^{\Delta/\Delta}$ mice may be related to a retardation of development [116].

The rise in the K^+ concentration during the neonatal phase of development was found to be delayed by ~3 days in *Slc26a4*$^{\Delta/\Delta}$ mice since K^+ concentrations reached similar levels at P0 in *Slc26a4*$^{\Delta/+}$ mice and P3 in *Slc26a4*$^{\Delta/\Delta}$ mice. This delay in the concentration change may in part be due to the ~10 fold larger volume of scala media in *Slc26a4*$^{\Delta/\Delta}$ mice compared to *Slc26a4*$^{\Delta/+}$ mice that would require a ~10 fold higher rate of K^+ secretion and Na^+ absorption [3]. This delay, however, may also, at least in part, be due to a delayed vascularization of stria vascularis in *Slc26a4*$^{\Delta/\Delta}$ mice that had been observed at P3 [102].

The endolymphatic sac has been shown to reabsorb fluid and thereby drain the cochlea during the phase of cochlear lumen formation in *Slc26a4*$^{\Delta/+}$ mice. Failure to drain the cochlea leads to enlargement of the cochlea in *Slc26a4*$^{\Delta/\Delta}$ mice [3]. It is conceivable that loss of *Slc26a4* disrupts NaCl absorption and thereby leads to the enlargement. The negative transepithelial potential found in the prenatal endolymphatic sac (*Figure 2.4D*) is consistent with electrogenic Na^+ absorption mediated by a channel such as ENaC, which has been found to be expressed in the endolymphatic sac [143]. Whether ENaC or other ion transporters mediate fluid absorption in the endolymphatic sac is beyond the scope of the present study.

In summary, we have determined 1) that endolymph in the cochlea and the endolymphatic sac of *Slc26a4*$^{\Delta/+}$ and *Slc26a4*$^{\Delta/\Delta}$ mice is a NaCl rich fluid during the phase of cochlear growth and enlargement, 2) that the onset of K^+ secretion occurs in

the cochlea prenatally, and 3) that the rise in the K^+ concentration coincides with the onset of expression of the K^+ channel KCNQ1 and the $Na^+/2Cl^-/K^+$ cotransporter SLC12A2. The determination of the ionic composition of endolymph during the phase of cochlear growth in *Slc26a4*$^{\Delta/+}$ mice and enlargement in *Slc26a4*$^{\Delta/\Delta}$ mice presents an important first step toward elucidating mechanisms that cause the enlargement. The elucidation of these mechanisms is important for the identification of drug targets that can be exploited to prevent enlargement and restore normal cochlear development in patients carrying mutations of *SLC26A4*.

Acknowledgments

We thank Dr. Tracy Miesner and Mr. James Dille (Comparative Medicine Group, Kansas State University) for excellent mouse care.

Funding

This work was supported by a grant from the National Institutes on Deafness and Other Communication Disorders, NIH-R01-DC012151 (to P.W.) and by a grant from the Kansas City Area Life Sciences Institute (to P.W.) that was in turn funded by the Patton Trust. The Confocal Microscopy Core facility was supported by Kansas State University - College of Veterinary Medicine and a grant from the National Institutes of Health, NIH-P20-RR017686 (to D.C.M.). The funders had no role in study design, data collection and analysis, decision to publish, or preparation of the manuscript.

Chapter 3 Rescue of hearing and balance in *Slc26a4* mutant mice

These data have been published in the following refereed journal article:

Xiangming Li, Joel D. Sanneman, Donald G. Harbidge, Fei Zhou, Taku Ito, Raoul Nelson, Nicolas Picard, Régine Chambrey, Dominique Eladari, Tracy Miesner, Andrew J. Griffith, Daniel C. Marcus, Philine Wangemann

SLC26A4 targeted to the endolymphatic sac rescues hearing and balance in *Slc26a4* mutant mice

PLoS Genet 9(7): e1003641. doi:10.1371/journal.pgen.1003641

Author Contributions

PW DCM AJG	Conceived and designed the experiments
XL JDS DGH FZ PW	Performed the experiments
XL JDS DGH FZ PW	Analyzed the data
PW RN NP RC DE TI AJG	Contributed reagents/materials/analysis tools
XL PW	Wrote the paper
TM	Mouse colony management and genotyping

Abstract

Mutations of *SLC26A4* are a common cause of human hearing loss associated with enlargement of the vestibular aqueduct. *SLC26A4* encodes pendrin, an anion exchanger expressed in a variety of epithelial cells in the cochlea, the vestibular labyrinth and the endolymphatic sac. *Slc26a4*$^{\Delta/\Delta}$ mice are devoid of pendrin and develop a severe enlargement of the membranous labyrinth, fail to acquire hearing and balance, and thereby provide a model for the human phenotype. Here, we generated a transgenic mouse line that expresses human *SLC26A4* controlled by the promoter of *ATP6V1B1.* Crossing this transgene into the *Slc26a4*$^{\Delta/\Delta}$ line restored protein expression of pendrin in the endolymphatic sac without inducing detectable expression in the cochlea or the vestibular sensory organs. The transgene prevented abnormal enlargement of the membranous labyrinth, restored a normal endocochlear potential, normal pH gradients between endolymph and perilymph in the cochlea, normal otoconia formation in the vestibular labyrinth and normal sensory functions of hearing and balance. Our study demonstrates that restoration of pendrin to the endolymphatic sac is sufficient to restore normal inner ear function. This finding in conjunction with our previous report that pendrin expression is required for embryonic development but not for the maintenance of hearing opens the prospect that a spatially and temporally limited therapy will restore normal hearing in human patients carrying a variety of mutations of *SLC26A4.*

Author Summary

Mutations of *SLC26A4* are the most common cause for hearing loss associated with a swelling of the inner ear. This human disease is largely recapitulated in a mutant mouse model. Mutant mice lack *Slc26a4* expression and their inner ears swell during embryonic development, which leads to failure of the cochlea and the vestibular organs resulting in deafness and loss of balance.

SLC26A4 is normally found in the cochlea and vestibular organs of the inner ear as well as in the endolymphatic sac, which is a non-sensory part of the inner ear. The multitude of sites where *SLC26A4* is located made the goal to restore function through restoration look futile, unless some sites were more important than others.

Here, we generated a new mutant mouse that expresses *SLC26A4* in the endolymphatic sac but not in the cochlea or the vestibular organs of the inner ear. Fantastically, this mouse did not develop the detrimental swelling of the inner ear and even more exciting, the mouse developed normal hearing and balance.

Our study provides the proof-of-concept that a therapy aimed at repairing the endolymphatic sac during embryonic development is sufficient to restore a life-time of normal hearing and balance.

Introduction

Enlargement of the vestibular aqueduct (EVA; OMIM #600791) is a malformation of the temporal bone that is commonly observed in children with sensorineural hearing loss [30,31,144–146]. Mutations of *SLC26A4* are the most common cause for EVA-associated hearing loss that can either be non-syndromic (*DFNB4*; OMIM # 600791) or syndromic with enlargement of the thyroid gland (Pendred syndrome; OMIM #274600). *SLC26A4* codes for the anion exchanger pendrin that transports anions such as Cl^-, I^- and HCO_3^- [63,65].

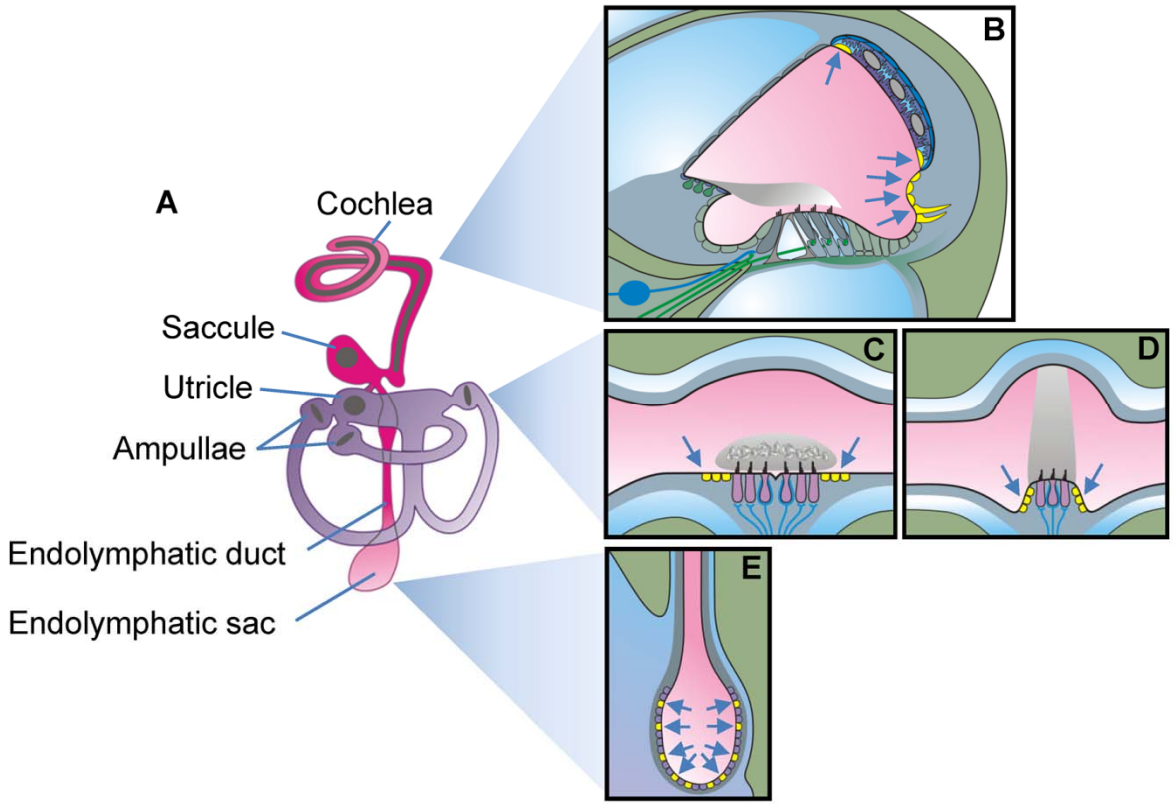

Figure 3.1: Schematic diagram of the inner ear.

A) *Diagram of the membranous labyrinth. The two continuous luminal fluid spaces of the mature inner ear are filled with endolymph (pink and purple).* ***B-E****) Diagrams of a cross section of one cochlear turn (****B****), of the utricle or saccule (****C****), of one ampulla (****D****) and the endolymphatic sac (****E****). Cells that express pendrin (yellow cells pointed to by arrows) are diagrammed in mature tissues.*

Although EVA is a malformation of the temporal bone, it is not the cause for hearing loss since no correlation was found between the degree of EVA and the severity of

hearing impairment [36]. EVA, however, is an indication of an enlargement of the endolymphatic duct epithelium that was present during embryonic development. Cartilage cells that form in the periphery of the endolymphatic duct epithelium preserve the diameter of the duct in a 'fossil-like' record when they give rise to the bone of the vestibular aqueduct.

The mature inner ear consists of seven interconnected fluid spaces that house six sensory organs (*Figure 3.1*): The cochlea for hearing, the utricle and saccule for sensing linear acceleration including gravity, and three ampullae with semicircular canals for sensing angular acceleration in three spatial axes. The seventh fluid compartment is the endolymphatic duct and sac, which is devoid of sensory cells and which is suspected to play a role in fluid homeostasis [3,147]. Pendrin is expressed in a variety of epithelial cells that enclose endolymph, which is the luminal fluid of the inner ear (*Figure 3.1*). Pendrin is expressed in outer sulcus, spiral prominence and spindle-shaped cells in the cochlea, transitional cells in the utricle, saccule and ampullae and mitochondria-rich cells (synonym: Forkhead-related or FORE cells) of the endolymphatic sac [66,101]. Each cell type represents a small domain in the heterogeneous epithelium that encloses endolymph. The many locations and cell types that express pendrin in a normal inner ear made the goal to restore function through restoration of expression look futile unless some sites of expression were more important than others.

The earliest onset of pendrin expression in the murine inner ear occurs in the endolymphatic sac at embryonic day E11.5, which precedes the onset of expression in the cochlea by 3 days, in the saccule and utricle by 4 days, and in the ampullae by 5 days [102]. The expression in the endolymphatic sac surges dramatically at E14.5, a time in development when there is very little pendrin expressed elsewhere in the inner ear [102].

Studies in a mouse model, *Slc26a4*$^{\Delta/\Delta}$, have revealed that loss of pendrin leads to an enlargement of endolymph volume followed by an acidification and a failure to develop

normal hearing and balance [102,103]. The onset of the enlargement in the cochlea and the endolymphatic sac occurs at E14.5 which precedes the onset of the luminal acidification by 1 day in the cochlea and by 3 days in the endolymphatic sac [102]. The enlargement develops in *Slc26a4*$^{\Delta/\Delta}$ mice between E14.5 and E18.5, which is the phase of rapid growth of the cochlea [31]. The coincidence of the surge in pendrin expression in the endolymphatic sac at E14.5 and the onset of the enlargement in *Slc26a4*$^{\Delta/\Delta}$ mice points to the importance of pendrin expression in the endolymphatic sac for inner ear fluid homeostasis.

We hypothesized that restoration of pendrin expression in the endolymphatic sac would prevent enlargement and permit normal development of the cochlea and the vestibular labyrinth including the acquisition of sensory function. To test this hypothesis, we generated a mouse line that expresses human pendrin *SLC26A4* controlled by the promoter of the B1-subunit of the human vacuolar H^+ ATPase (*ATP6V1B1*) and crossed this transgene into the *Slc26a4*$^{\Delta/\Delta}$ line to generate mice that lack expression of mouse pendrin but express human pendrin in the endolymphatic sac. No expression of pendrin protein was detected in these mice in the cochlea or the vestibular labyrinth but in mitochondria-rich cells of the endolymphatic sac. Analysis of this mouse model revealed normal hearing and balance function. Our data indicate that the expression of pendrin solely in the endolymphatic sac of the inner ear is sufficient to permit the development of normal hearing and balance.

Results

Generation of Tg(+);Slc26a4$^{\Delta/\Delta}$ transgenic mice

A transgenic mouse line, referred to as Tg*(B1-hPDS)*$^{Tg/+}$;*Slc26a4*$^{+/+}$ and abbreviated here to Tg(+);*Slc26a4*$^{+/+}$, was created by the laboratory of Dr. Dominique Eladari (Paris, France) [148]. This mouse expresses human *SLC26A4* (formerly named *hPDS*) controlled by the promoter of *ATP6V1B1,* which codes for the B1-subunit of the vH^+ATPase. Transgenic founders were crossed with wild-type C57BL/6 x CBA F1 mice

and three Tg(+);*Slc26a4*$^{+/+}$ mice were shipped to Kansas State University (Manhattan, Kansas, USA).

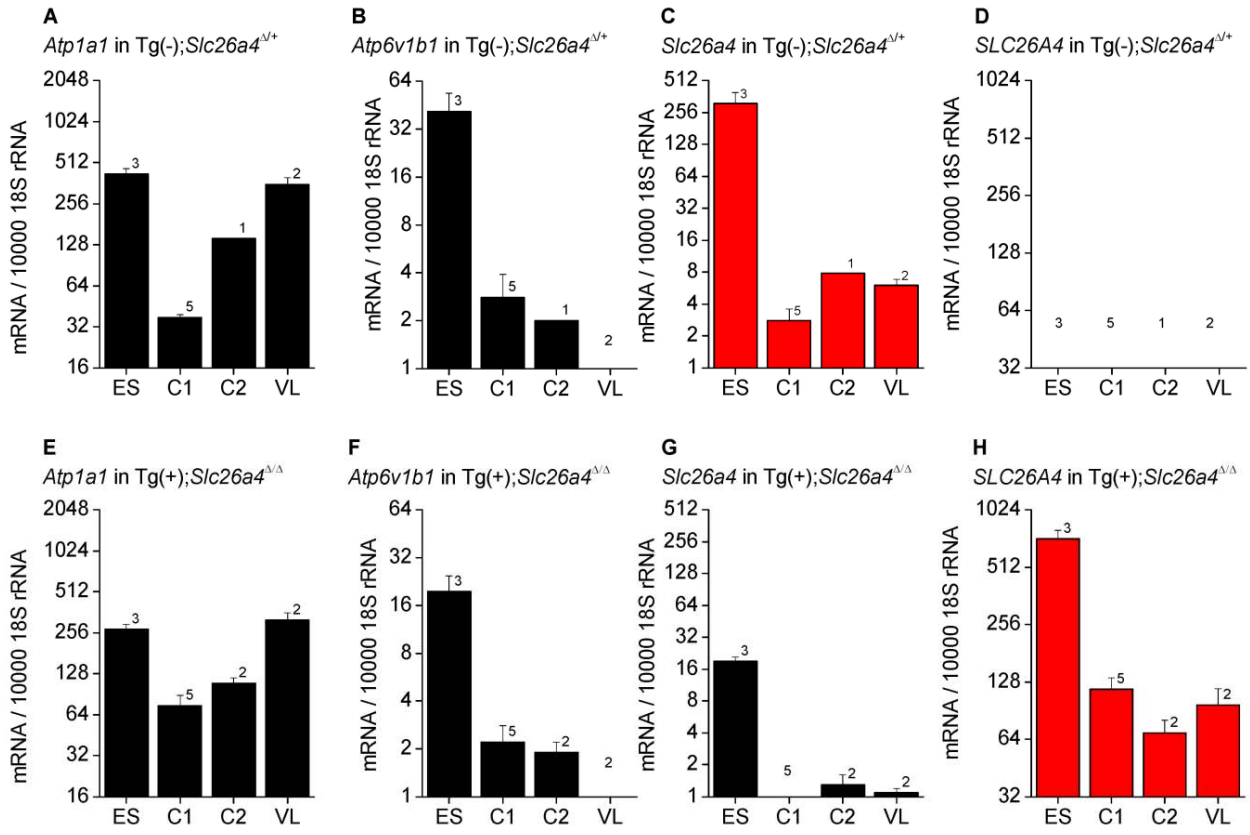

Figure 3.2: Atp1a1, Atp6v1b1, Slc26a4 & SLC26A4 mRNA levels in inner ear

Expression was determined by quantitative RT-PCR performed on total RNA. Total RNA was isolated from microdissected tissues obtained from Tg(-);Slc26a4$^{\Delta/+}$ *(**A-D**) and Tg(+);Slc26a4*$^{\Delta/\Delta}$ *mice (**E-H**). Endolymphatic sacs (ES) were isolated from mice at age E17.5. Cochleae were isolated at ages E17.5 (C1) and P2 (C2). Vestibular labyrinths (VL), consisted of saccule, utricle, ampullae and semicircular canals without endolymphatic sacs, were isolated at age P8. The expression of endogenous mouse Atp1a1, Atp6v1b1, and Slc26a4, and of transgenic human SLC26A4 mRNA was normalized to the expression of 18S rRNA. Note that the expression pattern of human SLC26A4 in Tg(+);Slc26a4*$^{\Delta/\Delta}$ *mice resembles the pattern of mouse Slc26a4 in Tg(-);Slc26a4*$^{\Delta/+}$ *mice (both patterns highlighted in red). Numbers inside graphs represent the number of experiments. (Experiments conducted by XL and FZ)*

At Kansas State University, Tg(+);*Slc26a4*$^{+/+}$ mice were crossed with *Slc26a4*$^{\Delta/\Delta}$ mice, which are maintained in an isogenic 129S6SvEv background, to generate the desired

Tg(+);*Slc26a4*$^{\Delta/\Delta}$ mice in an F2 generation. Expression of *SLC26A4* (human pendrin) in this mouse was expected to originate solely from the transgene since Exon 8 in the *Slc26a4*$^{\Delta}$ allele was replaced with a neomycin-cassette that introduced a frame-shift [103]. Littermates with the genotype Tg(-);*Slc26a4*$^{\Delta/\Delta}$ served as negative controls. These mice were expected to lack functional pendrin protein expression. Further, littermates with genotypes Tg(-);*Slc26a4*$^{\Delta/+}$, Tg(+);*Slc26a4*$^{\Delta/+}$, and Tg(+);*Slc26a4*$^{+/+}$ served as positive controls. These mice were expected to express murine pendrin with or without augmentation of human pendrin and have normal hearing and balance.

mRNA expression

Expression of *Atp1a1*, *Atp6v1b1, Slc26a4* and *SLC26A4* was determined by quantitative RT-PCR and normalized to the expression of 18S rRNA (*Figure 3.2*). The highest levels of *Atp6v1b1* and *Slc26a4* mRNA among the different inner ear tissues were found in the endolymphatic sac (*Figure 3.2B and C*). Expression of *Slc26a4* was reduced by factors between 6 and 16 in Tg(+);*Slc26a4*$^{\Delta/\Delta}$ mice compared to Tg(-);*Slc26a4*$^{\Delta/+}$ mice (*Figure 3.2C vs G*). Expression levels of *Atp1a1 and Atp6v1b1* exhibited a similar pattern among inner ear tissues of Tg(-);*Slc26a4*$^{\Delta/+}$ and Tg(+);*Slc26a4*$^{\Delta/\Delta}$ mice (*Figure 3.2A vs E and Figure 3.2B vs F*). Most interesting, expression levels of human *SLC26A4* in Tg(+);*Slc26a4*$^{\Delta/\Delta}$ resembled the pattern of mouse *Slc26a4* in Tg(-);*Slc26a4*$^{\Delta/+}$ mice with the highest levels being expressed in the endolymphatic sac (*Figure 3.2C vs H*). Whether or not expression levels of human *SLC26A4* in Tg(+);*Slc26a4*$^{\Delta/\Delta}$ exceeded expression levels of mouse *Slc26a4* in Tg(-);*Slc26a4*$^{\Delta/+}$ mice remained undetermined, since the efficiency of the reverse transcription of mRNA into cDNA remains generally unknown in quantitative RT-PCR experiments. Taken together, the data demonstrate that the transgene restored pendrin mRNA expression to the endolymphatic sac, the cochlea and the vestibular labyrinth of the inner ear.

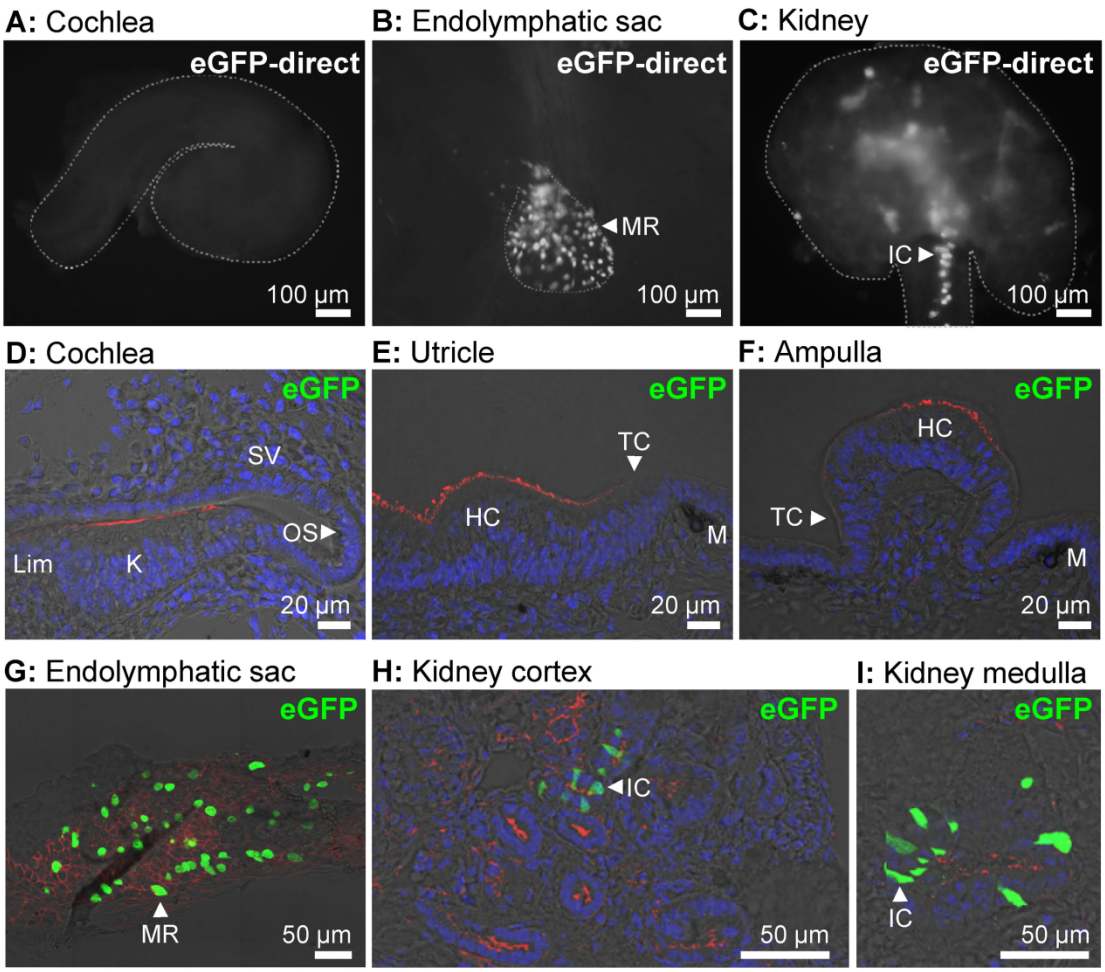

Figure 3.3: Transgene-encoded eGFP expression.

A-C*) Expression of eGFP was monitored as direct fluorescence in cochlear ducts (**A**), endolymphatic sacs (**B**), and kidney slices (**C**) freshly isolated from E15.5 Tg(B1-eGFP) mice. The outline of the imaged tissues is marked (dashed-line).* ***D-I****) Expression of eGFP was evaluated by immunocytochemistry in the cochlea (**D**), utricle (**E**), ampulla (**F**), endolymphatic sac (**G**), kidney cortex (**H**), and kidney medulla (**I**) from E15.5 Tg(B1-eGFP) mice. Staining consisted of immunocytochemistry of eGFP (green), F-actin (red) and nucleic acids (blue). The number of mice represented by these images are 2 for images **A-C** and 2 for images **D-I**. MR, mitochondria-rich cells; IC, intercalated cells; Lim, spiral limbus; K, Kölliker's organ; OS, outer sulcus; SV, stria vascularis; HC, vestibular hair cells; TC, transitional cells; M, melanocytes*. (Experiments conducted by PW, NP and XL)

Protein expression - eGFP expression

The ability of the *ATP6V1B1* promoter to drive protein expression in different tissues including the cochlea, the vestibular labyrinth and the endolymphatic sac was evaluated

in a transgenic mouse line, Tg(*B1-eGFP*) in which the expression of eGFP is controlled by the same 6.9 kb promoter of the human *ATP6V1B1* gene that drives the expression of human pendrin in Tg(+);*Slc26a4*$^{\Delta/\Delta}$ mice [149]. No expression of eGFP was detected in the cochlea or the vestibular labyrinth of E15.5 Tg(*B1-eGFP*) mice, although expression was present in the endolymphatic sac and the kidney (*Figure 3.3*). These data suggest that the *ATP6V1B1* promoter does not drive protein expression in the cochlea or the vestibular labyrinth.

Protein expression - Western blotting

Soft tissues of the cochlea and the vestibular labyrinth, exclusive of the endolymph sac, were collected from adult mice by microdissection and pooled into an 'inner ear' sample. Crude membrane protein preparations were obtained from these inner ear samples and from kidneys and subjected to gel-electrophoresis and Western blotting. Membrane proteins were obtained from Tg(+);*Slc26a4*$^{\Delta/\Delta}$ mice as well as from Tg(-);*Slc26a4*$^{\Delta/+}$ mice, which served as positive controls, and from Tg(-);*Slc26a4*$^{\Delta/\Delta}$ mice, which served as negative controls. Pendrin was detected in the inner ear and kidney of Tg(-);*Slc26a4*$^{\Delta/+}$ mice as a ~110 kDa band (*Figure 3.4A*). Inner ear from Tg(+);*Slc26a4*$^{\Delta/\Delta}$ mice lacked this band. The observation that there was no difference in the pattern of faint bands between inner ears from Tg(+);*Slc26a4*$^{\Delta/\Delta}$ mice and Tg(-);*Slc26a4*$^{\Delta/\Delta}$ mice, which is the negative control, suggests that pendrin was either not detectable or not present. The pendrin band, however, was found in kidney from Tg(+);*Slc26a4*$^{\Delta/\Delta}$ mice (*Figure 3.4B*), which suggests that the antibody recognizes both mouse and human pendrin. The observation that pendrin was detected at similar levels in descending amounts of kidney proteins isolated from Tg(-);*Slc26a4*$^{\Delta/+}$ mice (*Figure 3.4A*) and Tg(+);*Slc26a4*$^{\Delta/\Delta}$ mice (*Figure 3.4C*) suggests that the detection threshold for mouse and human pendrin was similar. Whether the antibody differed in the sensitivity between mouse and human pendrin remains unknown, since the relative abundance of mouse pendrin in kidneys of Tg(-);*Slc26a4*$^{\Delta/+}$ mice and human pendrin in kidneys of Tg(+);*Slc26a4*$^{\Delta/\Delta}$ mice is not known.

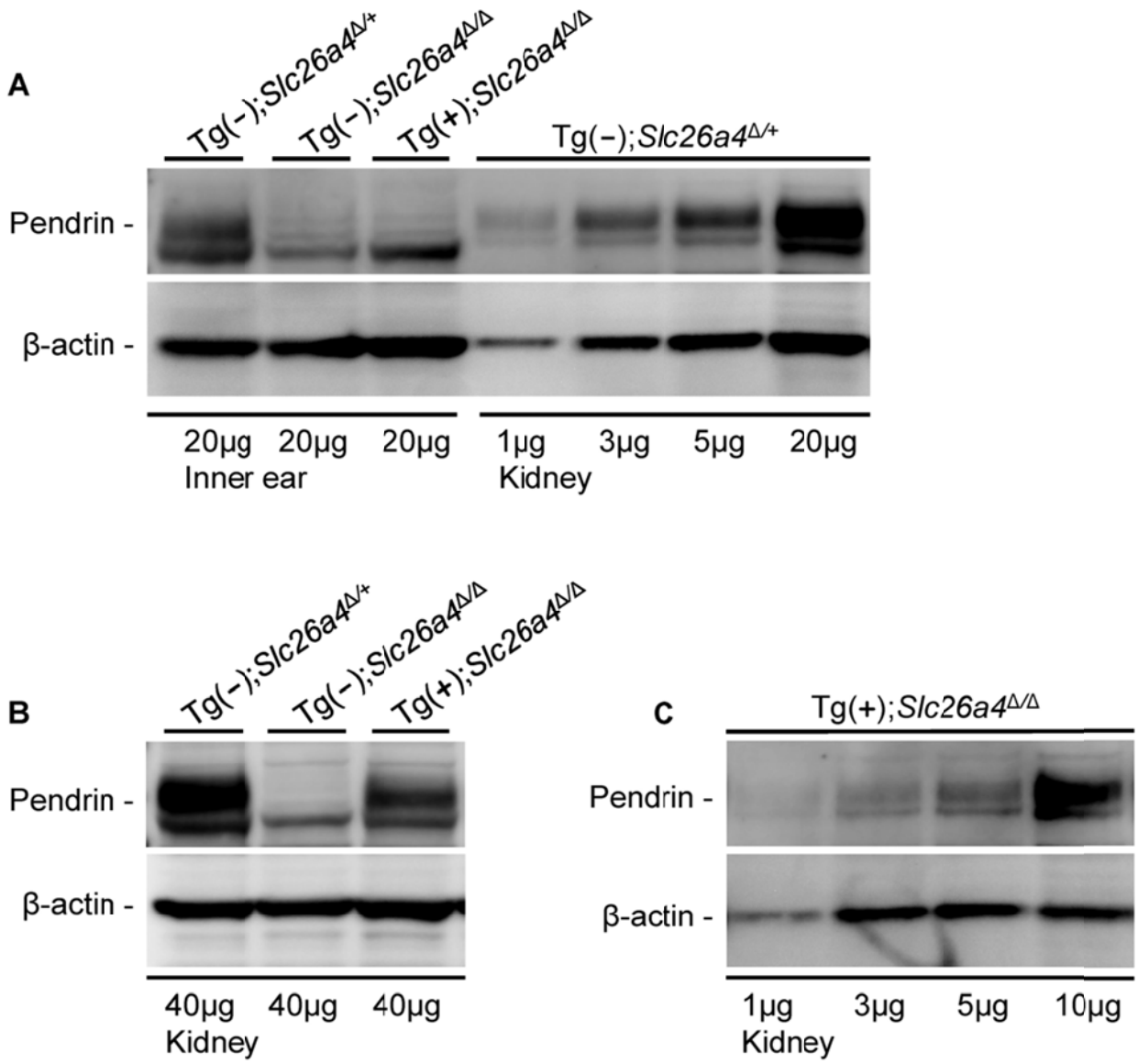

Figure 3.4: Pendrin expression evaluated by Western blotting.

Proteins in crude membranes prepared from pooled inner ear tissues consisting of soft tissues from the cochlea and the vestibular labyrinth devoid of endolymphatic sac and crude membranes prepared from kidneys of Tg(-)Slc26a4$^{\Delta/+}$, Tg(-)Slc26a4$^{\Delta/\Delta}$ and Tg(+)Slc26a4$^{\Delta/\Delta}$ mice were resolved by gel-electrophoresis and detected with an anti-pendrin antibody (Pds #1) and an anti-β-actin antibody. β-actin served as a loading control. ***A****) Comparison of pendrin expression in membranes prepared from inner ears of Tg(-)Slc26a4$^{\Delta/+}$, Tg(-)Slc26a4$^{\Delta/\Delta}$ and Tg(+)Slc26a4$^{\Delta/\Delta}$ mice to expression levels in descending amounts of membranes prepared from kidneys of Tg(-)Slc26a4$^{\Delta/+}$ mice.* ***B****) Comparison of pendrin expression in membranes prepared from kidneys of Tg(-)Slc26a4$^{\Delta/+}$, Tg(-)Slc26a4$^{\Delta/\Delta}$ and Tg(+)Slc26a4$^{\Delta/\Delta}$ mice.* ***C****) Expression levels of pendrin in descending amounts of membranes prepared from kidneys of Tg(+)Slc26a4$^{\Delta/\Delta}$ mice. Data shown in* ***A****,* ***B*** *and* ***C*** *are each representative of 2 biological replicates. (Experiments conducted by XL)*

The meaning of pendrin being not detectable in the inner ear was evaluated by comparison of the intensity of the pendrin band in inner ear to the intensities in descending amounts of kidney protein (*Figure 3.4A*). This comparison suggests that a ~5-fold lower amount pendrin should have been detectable in the inner ear. This means that pendrin expression in the inner ear of Tg(+);*Slc26a4*$^{\Delta/\Delta}$ mice is either absent or expressed at a level that does not exceed 20% of the expression level in Tg(-);*Slc26a4*$^{\Delta/+}$ mice.

Paint-fill of the cochlea and the endolymphatic sac

Temporal bones from Tg(+);*Slc26a4*$^{\Delta/+}$ and Tg(+);*Slc26a4*$^{\Delta/\Delta}$ mice were isolated at E15.5, fixed and injected with white paint (*Figure 3.5A and B*). Most striking is that there was no enlargement of the endolymphatic sac, duct or cochlea in Tg(+);*Slc26a4*$^{\Delta/\Delta}$ mice and that the morphology of Tg(+);*Slc26a4*$^{\Delta/+}$ and Tg(+);*Slc26a4*$^{\Delta/\Delta}$ mice was grossly similar. These data demonstrate that the introduction of the transgene rescued the malformation previously described in *Slc26a4*$^{\Delta/\Delta}$ mice [3,103].

Histology and pendrin expression in the endolymphatic sac

Whole-mounted specimens of the endolymphatic sac were prepared for immunocytochemistry from Tg(+);*Slc26a4*$^{\Delta/\Delta}$, Tg(-);*Slc26a4*$^{\Delta/\Delta}$, and Tg(+);*Slc26a4*$^{\Delta/+}$ mice (*Figure 3.5C-E*). Most striking is the enlargement and lack of pendrin expression in the endolymphatic sac of Tg(-);*Slc26a4*$^{\Delta/\Delta}$ mice (*Figure 3.5E*) and the similarity in size and similarity in pendrin expression between the endolymphatic sac of Tg(+);*Slc26a4*$^{\Delta/\Delta}$ mice (*Figure 3.5C*) and Tg(+);*Slc26a4*$^{\Delta/+}$ mice (*Figure 3.5D*). These data demonstrate that the transgene drives pendrin expression in the endolymphatic sac and that the introduction of the transgene rescued the malformation[3,103].

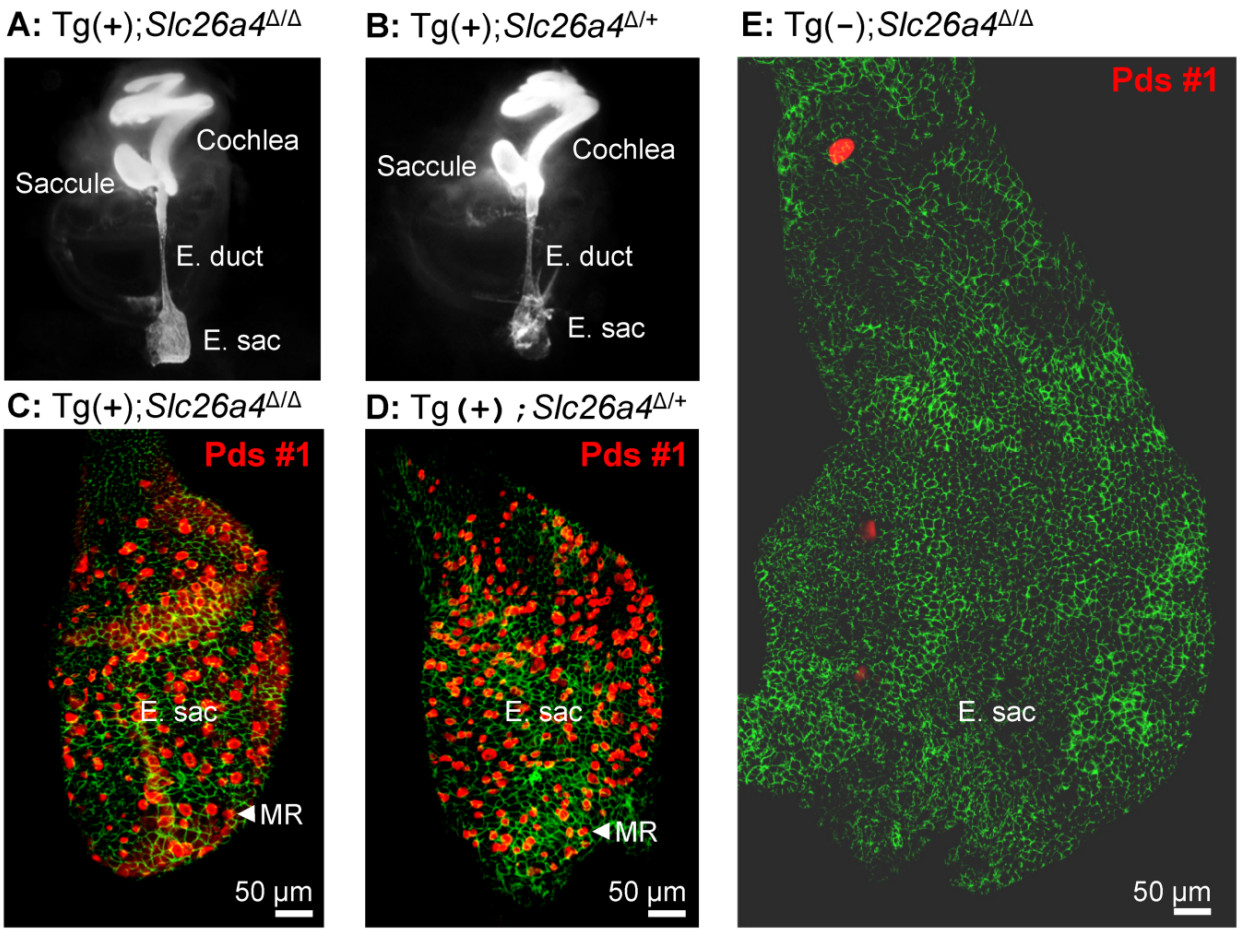

Figure 3.5: Histology and pendrin expression in the endolymphatic sac.

***A-B**) Paint filled inner ears from Tg(+);Slc26a4$^{\Delta/\Delta}$ and Tg(+);Slc26a4$^{\Delta/+}$ mice at age E15.5. Note that neither the endolymphatic duct (E. duct) nor the endolymphatic sac (E. sac) were enlarged. **C-E**) Pendrin protein expression in the endolymphatic sac at age E16.5. Staining consisted of immunocytochemistry of pendrin (red) and F-actin (green). Images provide comparison of whole mounts from Tg(+);Slc26a4$^{\Delta/\Delta}$ mice (**C**), Tg(+);Slc26a4$^{\Delta/+}$ mice (**D**), and Tg(-);Slc26a4$^{\Delta/\Delta}$ mice (**E**). Note that images **C-E** are presented at the same scale. The number of mice represented by these images is 2 for **A**, 2 for **B**, 3 for **C**, 4 for **D**, and 1 for **E**. MR, mitochondria-rich cells. (Experiments conducted by XL)*

Gross morphology of the cochlea

Gross morphological examination of inner ears revealed greater similarity between Tg(+);*Slc26a4*$^{\Delta/\Delta}$ mice and Tg(+);*Slc26a4*$^{\Delta/+}$ than between Tg(+);*Slc26a4*$^{\Delta/\Delta}$ mice and Tg(-);*Slc26a4*$^{\Delta/\Delta}$ mice (*Figure 3.6A-C*). Cochlear turns in Tg(+);*Slc26a4*$^{\Delta/\Delta}$ mice appeared normal in width and did not show widening of turns or thinning of the otic

capsule that was seen in Tg(-);*Slc26a4*$^{\Delta/\Delta}$ and that was previously described in *Slc26a4*$^{\Delta/\Delta}$ mice [101,116]. Inspection of the oval window revealed 'glittering' otoconia in the saccule in Tg(+);*Slc26a4*$^{\Delta/\Delta}$ and Tg(+);*Slc26a4*$^{\Delta/+}$ mice in contrast to Tg(-);*Slc26a4*$^{\Delta/\Delta}$ mice where no 'glittering' was visible (*Figure 3.6D-F*).

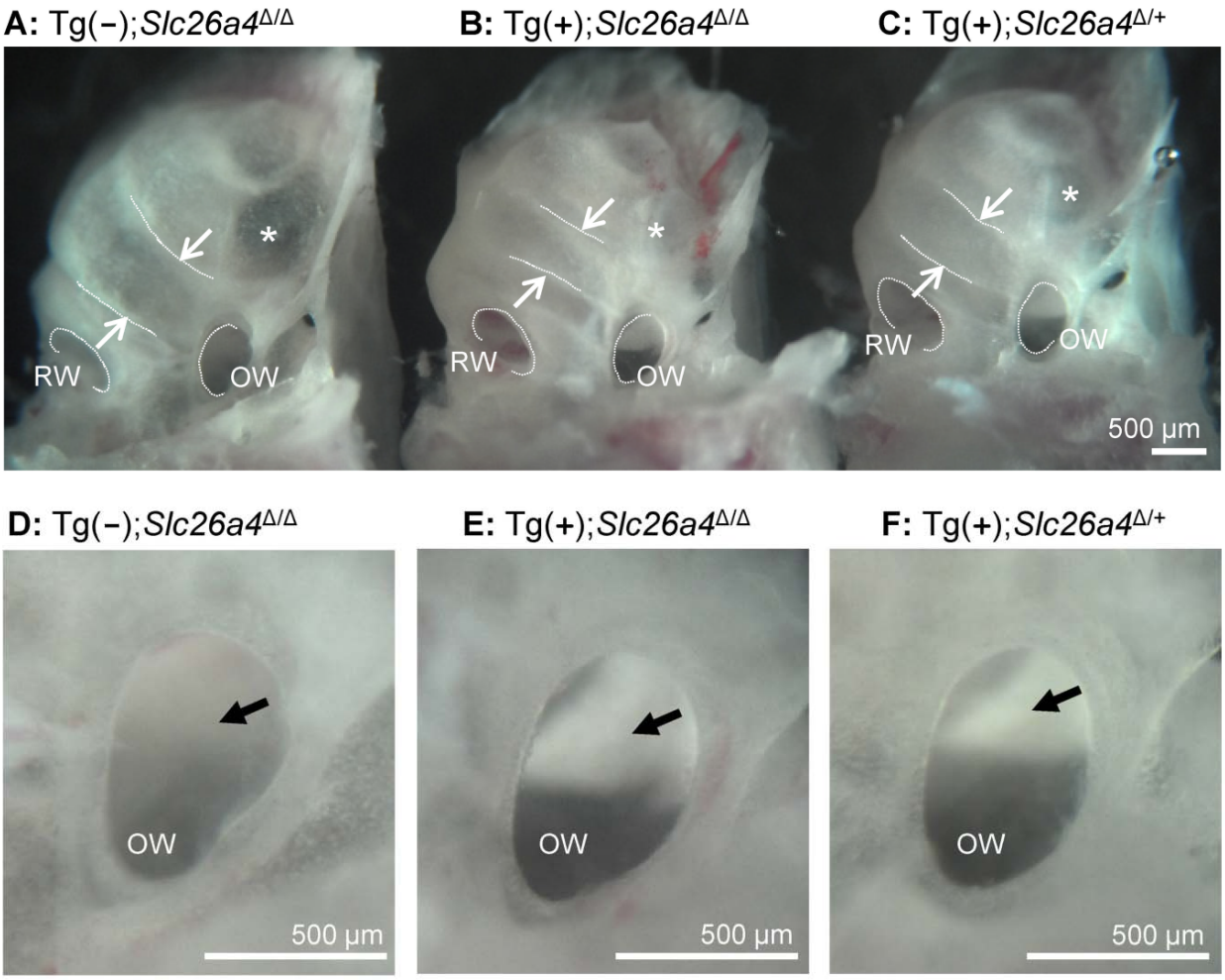

Figure 3.6: Gross morphology of the cochlea isolated by microdissection.

A-C*) Overview images of cochleae from a Tg(-);Slc26a4*$^{\Delta/\Delta}$*, Tg(+);Slc26a4*$^{\Delta/\Delta}$ *and Tg(+);Slc26a4*$^{\Delta/+}$ *mice. The width of the lower cochlear turn is marked with arrows and the round (RW) and oval window (OW) are labeled. A region with apparently thinner bone is marked (*).* ***D-F****) Enlarged view of the oval window. Normal otoconia in the saccule that reflect the light and appear bright white were seen in Tg(+);Slc26a4*$^{\Delta/\Delta}$ *and Tg(+);Slc26a4*$^{\Delta/+}$ *mice but not in Tg(-);Slc26a4*$^{\Delta/\Delta}$ *(arrow). The number of mice represented by these images is 1 for* ***A*** *and* ***D****, and 3 pairs for images* ***B*** *&* ***C*** *and* ***E*** *&* ***F****. (Experiments conducted by XL)*

Histology and pendrin expression in the cochlea

Midmodiolar sections of cochlear tissues were prepared for immunocytochemistry from Tg(+);*Slc26a4*$^{\Delta/\Delta}$ mice and positive controls consisting of Tg(-);*Slc26a4*$^{\Delta/+}$ or Tg(+);*Slc26a4*$^{\Delta/+}$ mice. No evidence for cochlear enlargement was found in Tg(+);*Slc26a4*$^{\Delta/\Delta}$ mice at E16.5 (*Figure 3.7B*), P1 (*Figure 3.13A*), P16 (*Figure 3.7A; Figure 3.13E*) or P18 (*Figure 3.13C*) suggesting that the introduction of the transgene rescued the cochlear malformation previously described in *Slc26a4*$^{\Delta/\Delta}$ mice, which includes a ~10-fold enlargement of the cochlea [101,103]. No detectable pendrin expression was found in the spiral prominence or outer sulcus epithelium of the cochlea in Tg(+);*Slc26a4*$^{\Delta/\Delta}$ mice although prominent expression was observed in these cells in positive controls (*Figure 3.7 and Figure 3.13*). The absence of pendrin in Tg(+);*Slc26a4*$^{\Delta/\Delta}$ mice was observed with two different anti-pendrin antibodies (Pds #1 and Pds #2). The patterns of pendrin expression in the positive controls, Tg(-);*Slc26a4*$^{\Delta/+}$ and Tg(+);*Slc26a4*$^{\Delta/+}$ mice, were similar for both antibodies to the pattern previously observed in *Slc26a4*$^{\Delta/+}$ mice [101,102,150]. Expression of pendrin was further examined in whole-mounted specimens that encompassed the spiral limbus, organ of Corti and outer sulcus. No detectable pendrin expression was found at age P35 in the spiral limbus of Tg(+);*Slc26a4*$^{\Delta/\Delta}$ mice (*Figure 3.7C*) or Tg(-);*Slc26a4*$^{\Delta/+}$ mice (*Figure 3.7H*) in contrast to the prominent expression of pendrin in the outer sulcus epithelia of Tg(-);*Slc26a4*$^{\Delta/+}$ mice (*Figure 3.7J*). For completeness, it needs to be reported that some punctate staining was found in nerve terminals near inner hair cells of Tg(+);*Slc26a4*$^{\Delta/\Delta}$ (*Figure 3.7D*) and Tg(-);*Slc26a4*$^{\Delta/+}$ mice (*Figure 3.7I*).

Endocochlear potential and pH

The endocochlear potential and the difference in pH between endolymph and perilymph was measured with double-barreled ion selective electrodes in Tg(-);*Slc26a4*$^{\Delta/\Delta}$ mice, Tg(+);*Slc26a4*$^{\Delta/+}$ mice, and Tg(+);*Slc26a4*$^{\Delta/\Delta}$ mice (*Figure 3.8*). Tg(-);*Slc26a4*$^{\Delta/\Delta}$ mice failed to develop a normal endocochlear potential and the pH of endolymph was lower (= more acidic) than in perilymph, as previously reported [81]. In contrast, Tg(+);*Slc26a4*$^{\Delta/+}$ mice, as reported for *Slc26a4*$^{\Delta/+}$ mice [81], developed a normal

endocochlear potential and a normal endolymphatic pH that was higher (=more alkaline) than in perilymph. Similar to Tg(+);*Slc26a4*$^{\Delta/+}$ mice, Tg(+);*Slc26a4*$^{\Delta/\Delta}$ mice developed a normal endocochlear potential and a normal endolymphatic pH even though no detectable pendrin expression was observed in the cochlear epithelium. These data demonstrate that the introduction of the transgene, which rescued the malformation, also rescued the loss of the endocochlear potential and the loss of normal endolymphatic pH homeostasis.

Hearing

Hearing tests were based on auditory brain stem recordings and thresholds in response to tone bursts of 8 kHz, 16 kHz and 32 kHz. Tests performed in Tg(+);*Slc26a4*$^{+/+}$, Tg(-);*Slc26a4*$^{\Delta/\Delta}$ and Tg(+);*Slc26a4*$^{\Delta/\Delta}$ mice confirmed profound deafness in Tg(-);*Slc26a4*$^{\Delta/\Delta}$ mice (*Figure 3.9B*) consistent with previous findings in *Slc26a4*$^{\Delta/\Delta}$ mice [81,81,103]. Waveforms of auditory brain stem recordings as well as thresholds were similar between Tg(+);*Slc26a4*$^{\Delta/\Delta}$ mice (*Figure 3.9A*) and Tg(+);*Slc26a4*$^{\Delta/+}$ (*Figure 3.9C*). These findings demonstrate that the introduction of the transgene rescued normal hearing although the cochlea did not express detectable levels of pendrin. We next evaluated whether the rescued hearing phenotype in Tg(+);*Slc26a4*$^{\Delta/\Delta}$ would be stable through at least 3 months of age. Auditory brain stem recordings were performed in Tg(+);*Slc26a4*$^{\Delta/+}$ mice (*Figure 3.9D-F*), in Tg(+);*Slc26a4*$^{\Delta/\Delta}$ mice (*Figure 3.9J-L*), and in Tg(+);*Slc26a4*$^{+/+}$ mice (*Figure 3.9G-I*) at 1, 2 and 3 month of age. Hearing in Tg(+);*Slc26a4*$^{\Delta/\Delta}$ mice at 8 kHz and 16 kHz was stable through 3 months. Thresholds were very similar among individuals and did not differ from Tg(+);*Slc26a4*$^{\Delta/+}$ and Tg(+);*Slc26a4*$^{+/+}$ mice. A greater variability in hearing thresholds was observed at 32 kHz (*Figure 3.9L*), with 10 of the 19 Tg(+);*Slc26a4*$^{\Delta/\Delta}$ mice maintaining excellent hearing (thresholds ≤30 dB at 32 kHz) and 5 developing a high-frequency hearing loss (thresholds ≥60 dB at 32 kHz). About one half of the Tg(+);*Slc26a4*$^{\Delta/\Delta}$ mice (9 of 19) developed progressive threshold elevations at 32 kHz with thresholds increasing by ≥10 dB between the monthly measurements. This variability is reflected in the greater error

bars at 32 kHz but did not lead to a statistically significant difference between Tg(+);*Slc26a4*$^{\Delta/\Delta}$ and Tg(+);*Slc26a4*$^{+/+}$ mice.

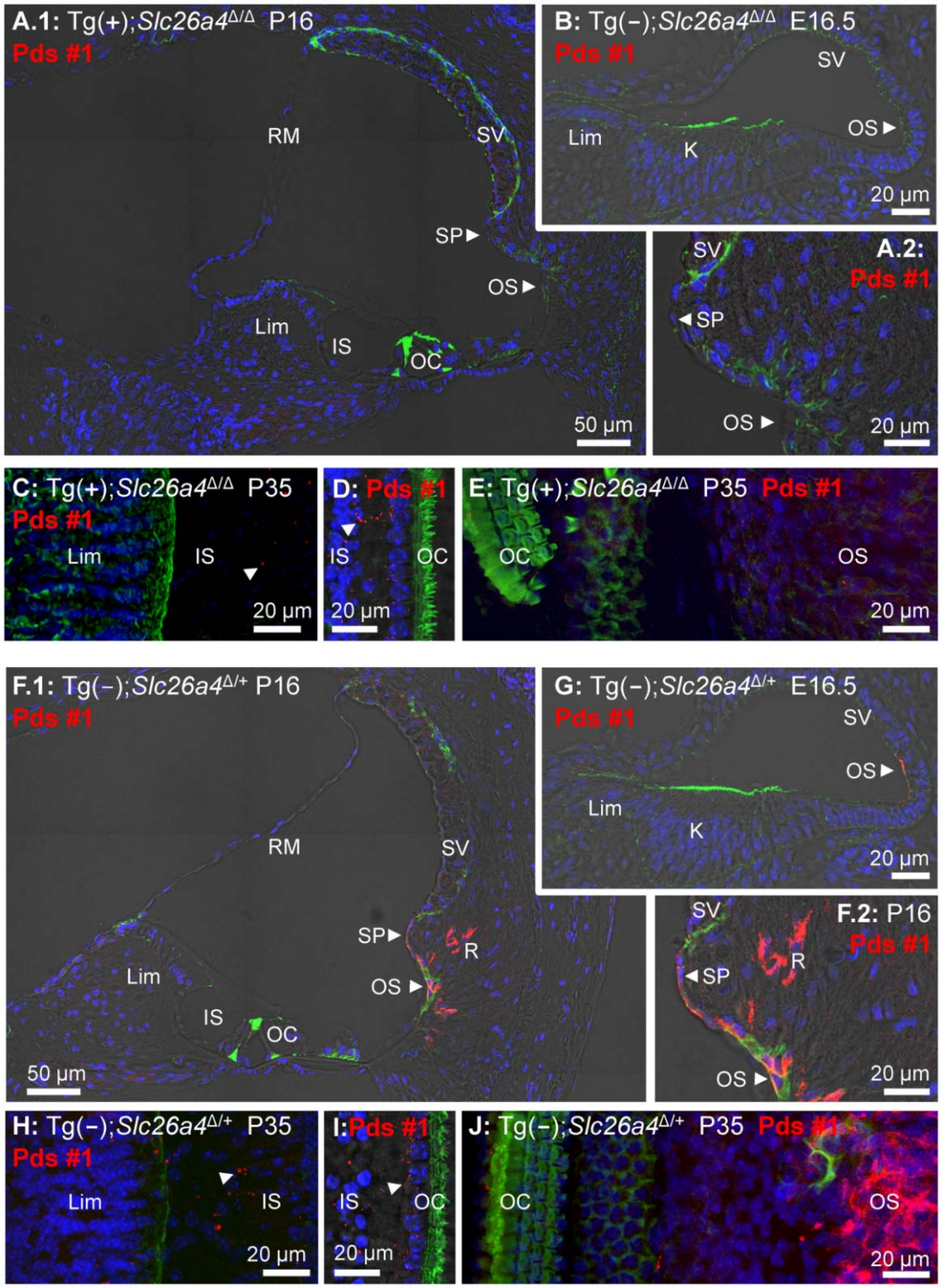

Figure 3.7: Histology and pendrin expression in the cochlea.

*Staining in all images consisted of immunocytochemistry of pendrin (Pds #1 antibody; red), F-actin (green) and nucleic acids (blue). Images provide comparison of cryosections (**A-B**) and whole-mounted specimens (**C-E**) from Tg(+);Slc26a4$^{\Delta/\Delta}$ mice to cryosections (**F-G**) and whole-mounted specimens (**H-J**) from Tg(-);Slc26a4$^{\Delta/+}$ mice. Whole-mounted specimens in **C**, **E**, **H** and **J** were imaged by detecting fluorescence in 25 optical sections that were recorded in 1 µm intervals and projected into a single plane. Whole-mounted specimens in **D** and **I** were imaged by detecting fluorescence in 8 optical sections that were recorded in 1 µm intervals, projected into a single plane and overlaid onto a single brightfield image. The number of pairs of mice represented by these images are 2 for image **A** & **F**, 3 for **B** & **G**, and 1 for **C-E** & **H-J** with 3 sections being evaluated per animal. K, Kölliker's organ; OS, outer sulcus; Lim, spiral limbus; IS, inner sulcus; OC, organ of Corti; SP, spiral prominence; SV, stria vascularis; RM, Reissner's membrane. Additional images using an alternative anti-pendrin antibody (Pds #2) and alternative positive controls (Tg(+);Slc26a4$^{\Delta/+}$ mice) are provided in the Supplement (Fig. 3.13). (Experiments conducted by XL)*

Histology and pendrin expression in the vestibular labyrinth

Sections and whole-mounted specimens of vestibular tissues were prepared for immunocytochemistry from Tg(+);*Slc26a4*$^{\Delta/\Delta}$ mice and positive controls consisting of Tg(-);*Slc26a4*$^{\Delta/+}$ or Tg(+);*Slc26a4*$^{\Delta/+}$ mice. No evidence of pendrin expression was found in the three sensory organs in Tg(+);*Slc26a4*$^{\Delta/\Delta}$ mice at P14 (*Figure 3.14A*), P16 (*Figure 3.10A,C,D and Figure 3.14C,G,K*), P18 (*Figure 3.14E*), and P35 (*Figure 3.10B*). The absence of pendrin in Tg(+);*Slc26a4*$^{\Delta/\Delta}$ mice was observed with two different anti-pendrin antibodies (Pds #1 and Pds #2). In contrast, pendrin expression was found in transitional cells of the utricle, saccule and ampullae of controls that consisted of Tg(-);*Slc26a4*$^{\Delta/+}$ or Tg(+);*Slc26a4*$^{\Delta/+}$ mice. The expression patterns in Tg(-);*Slc26a4*$^{\Delta/+}$ and Tg(+);*Slc26a4*$^{\Delta/+}$ mice with both antibodies were similar to the pattern previously described in *Slc26a4*$^{\Delta/+}$ mice [101,150].

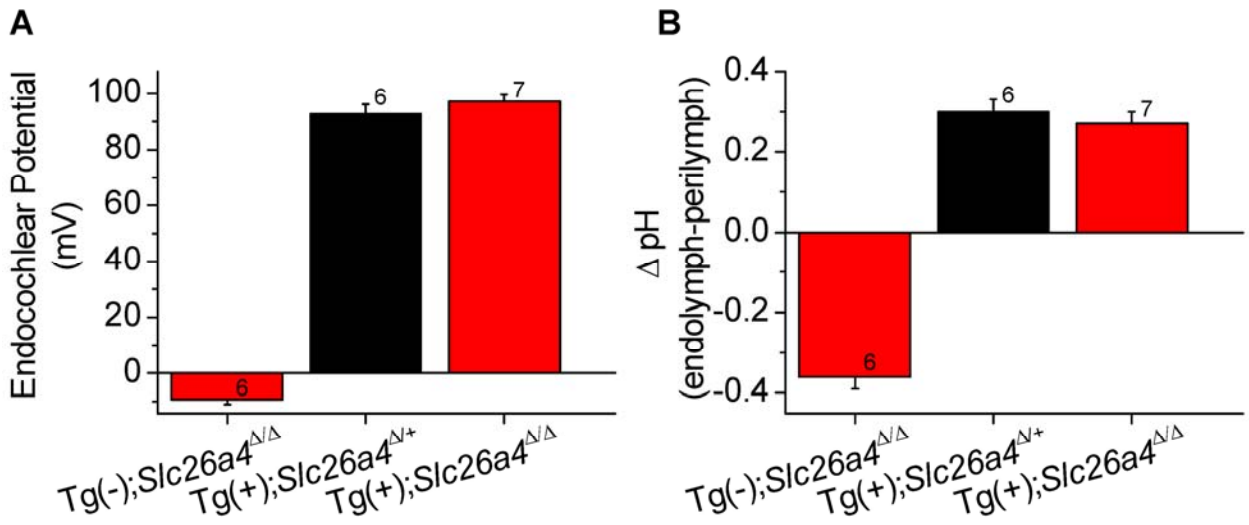

Figure 3.8: Endocochlear potential and pH.

*Endocochlear potential (**A**) and the difference between endolymphatic and perilymphatic pH (**B**) were measured in Tg(-);Slc26a4$^{\Delta/\Delta}$, Tg(+);Slc26a4$^{\Delta/+}$, and Tg(+);Slc26a4$^{\Delta/\Delta}$ mice. Numbers near the error bars represent the number of experiments. (Experiments conducted by DH)*

Otoconia

Vestibular labyrinths were isolated by microdissection from Tg(-);*Slc26a4*$^{\Delta/\Delta}$, Tg(+);*Slc26a4*$^{\Delta/\Delta}$ and Tg(+);*Slc26a4*$^{\Delta/+}$ mice and the roof of the utricle was removed to permit an unobstructed view onto the utricular macula (*Figure 3.11A-C*). Glittering otoconia were observed in Tg(+);*Slc26a4*$^{\Delta/\Delta}$ and Tg(+);*Slc26a4*$^{\Delta/+}$ mice and giant otoconia in Tg(-);*Slc26a4*$^{\Delta/\Delta}$. Otoconia were transferred into glass-bottom dishes and inspected by laser-scanning microscopy using a 405 nm laser. Giant otoconia from Tg(-);*Slc26a4*$^{\Delta/\Delta}$ mice were ~10-fold larger than normal otoconia (*Figure 3.11D*). The shape of the giant otoconia resembled the shape previously observed in *Slc26a4*$^{\Delta/\Delta}$ mice [101]. Otoconia in Tg(+);*Slc26a4*$^{\Delta/\Delta}$ and Tg(+);*Slc26a4*$^{\Delta/+}$ mice were similar consisting in both genotypes of larger (~20 µm, *Figure 3.11E.1 and F.1*) and smaller (~10 µm; *Figure 3.11E.2 and F.2*) otoconia, some of which revealed a concentric structure (*Figure 3.11E.3 and F.3*). These data suggest that the introduction of the transgene rescued normal otoconia formation.

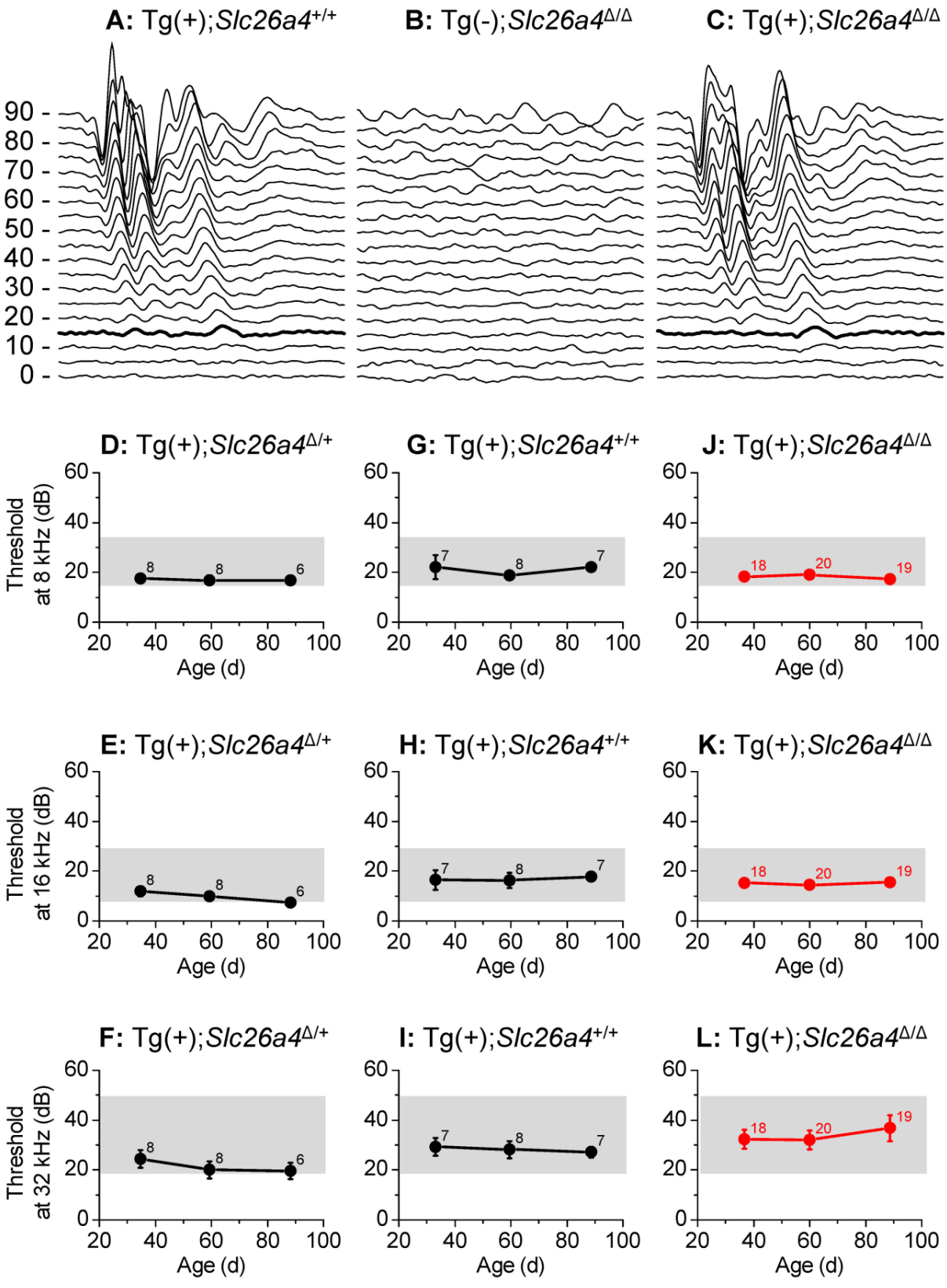

Figure 3.9: Hearing tests based on auditory brain stem responses.

***A-C**) Examples of recordings of auditory brain stem responses to tone bursts of 16 kHz at amplitudes between 0 and 90 dB-SPL that were presented to Tg(+);Slc26a4$^{+/+}$ mice at P35 (**A**), Tg(-);Slc26a4$^{\Delta/\Delta}$ mice at P35 (**B**), and Tg(+);Slc26a4$^{\Delta/\Delta}$ mice at P35 (**C**). Thresholds at 15 dB-SPL are marked (thickened trace). **D-L**) Hearing thresholds based on auditory brain stem responses, were determined in Tg(+);Slc26a4$^{\Delta/+}$ mice (**D-F**), Tg(+);Slc26a4$^{+/+}$ mice (**G-I**), and Tg(+);Slc26a4$^{\Delta/\Delta}$ mice (**J-L**; highlighted in red). Frequencies evaluated at 8 kHz (**D, G, J**), 16 kHz (**E, H, K**), and 32 kHz (**F, I, L**). The combined ranges of normal hearing in the three mouse strains (129S6, C57BL/6 and CBA) that contributed to the background of the mice are marked (grey rectangles). Numbers next to symbols in **D-L** represent the number of mice tested. (Experiments conducted by JS)*

Balance

Balance tests were performed in Tg(+);*Slc26a4*$^{\Delta/\Delta}$ mice and Tg(+);*Slc26a4*$^{\Delta/+}$ mice as well as in Tg(-);*Slc26a4*$^{\Delta/+}$ and Tg(-);*Slc26a4*$^{\Delta/\Delta}$ mice (*Figure 3.12*). Tg(-);*Slc26a4*$^{\Delta/\Delta}$ mice failed the test, which confirmed the vestibular phenotype previously described in *Slc26a4*$^{\Delta/\Delta}$ mice [103]. There was no apparent difference in the performance of Tg(+);*Slc26a4*$^{\Delta/\Delta}$, Tg(+);*Slc26a4*$^{\Delta/+}$ and Tg(-);*Slc26a4*$^{\Delta/+}$ mice. These data demonstrate that the introduction of the transgene rescued normal gross motor vestibular function.

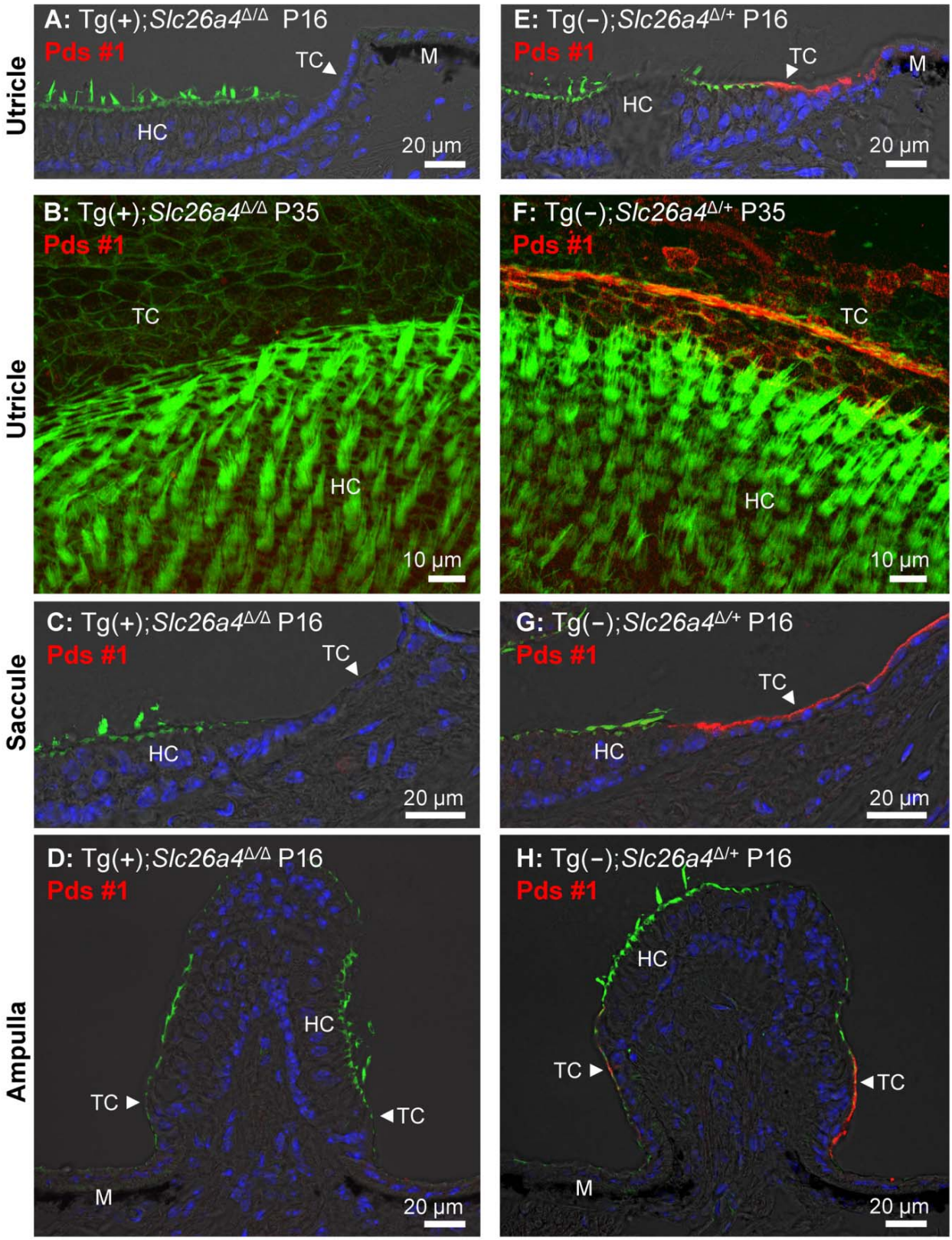

Figure 3.10: Histology and pendrin expression in the vestibular labyrinth.

*Staining in all images consisted of immunocytochemistry of pendrin (Pds #1 antibody; red) and F-actin (green) and of nucleic acids (blue), the latter with the exception of images **B** and **F**. Images provide comparison of cryosections (**A, C-D**) and whole-mounted specimens (**B**) from Tg(+);Slc26a4$^{\Delta/\Delta}$ to cryosections (**E, G-H**) and whole-mounted specimens (**F**) from Tg(-);Slc26a4$^{\Delta/+}$ mice. Whole-mounted specimens were imaged by detecting fluorescence in 25 optical sections that were recorded in 1 µm intervals and projected into a single plane. The number of pairs of mice represented by these images are 2 for image **A** & **E**, 1 for **B** & **F**, 2 for **C** & **G**, and 2 for **D** & **H** with 3 sections being evaluated per animal. HC, vestibular hair cells; TC, transitional cells; M, melanocytes. Additional images using an alternative anti-pendrin antibody (Pds #2) and alternative positive controls (Tg(+);Slc26a4$^{\Delta/+}$ mice) are provided in the Supplement (Fig. 3.14). (Experiments conducted by XL)*

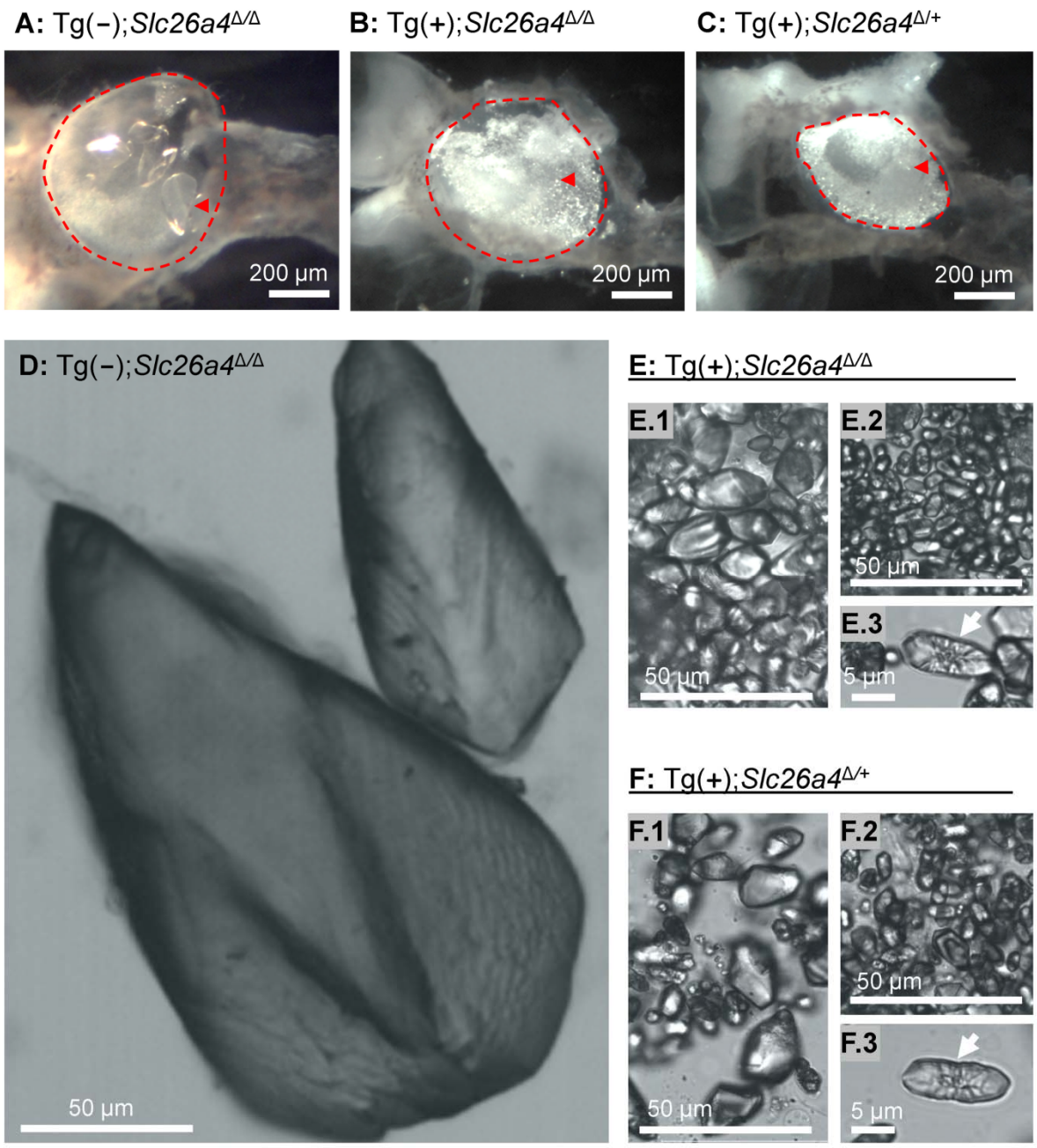

Figure 3.11: Otoconia.

A-C*) Microdissected maculae utriculi from a Tg(-);Slc26a4$^{\Delta/\Delta}$, Tg(+);Slc26a4$^{\Delta/\Delta}$ and Tg(+);Slc26a4$^{\Delta/+}$ mice. The macula utriculi have been marked (red dashed line) and a single otoconium is indicated (red arrow head).* ***D-F****) Isolated otoconia from Tg(-);Slc26a4$^{\Delta/\Delta}$, Tg(+);Slc26a4$^{\Delta/\Delta}$ and Tg(+);Slc26a4$^{\Delta/+}$ mice. Note that images* ***D****,* ***E.1****,* ***E.2****,* ***F.1*** *and* ***F.2*** *are presented at the same scale. Mega-otoconia were found only in Tg(-);Slc26a4$^{\Delta/\Delta}$ mice. Tg(+);Slc26a4$^{\Delta/\Delta}$ mice contained a mixture of larger and smaller otoconia, some of which showed a concentric pattern (****E.1, E.2*** *and* ***E.3****) that was similar to the mixture found in Tg(-);Slc26a4$^{\Delta/+}$ mice (****F.1, F.2*** *and* ***F.3****). (Experiments conducted by XL and PW)*

Discussion

In this study we generated a mouse that expresses human pendrin in the endolymphatic sac but lacks detectable pendrin protein expression in the cochlea or in the vestibular labyrinth. The most biologically interesting and clinically relevant observation of this study is that this mouse develops normal hearing and balance. Our findings support the hypothesis that pendrin expression in the endolymphatic sac is chiefly responsible for the development of normal endolymph volume, that lack of pendrin in the endolymphatic sac is mainly responsible for the development of the membranous labyrinth enlargement in *Slc26a4*$^{\Delta/\Delta}$ mice, and that the complex inner ear pathology found in *Slc26a4*$^{\Delta/\Delta}$ mice is largely a consequence of the enlargement during embryonic development. This hypothesis was based on the studies in *Slc26a4*$^{\Delta/\Delta}$ mice that revealed that the enlargement is a key event on the path toward organ failure resulting in deafness and vestibular dysfunction [81,101,102] and on studies in *Foxi1*$^{-/-}$ mice that lack pendrin expression in the endolymphatic sac, develop an enlargement of the inner ear, but express pendrin in the cochlea and the vestibular labyrinth [123].

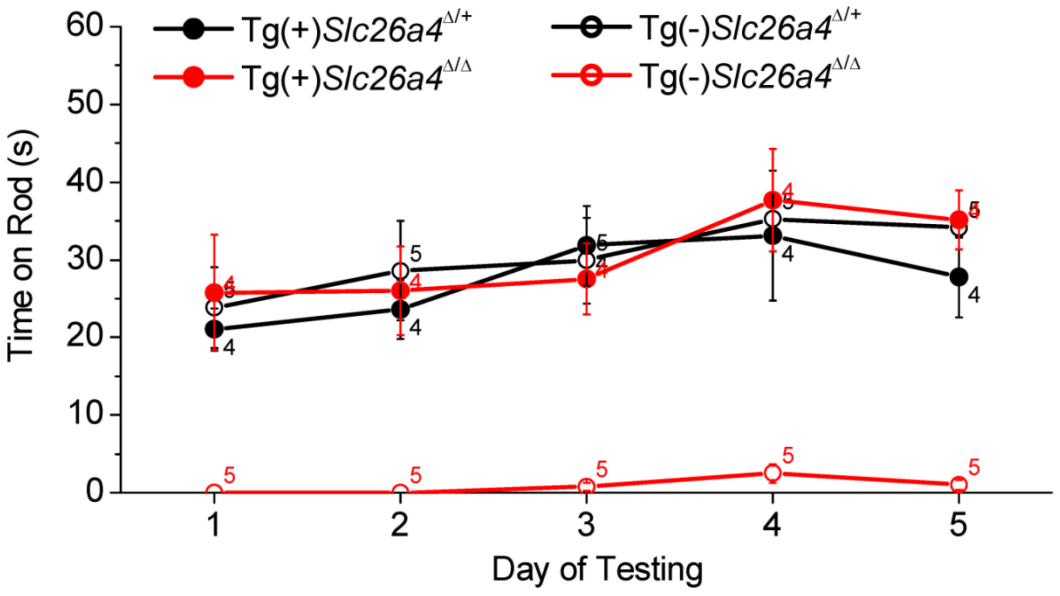

Figure 3.12: Balance tests

Tests were based on the ability of Tg(+);Slc26a4$^{\Delta/+}$*, Tg(+);Slc26a4*$^{\Delta/\Delta}$*, Tg(-);Slc26a4*$^{\Delta/+}$*, Tg(-);Slc26a4*$^{\Delta/\Delta}$ *mice to balance on a rotating rod that was accelerated from 4 to 40 rpm over 60 s. Numbers near the symbols indicate the number of mice evaluated. (Experiments conducted by DH)*

To test our hypothesis, we generated a transgenic mouse, Tg(*B1-hPDS*), which expresses human *SLC26A4* (previously named *PDS*) controlled by the promoter of *ATP1V1B1* [151]. The ability of the promoter of *ATP1V1B1* to control gene expression had previously been evaluated in a transgenic mouse that expresses eGFP controlled by the promoter of *ATP6V1B1* [149,152]. Expression of eGFP had been found in this mouse in intercalated cells of the renal collecting duct, and in narrow and clear cells of the epididymal epithelium of adult mice [149]. We found expression of eGFP in the embryonic kidney and in mitochondria-rich cells of the endolymphatic sac but not in the cochlea or the vestibular labyrinth (*Figure 3.3*). Expression in mitochondria-rich cells of the endolymphatic sac was expected since these cells are members of the FORE family (forkhead related) of cells. FORE cells express FOXI1, which drives the expression of *Atp6v1b1* and *Slc26a4 [39,88,90]*. Consistently, mitochondria-rich cells of the endolymphatic sac express the mRNAs *Atp6v1b1* and *Slc26a4 [44,100]* and the corresponding proteins, the B1-subunit of the vH^+ATPase and pendrin [90,150]. The onset of expression of *Atp6v1b1* in the endolymphatic sac is at E11.5, which is similar to the onset of pendrin [48,102]. Thus, it was likely that the transgene Tg(*B1-hPDS*) would drive a timely expression of pendrin in mitochondria-rich cells of the endolymphatic sac.

Although FOXI1 drives the expression of *Atp6v1b1* and *Slc26a4* in FORE cells such as the mitochondria-rich cells of the endolymphatic sac, the expression of *Atp6v1b1* and *Slc26a4* is not limited to FORE cells. Indeed, *Slc26a4* is expressed in the inner ear in spiral prominence and outer sulcus epithelial cells as well as in spindle-shaped cells of the cochlea and in transitional cells of the vestibular labyrinth, none of which are FORE cells [101,150]. Further, *Atp6v1b1* expression has been found in the spiral limbus of the cochlea, which does not contain FORE cells [44,48]. The expression of *Atp6v1b1* in the cochlea provided the possibility that the transgene would drive an ectopic expression of pendrin in the spiral limbus. Our studies of eGFP expression (*Figure 3.3*) and of pendrin expression by Western blotting (*Figure 3.4*) and immunocytochemistry of whole-mounted specimens and sections using two different anti-pendrin antibodies (Pds #1 and Pds #2, *Figure 3.7 and 3.13*) revealed no detectable expression in the cochlea or vestibular labyrinth of Tg(+);*Slc26a4*$^{\Delta/\Delta}$ mice. The observed absence of pendrin

expression in the vestibular labyrinth of Tg(+);*Slc26a4*$^{\Delta/\Delta}$ mice (*Figure 3.10 and 3.14*) is consistent with the reported lack of *Atp6v1b1* expression in the vestibular labyrinth based on detection by *in situ* hybridization [44,48] and by quantitative RT-PCR (*Figure 3.2B and F*), which is a more sensitive technique. The observation that human *SLC26A4* mRNA but no pendrin nor eGFP protein was detected in the cochlea or the vestibular labyrinth suggests the presence of strong translational regulation[153]. Taken together, our data demonstrate that we have generated a mouse that expresses pendrin in the endolymphatic sac but not in the cochlea or the vestibular labyrinth, although we cannot completely rule out that low levels of pendrin protein expression escaped our detection. Such low pendrin expression is unlikely the reason for the restored endolymphatic volume, since pendrin expression in the cochlea and vestibular labyrinth of *Foxi*$^{-/-}$ mice, which lack pendrin expression in the endolymphatic sac, did not prevent endolymphatic enlargement [123] and since mice that express a mutant pendrin protein that supports anion exchange at a reduced rate are deaf, develop mega-otoconia and are balance impaired [105]. Moreover, hypomorphic mutant alleles of *SLC26A4* show no difference in the resulting auditory phenotype from that of functional null alleles in patients with Pendred syndrome [126], indicating that small amounts of pendrin activity are insufficient to rescue hearing in humans.

Measurements of the endocochlear potential and pH revealed that the introduction of the transgene, which rescued normal endolymph volume, also rescued the loss of the normal endocochlear potential and the loss of the normal endolymphatic pH homeostasis (*Figure 3.8*). It appears that the Cl^-/HCO_3^- exchanger pendrin, which is normally expressed in the apical membranes of spiral prominence and outer sulcus epithelial cells, is not the sole mechanism responsible for the alkaline pH of endolymph in a normally developed cochlea. A similar conclusion can be drawn based on measurements in the doxycycline-inducible *Slc26a4* mouse model where termination of pendrin expression at P6 led to the development of a nearly normal endocochlear potential and of a nearly normal alkaline pH [114]. We hypothesize that the epithelial barrier enclosing endolymph is permeable to H^+, OH^- and HCO_3^- and that the pH of endolymph follows the endocochlear potential.

Hearing and balance tests in Tg(+);*Slc26a4*$^{\Delta/\Delta}$ mice revealed normal sensory function (*Figure 3.9 and 3.12*). The observation that hearing thresholds at 32 kHz had some variability in Tg(+);*Slc26a4*$^{\Delta/\Delta}$ mice and that some Tg(+);*Slc26a4*$^{\Delta/\Delta}$ mice developed progressive high-frequency hearing loss is most likely a function of the genetic background. Tg(+);*Slc26a4*$^{\Delta/\Delta}$ were generated in a F2 generation from *Slc26a4*$^{\Delta/\Delta}$ mice that were maintained isogenic in the 129S6 background and Tg(+);*Slc26a4*$^{\Delta/\Delta}$ mice that were recently generated in a mixed background of C57BL/6 and CBA. DNA from the three background strains, 129S6, C57BL/6 and CBA, which differ in their hearing thresholds, are expected to comprise variable amounts of the genomes of individual mice. Hearing thresholds for 1 to 3 month-old 129S6, C57BL/6 and CBA mice range between 20-35 dB-SPL at 8 kHz, 10-28 dB-SPL at 16 kHz and 20-50 dB-SPL at 32 Hz [81,154–158]. In general, 129S6, C57BL/6 and CBA mice have similar thresholds at 8 kHz, whereas at 16 and 32 kHz CBA mice have lower thresholds than 129S6 and C57BL/6 mice. Thus, the greater variability in hearing thresholds that was observed at 32 kHz particularly in Tg(+);*Slc26a4*$^{\Delta/\Delta}$ may be due to a variability in the mixture of these background strains.

Our observation that normal hearing developed in the absence of pendrin expression in the cochlea in combination with the published finding that normal hearing was maintained when pendrin expression was terminated after completed development [114], could suggest that pendrin in the cochlea has no physiologic significance beyond the developmental phase. However, it is also conceivable that pendrin-mediated HCO_3^- secretion provides a buffer that stabilizes the pH in the lateral wall tissues as well as in endolymph, and that this buffering is important during stress situations associated with normal life. Pendrin expression may indeed be important for the maintenance of hearing into advanced age.

In summary, we demonstrated that restoration of pendrin to the endolymphatic sac is sufficient to restore normal inner ear function. This implies that pendrin in the endolymphatic sac is more important for the development of normal hearing than pendrin expression in the cochlea and more important for the development of normal balance than pendrin expression in the vestibular labyrinth. This finding, in conjunction with our previous report that pendrin expression is required for embryonic development

but not for the maintenance of hearing, opens the prospect that a spatially and temporally limited therapy will restore normal hearing in human patients carrying a variety of mutations of *SLC26A4.*

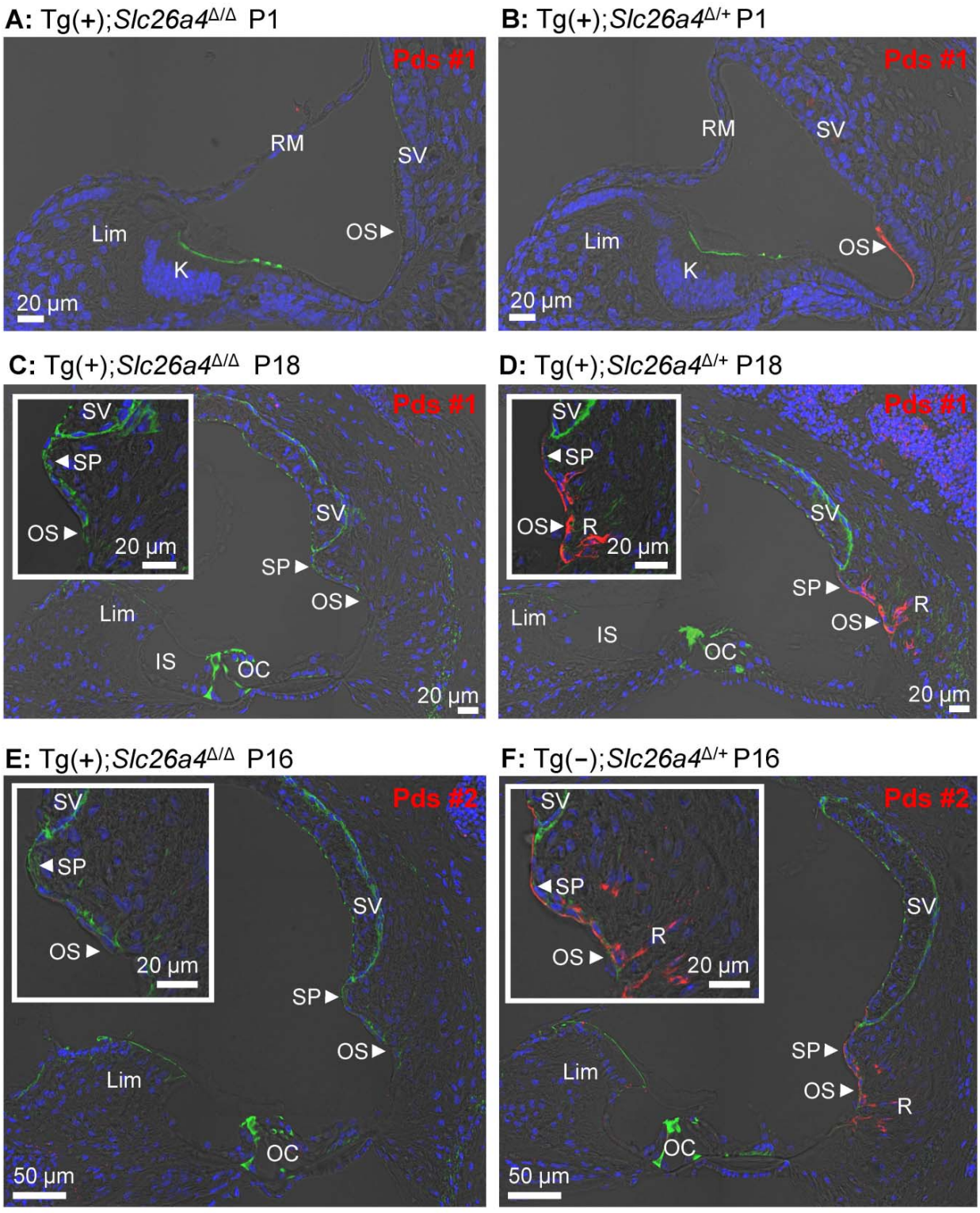

Figure 3.13 Histology and pendrin expression in the cochlea.

Staining in all images consisted of immunocytochemistry of pendrin (Pds #1 antibody or Pds #2 antibody; red*), F-actin (*green*) and nucleic acids (*blue*). Images provide comparison of pendrin expression in Tg(+);*Slc26a4$^{\Delta/\Delta}$ *mice (**A, C, E**) to positive controls consisting of Tg(+);*Slc26a4$^{\Delta/+}$ *(**B, D**) or Tg(−);*Slc26a4$^{\Delta/+}$ *mice (**F**). Note that both antibodies, Pds #1 and Pds #2, failed to detect pendrin expression in Tg(+);*Slc26a4$^{\Delta/\Delta}$ *mice and that the staining pattern for pendrin in positive controls was similar for both antibodies and for both positive controls. The number of pairs of mice represented by these images are 2 for images **A** & **B**, 1 for **C** & **D**, and 2 for **E** & **F** with 3 sections being evaluated per animal. K, Kölliker's organ; OS, outer sulcus; Lim, spiral limbus; IS, inner sulcus; OC, organ of Corti; SP, spiral prominence; SV, stria vascularis; RM, Reissner's membrane. Compare these images to those in* Figure 3.7. *(Experiments conducted by XL)*

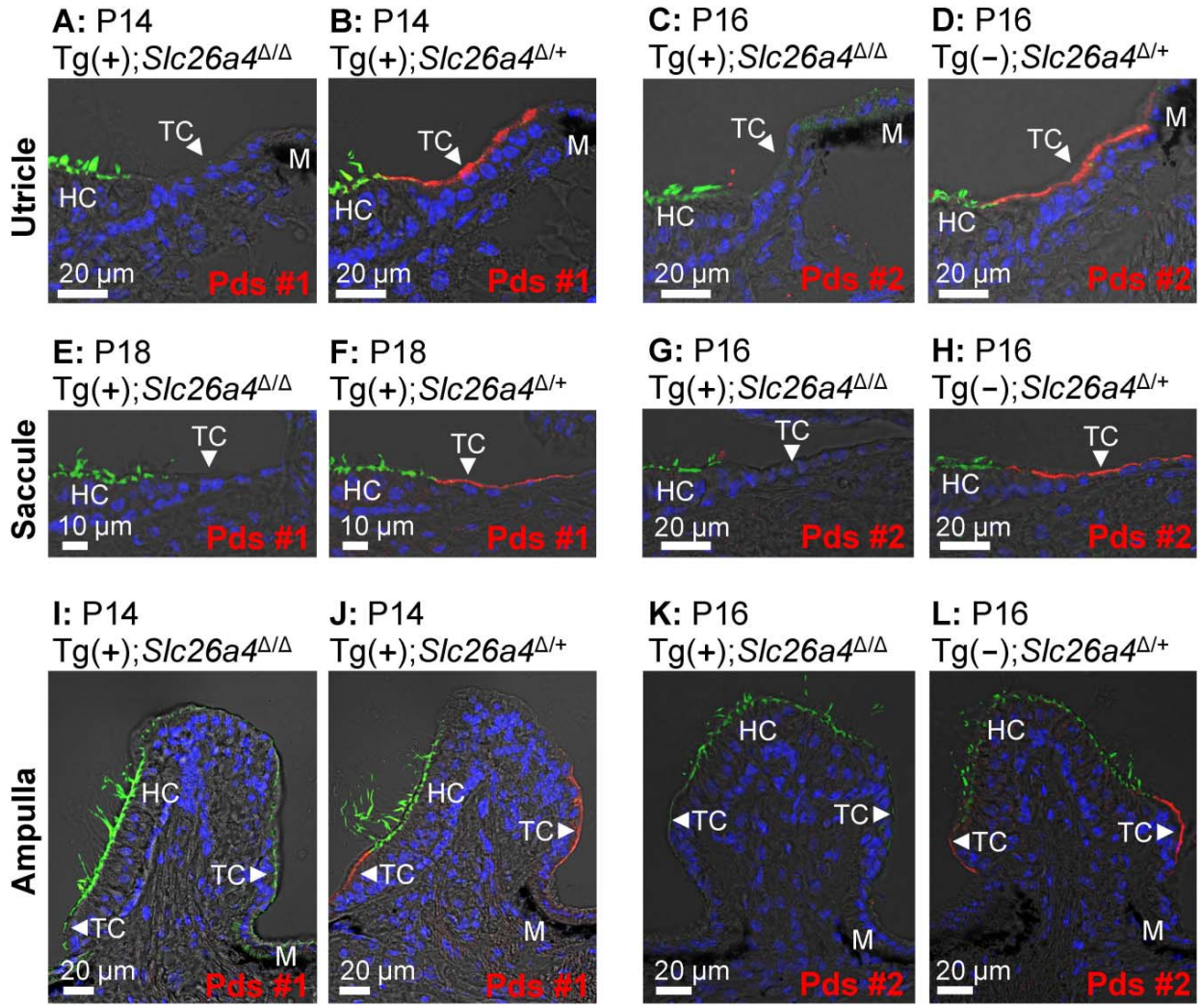

Figure 3.14 Histology and pendrin expression in the vestibular labyrinth.

Staining in all images consisted of immunocytochemistry of pendrin (Pds #1 antibody or Pds #2 antibody; red*) and F-actin (*green*) and of nucleic acids (*blue*). Images provide comparison of pendrin expression in Tg(+);*Slc26a4$^{\Delta/\Delta}$ *mice (**A,C,E,G,I,K**) to positive controls consisting of Tg(+);*Slc26a4$^{\Delta/+}$ *(**B, F, J**) or Tg(−);*Slc26a4$^{\Delta/+}$ *mice (**D,H,L**). Note that both antibodies, Pds #1 and Pds #2, failed to detect pendrin expression in Tg(+);*Slc26a4$^{\Delta/\Delta}$ *mice and that the staining pattern for pendrin in positive controls was similar for both antibodies and for both positive controls. The number of pairs of mice represented by these images are 2 for images **A** & **B**, 2 for images **C** & **D**, 1 for images **E** & **F**, 2 for images **G** & **H**, 2 for images **I** & **J**, and 2 for images **K** & **L**. HC, vestibular hair cells; TC, transitional cells; M, melanocytes. Compare these images to those in Figure 3.10 (Experiments conducted by XL)*

Methods

Ethics Statement

All animal experiments and procedures at Kansas State University were performed according to protocols approved by the Animal Care and Use Committees at Kansas State University (IACUC#: 2961). All animal procedures at Sorbonne University Paris Cité were performed according to protocols approved by the ethics committee from University Pierre et Marie Curie, and were performed in accordance with the Guide for the Care and Use of Laboratory Animals (NIH publication No.93-23, revised 1985).

Generation of Tg(B1-hPDS)$^{Tg/+}$;Slc26a4$^{+/+}$ transgenic mice

Human *SLC26A4* cDNA was ligated into a pBluescript vector that contained 6.9 kbp of the human *ATP6V1B1* promoter [149,152]. An SV40 late region polyadenylation signal was cloned downstream of the *SLC26A4* cDNA. The transgene Tg(*B1-hPDS*) included the 5'-flanking region of the *ATP6V1B1* gene extending to but excluding the endogenous translational start codon, the human *SLC26A4* cDNA, with its own translational start site, and the SV40 late region polyadenylation signal. The integrity of the transgene was confirmed by restriction digest and bidirectional sequencing of ligation sites. In preparation for injection, the transgene was linearized by SalI and NotI digestion, followed by gel purification using an electroelution method and then concentrated using ElutipD columns (Whatman). The transgene was then further

concentrated by ethanol precipitation and resuspended in low EDTA injection buffer (10 mM Tris with 0.1 mM EDTA). Tg(*B1-hPDS*) transgenic mice were created by the University of Utah transgenic mouse core facility using standard procedures [149,152]. Genotyping revealed that 63 pups were positive for transgene integration. One founder, which transmitted the transgene in a Mendelian fashion, was crossed with wild-type C57BL/6 x CBA F1 mice to establish a colony. Three Tg(*B1-hPDS*);*Slc26a4*$^{+/+}$ transgenic mice were shipped to Kansas State University in Manhattan, Kansas, USA.

Generation of Tg(B1-hPDS)$^{Tg/+}$;Slc26a4$^{\Delta/\Delta}$ transgenic mice

At Kansas State University, a colony of Tg*(B1-hPDS)*$^{Tg/+}$*;Slc26a4*$^{\Delta/\Delta}$ mice was established. Colony management was supported by software (Litter tracker, written in Microsoft Visual Basic and Excel 2010 by P.W.) Tg(*B1-hPDS*)$^{Tg/+}$;*Slc26a4*$^{+/+}$ mice were crossed with *Slc26a4*$^{\Delta/\Delta}$ mice to generate Tg(*B1-hPDS*)$^{Tg/+}$;*Slc26a4*$^{\Delta/+}$ mice. Matings of Tg(*B1-hPDS*)$^{Tg/+}$;*Slc26a4*$^{\Delta/+}$ mice generated 28 Tg(*B1-hPDS*)$^{Tg/+}$;*Slc26a4*$^{+/+}$, 58 Tg(*B1-hPDS*)$^{Tg/+}$;*Slc26a4*$^{\Delta/+}$ and 39 Tg(*B1-hPDS*)$^{Tg/+}$;*Slc26a4*$^{\Delta/\Delta}$ mice in a near Mendelian ratio of 1 : 2 : 1 with a 75% rate of transmission for the transgene (based on 169 pups).

Genotyping

Mice were genotyped for *Slc26a4*$^{+}$ and *Slc26a4*$^{\Delta}$ alleles by PCR using established primers [103] and for the transgene *Tg(B1-hPDS)* (Transnetyx, Cordova, TN). Primers for the transgene were designed to amplify a 345 bp PCR-product spanning the *hPDS* cDNA and the SV40 polyadenylation signal sequence (left primer: 5'-aga ggg tca agg ttc cat ttt ag-3'; right primer: 5'-caa acc aca act aga atg cag tg-3') [148].

Isolation of embryonic tissues

Time-pregnant dams were deeply anesthetized with 4% tri-bromo-ethanol (0.014 ml/g body weight, i.p.) and embryos were harvested by laparotomy. Dams and embryos were sacrificed by decapitation. Gestational age was counted from the day when the vaginal plug was detected. This day was set to embryonic (E) day 0.5. Gestational age,

however, was verified by evaluating gross morphological features including limbs, digits and the appearance of the pinna and auditory meatus [159,160].

Isolation of tissues from postnatal mice

The age of mice was counted from the day of birth, which was set to postnatal (P) day 0. Postnatal mice were deeply anesthetized with 4% tri-bromo-ethanol (0.014 ml/g body weight, i.p.) and sacrificed by decapitation or cardiac perfusion with fixative.

Quantitative RT-PCR

Quantitative RT-PCR was performed on total RNA [116]. Total RNA was isolated from tissues obtained by microdissection from Tg(-);*Slc26a4*$^{\Delta/+}$ and Tg(+);*Slc26a4*$^{\Delta/\Delta}$ mice and subjected to quantitative RT-PCR using gene-specific primers for 18S rRNA as well as for mRNA coding for the α-subunit of the mouse Na^+/K^+ ATPase *Atp1a1*, the B1-subunit of the mouse vH^+ ATPase *Atp6v1b1*, mouse pendrin *Slc26a4* and human pendrin *SLC26A4*, which was introduced via the transgene.

Postnatal mice were genotyped by PCR prior to tissue collection. Embryonic Tg(-);*Slc26a4*$^{\Delta/+}$ mice were generated by mating Tg(-);*Slc26a4*$^{\Delta/\Delta}$ dams and Tg(-);*Slc26a4*$^{+/+}$ sires, which yielded 100% of the desired genotype. Embryonic Tg(+);*Slc26a4*$^{\Delta/\Delta}$ mice were generated by mating Tg(+);*Slc26a4*$^{\Delta/\Delta}$ dams and sires, which yielded Tg(+);*Slc26a4*$^{\Delta/\Delta}$ and Tg(-);*Slc26a4*$^{\Delta/\Delta}$ mice in a ratio of 3 : 1. Since embryonic mice could not be genotyped prior to tissue collection, the desired Tg(+);*Slc26a4*$^{\Delta/\Delta}$ mice among Tg(-);*Slc26a4*$^{\Delta/\Delta}$ mice were initially identified by visual inspection of the size of the endolymphatic sac and the presence of 'glittering' otoconia, This phenotypic identification was subsequently confirmed by the presence of human pendrin *SLC26A4* transgene by RT-PCR.

Tissues were obtained by microdissection. Endolymphatic sacs (8-10 endolymphatic sacs from 4-5 animals per sample) were obtained from mice at age E17.5. Cochlear ducts (4 cochlear ducts from 2 animals per sample and 2 cochlear ducts from 1 animal per sample) were obtained from mice at ages E17.5 and P2, respectively. Vestibular

labyrinths (6 vestibular labyrinths from 3 animals per sample) were obtained from mice at age P8. Total RNA was isolated from microdissected tissues (RNeasy micro kit, Qiagen, Valencia, CA, USA), treated with DNAse (RNeasy micro kit), combined with RNA storage solution (Applied Biosystems/Ambion, Austin, TX), adjusted to a concentration of 10 ng/µl, and stored at -80 °C.

Quantity and quality of total RNA were evaluated by microfluidic electrophoresis (BioAnalyzer, Agilent, Santa Clara, CA), by microliter absorption photometry (Nanodrop, Wilmington, DE) and by quantitative RT-PCR of 18S rRNA. RNA samples were accepted for quantitative RT-PCR only when they were free of contamination and excellent RNA quality. RNA quality was quantified by the RNA integrity number (RIN) on a scale from 0 (worst) to 10 (best) (BioAnalyzer, Agilent). RIN numbers for total RNA isolated from E17.5 endolymphatic sac and cochlea were 8.2 ± 0.3 (n=3) and 9.2 ± 0.1 (n=10).

Chemicals were assembled with the assistance of an automatic pipetting station (Biomek NX^{p}, Beckman Coulter, Fullerton, CA) with hardware modifications and software programming by P.W. Quantitative RT-PCR reactions were carried out in 96-well plates with each well containing ~10 ng of total RNA, gene specific primers, and an enzyme mix containing reverse transcriptase and DNA polymerase (iScript, BioRad, Hercules, CA) in a total volume of 25 µl. Reverse transcription was performed for 10 min at 50°C and terminated by heating to 95°C for 5 min (OneStepPlus, Applied Biosystems, Foster City, CA). PCR consisted of 40 cycles of 10 s melting at 95°C, 30 s annealing and elongation at 58°C, and 15 s hot-measurement at 78°C (OneStepPlus, Applied Biosystems).

Left and right primers (exon, product size) were for 18S 5'-gag gtt cga aga cga tca ga-3' and 5'-tcg ctc cac caa cta aga ac-3' (316 bp), for *Atp1a1* 5'-tgc ccg cct caa cat tcc-3' (exon 14) and 5'-gac aca tca gag cca aca atc c-3' (exon 16, 291 bp), for *Atp6v1b1* 5'-tga ccc gaa act aca tca cc-3' (exon 1) and 5'-gcc aga gcc att gaa aat cc-3' (exon 5, 305 bp), for mouse *Slc26a4* 5'-tct gat gga ggc aga gat ga-3' (exon 20) and 5'-ggc cag cct aac aga gac ag-3' (exon 21, 430 bp), and for human *SLC26A4* were 5'-tcc caa agt gcc aat cca ta-3' and 5'-aca tca agt tct tct tcc gtc ag-3' (360 bp). Primer pairs for *Atp1a1*,

Atp6v1b1, mouse *Slc26a4* spanned introns to prevent amplification of genomic DNA. Primer pairs for mouse *Slc26a4* detected the *Slc26a4*$^{+}$ allele as well as the *Slc26a4*$^{\Delta}$ allele that is lacking exon 8 [103]. Left and right primers for mouse *Slc26a4* differed by 7 and 10 nucleotides from the corresponding human sequence and left and right primers for human *SLC26A4* differed in 4 and 6 nucleotides from the corresponding mouse sequence, thereby maximizing species-specific amplification. Since the human transgene did not contain introns, some reactions were carried out without reverse transcriptase to determine whether products of *SLC26A4* originated from cDNA rather than from genomic DNA. These experiments revealed no evidence for significant amplification of genomic DNA. Amplification of a single product of the appropriate size was verified by microfluidic electrophoresis (BioAnalyzer, Agilent).

The number of template molecules ($cDNA_{Template}$) was estimated according to

$$cDNA_{Template}[molecules] = \frac{6.02 \cdot 10^{23}[molecules] \cdot Product_{Threshold}[g] \cdot [mol] \cdot [bp]}{[mol] \cdot Product_{Size}[bp] \cdot Weight_{bp}[g] \cdot [mol] \cdot Efficiency \wedge C_t}$$

where 6.02 x 10^{23} molecules/mol represents Avogadro's number, $Product_{Threshold}$ is the weight of the PCR-product at threshold (0.49 x 10^{-9} g) that was obtained from calibration experiments, $Product_{Size}$ is the size of the product in base pairs (bp), $Weight_{bp}$ is average weight of one bp (660 g/mol), *Efficiency* is the PCR-efficiency obtained from the slope of the log-linear phase of the growth curve [134] and C_t is the cycle at which the fluorescence of the product molecules reaches a common threshold chosen in the middle of the log-linear part of the growth curve.

Paint-fill

Bisected heads of embryos age E15.5 were fixed overnight in Bodian's fixative, contained (vol/vol) 75% ethanol, 5% acetic acid, and 5% formalin in water. Heads were then dehydrated overnight in 100% ethanol and cleared in methyl-salicylate [161,162]. The membranous labyrinth was injected via the lateral wall of the basal turn of the cochlea and via the endolymphatic sac with diluted paint (Liquid Paper, Newell Rubbermaid, Atlanta, GA, 0.1-0.2% in methyl-salicylate) using a fine glass-electrode, a

manipulator (NM-151 Narishige) and a micrometer-driven oil-filled microinjector (CellTram Vario, Eppendorf, Hamburg, Germany). For each genotype, at least three inner ears were injected.

Direct fluorescence of eGFP

Whole mounts of fresh cochlear ducts, endolymphatic sacs and slices of kidney were prepared from E15.5 Tg(*B1-eGFP*) mice and visualized with a fluorescence microscope (AxioScope, Carl Zeiss Göttingen).

Western blotting

Crude membrane preparations of the inner ear: Soft tissues from 8 cochleae and 8 vestibular labyrinths devoid of endolymphatic sacs from adult mice were collected by microdissection in Cl^--free solution and pooled and homogenized in 500 µl Tris-sucrose buffer. Cl^--free solution contained (mM) 150 Na-gluconate, 1.6 K_2HPO_4, 0.4 KH_2PO_4, 4 Ca-gluconate$_2$, 1 $MgSO_4$ and 5 glucose, pH 7.4. Tris-sucrose buffer contained (mM) 250 sucrose, 50 Tris-HCl, 5 EDTA, pH=7.4, and proteinase inhibitor cocktail (Cat# PI-87786 Fisher, Pittsburgh, PA). Homogenization involved a pestle/1.5 ml Eppendorf vial and a Potter-Elvehjem tissue grinder (3 strokes at 1,250 rpm; Cat# K885512-0020, Fisher). Nuclei and debris were sedimented by centrifugation (6 min, 600g, 4°C, Micromax RF, International equipment, Needham Heights, MA) and the supernatant containing membranes was collected. Pellets were washed 3x with 100 µl Tris-sucrose buffer. Supernatants were pooled and membranes were pelleted by centrifugation (1 hr, 21,000g, 4°C, Micromax RF). Membranes were suspended in 30 µl Tris-sucrose buffer and protein content was quantified (BCA assay, Cat# 23227, Fisher; Absorption photometer, Nanodrop).

Crude membrane preparations of kidneys: Kidneys (~1 g wet weight) were sliced, frozen in liquid N_2, pulverized, transferred into 8 ml Tris-sucrose buffer and homogenized. Homogenization involved pestles fitting 1.5 ml Eppendorf vials and the Potter-Elvehjem tissue grinder (3 strokes at 1,250 rpm). Nuclei and debris were

sedimented by centrifugation (6 min, 600g, 4°C, Micromax RF) and the supernatant containing membranes was collected. Pellets were washed 3x with 2 ml Tris-sucrose buffer. Supernatants were pooled and membranes were pelleted by centrifugation (1 hr, 21,000g, 4°C, Micromax RF). Membranes were suspended in 200 µl Tris-sucrose buffer and protein content was quantified (BCA assay).

Gel-electrophoresis, blotting and protein detection: Crude membranes were solubilized, denatured and reduced for 1 hr at 37 °C in LDS sample buffer (Cat#: NP0007; Invitrogen) supplemented with 50 mM DTT. Proteins were resolved by gel-electrophoresis (4-12% Bis-Tris gels (Cat#: NP0326, Invitrogen) using a MOPS-SDS running buffer supplemented with an antioxidant (Cat#: NP0005, Invitrogen) and transferred onto PVDF membranes (BioRad, 3 hrs at 30V). PVDF membranes were blocked for 1 hr at RT in TBST solution containing 3% BSA. TBST solution contained 20 mM Tris-base, 68 mM NaCl, and 1% Tween-20. Blocked PVDF membranes were incubated overnight at 4 °C with primary antibody in TBST solution with 3% BSA. Primary antibodies were a rabbit anti-pendrin antibody (Pds #2; 1:200) and a polyclonal rabbit anti-mouse β-actin antibody (1: 1,000; Cat#: A2066, Sigma-Aldrich). Pds #2 was raised against the last 15 amino acids of the C-terminal of mouse pendrin [114]. Human pendrin differs in only 1 of these 15 amino acids. PVDF membranes were washed 5 x 3 min in TBST solution and then incubated for 1 hr at RT with the secondary antibody, goat anti-rabbit poly-HRP (Cat#: PI32260, Fisher) diluted in TBST solution with 3% BSA. The dilution of the secondary antibody was 1:2,500 for labeling the Pds #2 antibody and 1:10,000 for labeling the β-actin antibody. The membranes were washed 3 x 5 min in TBST solution. HRP was detected by chemiluminescence (SuperSignal Femto, Cat# PI34095, Fisher). The signal was integrated over 2-5 min by cooled CCD camera (ImageStation 4000R, Kodak).

Immunocytochemistry

Fixation: Isolated tissues from embryonic mice were fixed by submersion in PBS-formaldehyde solution at 4 °C. PBS-formaldehyde solution consisted of 4% formaldehyde (Electron Microscopy Sciences, Hatfield PA) in a solution that contained

(in mM) 137 NaCl, 2.7 KCl, 10.1 Na_2HPO_4, 1.8 KH_2PO_4. Tissues from postnatal animals were fixed by cardiac perfusion followed by perilymphatic perfusion. Cardiac perfusion was initiated with Cl^--free solution (6 ml, 1 min) and followed by Cl^--free solution with 4% formaldehyde (12 ml, 2 min). Perilymphatic perfusion consisted of an infusion of Cl^--free solution with 4% formaldehyde (25 µl, 5 min) through the round and oval window of the cochlea.

Cryosections. Fixed temporal bones were decalcified 18-24 h in 10% EDTA, processed through a sucrose gradient and infiltrated with polyethylene glycol. Mid-modiolar cryosections (12 µm, CM3050S, Leica, Nussloch, Germany) were blocked in PBS-TX (137 mM NaCl, 10.1 mM Na_2HPO_4, 1.8 mM KH_2PO_4, 2.7 mM KCl, pH 7.4 with 0.15% Triton X 100) and 5% bovine serum albumin. Slides were incubated overnight at 4 °C with primary antibody in PBS-TX with 2.5% BSA. Primary antibodies were two rabbit anti-pendrin antibodies (Pds #1; 1:200; a kind gift from Dr. Søren Nielsen, University of Aarhus, Denmark and Pds #2, 1:1,000) and a polyclonal FITC-conjugated goat anti-eGFP antibody (Cat#: GTX26662, GeneTex, San Antonio, TX). Pds #1 was raised against the last 22 amino acids of the C-terminal of mouse pendrin. Human pendrin differs in 6 of these 22 amino acids [102,163]. Slides were washed with PBS-TX and, where appropriate, incubated for 1 h at RT with secondary antibody (1:1,000, goat anti-rabbit Alexa 594, Invitrogen, Carlsbad, CA). After washing with PBS-TX, sections, where appropriate, were stained with phalloidin 488 (1:40; Invitrogen) to mark F-actin and DAPI (1:1,000; Invitrogen) to mark nuclei, washed again and cover-slipped with mounting medium (Vectashield HardSet Mounting Medium, Vector laboratories, Burlingame, CA).

Whole-mounted specimens. Tissues were obtained by microdissection from fixed temporal bones, washed in PBS-TX, and blocked with 5% bovine serum albumin in PBS-TX. Tissues were incubated overnight at 4 °C with primary antibodies in PBS-TX with 2.5% BSA. Primary antibodies were a rabbit anti-pendrin antibody (Pds #1; 1:200) or a polyclonal FITC-conjugated goat anti-eGFP antibody (GeneTex). Slides were washed with PBS-TX and, where appropriate, incubated for 1 h at RT with secondary antibody (1:1,000, goat anti-rabbit Alexa 594, Invitrogen). After washing with PBS-TX, tissues were stained with phalloidin 488 or phalloidin 594 (1:40; Invitrogen) and DAPI

(1:1000; Invitrogen), washed again and cover-slipped with mounting medium (VectaShield HardSet Mounting Medium, Vector laboratories, Burlingame, CA).

Confocal microscopy. Immunocytochemistry of cryosections and whole-mounted specimens were viewed by confocal microscopy (LSM 510 Meta, Carl Zeiss, Göttingen, Germany). Laser scanning bright-field images were collected to aid orientation.

Endocochlear potential and pH difference between endolymph and perilymph

Mice were anesthetized with 4% tri-bromo-ethanol for *in situ* measurements of the endocochlear potential and pH with double-barreled microelectrodes. Measurements were made in the basal turn of the cochlea by a round-window approach through the basilar membrane of the first turn of the cochlea [81,164]. The surgical cavity was covered with liquid Sylgard 184 (Dow Corning) to limit the loss of tissue CO_2 into ambient air.

Double-barreled glass microelectrodes were pulled (micropipette puller PD-5; Narishige) from filament-containing glass tubing (1B100F-4; World Precision Instruments) and baked at 180 ºC for 2 h to ensure dryness. One barrel was silanized by a 30 s exposure to 0.008 ml dimethyldichlorosilane (40136; Fluka). After silanization, microelectrodes were baked again at 180 ºC for 3 h and tips were broken to a final O.D. of ~3 µm. The reference barrel was filled with 150 mM KCl and the ion-selective barrel was filled at the tip with liquid ion exchanger (Hydrogen ionophore II - Cocktail A, 95297; Fluka) and back-filled with buffer solution (500 mM KCl, 20 mM HEPES, pH 7.4).

Each barrel of the double-barreled microelectrode was connected via a $Ag/AgCl_2$ electrode to an electrometer (FD223, World Precision Instruments). A flowing KCl electrode (1 M KCl in 0.2% agar) was inserted under the skin of the animal to serve as ground electrode. Data were recorded in analog (BD12E Flatbed recorder, Kipp & Zonen, Delft, The Netherlands) and digital form (DIGIDATA 1322A and AxoScope 10, Axon Instruments, Union City, CA). pH electrodes were calibrated *in situ* at 37 ºC using three calibration solutions with different pH values. Calibration solutions contained (in

mM): pH 6: 130 NaCl, 20 MES; pH 7: 130 NaCl, 20 HEPES; and pH 8: 130 NaCl, 20 HEPES. pH-sensitive electrodes had a slope of 56.9 ± 0.3 mV/pH unit (n=11).

Hearing tests

Mice were deeply anesthetized with a mixture of medetomidine and xylazine (0.375 mg/Kg body weight medetomidine and 56 mg/kg body weight xylazine; i.p.) and placed on a thermal pad to maintain normal body temperature. The mastoid, vertex and ventral neck region of the animal were connected via sub-dermal platinum needle electrodes (F-E2, Astro Med, Rhode Island, RI) and short (31 cm) leads to the main channel, reference channel and ground of the preamplifier, respectively. Auditory brainstem recordings were performed in a custom constructed, electrically shielded and sound-attenuated chamber (inner dimensions: 23 cm x 23 cm x 23 cm) using a digital data acquisition system (BioSig32 software, RA4LI Preamplifier, RP2.1 Enhanced Real Time Processor, PA5 Programmable Attenuator, ED1 Electrostatic Speaker Driver, Tucker-Davis Technologies, Alachua, FL). Tone burst stimuli were presented (21 per sec) via a free field electrostatic speaker (SigGen software, ES1 speaker, Tucker Davis). Acoustic stimuli were calibrated using a 1/4 inch condenser microphone (SigCal IRP4.2 software, Tucker Davis, PS9200 microphone, Acoustical Interface, Belmont, CA) placed at the location of the mouse head. Tone bursts (2 ms duration, 0.5 ms gate time; 8, 16 and 32 kHz) were presented with alternating phase (0 and 180°). Responses, recorded over 10 ms, were filtered (300 Hz high pass, 3000 Hz low pass and 60 Hz notch) and 1000 recordings were averaged. Tone burst stimuli were presented at intensities varying between 90 and 0 dB SPL in 5 dB intervals. Auditory thresholds were obtained by a visual comparison of wave forms. After the procedure, mice were rapidly recovered from anesthesia with atipamizole (1.875 mg/kg body weight; i.p.).

Balance tests

Balance testing consisted of determining the time that mice could balance on a rotating 1” rod with rotations ramping up from 4 to 40 rpm in 60 s (RotaRod, IITC Life Science,

Woodland Hills, CA). Test chambers were cushioned with bubble-foil to provide a soft landing for mice falling off the rod.

Acknowledgments

We thank Dr. Thomas B. Friedman (Section on Human Genetics, NIDCD, Rockville, MD) and Dr. Steven Raft (Section on Sensory Cell Regeneration & Development, NIDCD, Rockville, MD) for critically reading the manuscript, Dr. Søren Nielsen (University of Aarhus, Denmark) for the gift of a rabbit anti-pendrin antibody, and Mr. James Dille (Comparative Medicine Group, Kansas State University) for excellent mouse care.

Funding

This work was supported by a grant from the National Institutes on Deafness and Other Communication Disorders, NIH-R01-DC012151 (to P.W.), a KINBRE grant (to P.W.) that in turn was funded by grants from the National Center for Research Resources (P20 RR016475) and the National Institute of General Medical Sciences (P20 GM103418), by a grant HYPERCLO BLANC 2010-R10164DD from l'Agence Nationale de la Recherche (to D.E.), by an INSERM grant “subvention de recherche" from the association pour l’information et la recherche sur les maladies rénales génétiques (AIRG) 2011 (to D.E.), by a grant Subvention de Recherche 2012 from the Société Française d'Hypertension (SFHTA) (to D.E.), and by a grant "RENPAR" ANR BLANC 2012-BSV1-0017 from l'Agence Nationale de la Recherche (to R.C. and D.E.), and by NIH intramural research fund DC-000060-10 (to A.J.G.). The Confocal Microscopy Core facility at Kansas State University was supported by Kansas State University – College of Veterinary Medicine and a grant from the National Institutes of Health, NIH-P20-RR017686 (to D.C.M.). The funders had no role in study design, data collection and analysis, decision to publish, or preparation of the manuscript.

Perspective

To summarize the present study, we demonstrated that during the phase of cochlear growth and enlargement, the endolymph in cochlea and endolymphatic sac of *Slc26a4*$^{\Delta/+}$ and *Slc26a4*$^{\Delta/\Delta}$ mice is a NaCl-rich fluid that is subsequently modified into KCl-rich fluid shortly before birth. The transition of ion composition from a NaCl-rich to a KCl-rich fluid likely results from transport by $Na^+/2Cl^-/K^+$ cotransporter, SLC12A2, and the K^+ channels, KCNQ1/E1. These observations suggest that expansion of the endolymph volume stems from the failure to reabsorb NaCl. Information gathered from our work on the mouse model expressing human pendrin specifically in the endolymphatic sac lead us to conclude that pendrin expression in endolymphatic sac is predominantly responsible for the development of a normal endolymphatic volume, as well as normal hearing and balance.

The present findings raise more intriguing questions for future investigations: 1) What are the apparatuses and transporters responsible for fluid secretion and absorption? What is the mechanism for ion transport, such as Na^+ and Cl^-, in the mitochondria-rich cells and the principal cells of endolymphatic sac? Answering these questions will help identify potential pharmacological targets that could be manipulated to correct fluid transport, and subsequently prevent endolymph volume expansion. 2) What is the physiological role of pendrin in the cochlea and the vestibular labyrinth? Does the lack of, or insufficient expression of pendrin in the cochlea increase the susceptibility for stress-induced hearing impairment? What is the compensatory mechanism for maintaining the acid-base status in the adult cochlear endolymph, when pendrin function is absent? Answering these questions would provide insights into the observed disease progression as well as provide potential treatments for EVA - related patients, who have fluctuated and progressive hearing loss in the adulthood.

References

1. Wain HM, Bruford EA, Lovering RC, Lush MJ, Wright MW, Povey S (2002) Guidelines for human gene nomenclature. Genomics 79: 464-470.

2. Chittka L, Brockmann A (2005) Perception space--the final frontier. PLoS Biol 3: e137.

3. Kim HM, Wangemann P (2010) Failure of fluid absorption in the endolymphatic sac initiates cochlear enlargement that leads to deafness in mice lacking pendrin expression. PLoS One 5: e14041.

4. Marcus DC, Wangemann P (2012) Acoustic Transduction. In: Sperelakis N, editors. Cell Physiolgy Sourcebook Essentials of Membrane Biophysics. Amsterdam: Elsevier. pp. 649-668.

5. Kimura RS (1967) Experimental blockage of the endolymphatic duct and sac and its effect on the inner ear of the guinea pig. A study on endolymphatic hydrops. Ann Otol Rhinol Laryngol 76: 664-687.

6. Wangemann P (2006) Supporting sensory transduction: cochlear fluid homeostasis and the endocochlear potential. J Physiol 576: 11-21.

7. Wangemann P (2011) The role of pendrin in the development of the murine inner ear. Cell Physiol Biochem 28: 527-534.

8. Kelley, Matthew W., Wu, Doris. K., and Fay, Richard. R. (2005) Development of the Inner Ear. New York City: Springer.

9. Morsli H, Choo D, Ryan A, Johnson R, Wu DK (1998) Development of the mouse inner ear and origin of its sensory organs. J Neurosci 18: 3327-3335.

10. Mansour LS, Schoenwolf GC (2005) Morphogenesis of the Inner Ear. In: Kelley MW, Wu DK, Popper AN, Fay RR, editors. Development of the Inner Ear. New York City: Springer Publishing. pp. 43-84.

11. Cantos R, Cole LK, Acampora D, Simeone A, Wu DK (2000) Patterning of the mammalian cochlea. Proc Natl Acad Sci U S A 97: 11707-11713.

12. Boron, Walter F and Boulpaep, Emile L. (2011) Medical Physiology. Philadelphia: Saunders.

13. Hudspeth AJ (1989) How the ear's works work. Nature 341: 397-404.

14. Lim DJ (1980) Cochlear anatomy related to cochlear micromechanics. A review. J Acoust Soc Am 67: 1686-1695.

15. Colclasure JC, Holt JR (2003) Transduction and adaptation in sensory hair cells of the mammalian vestibular system. Gravit Space Biol Bull 16: 61-70.

16. Marcus DC, Wangemann P (2010) Cochlear and Vestibular Function and Dysfunction. In: F.Javier Alvarez-Leefmans, Eric Delpire, editors. Physiology and Pathology of Chloride Transporters and Channels in the Nervous System from Molecules to Diseases. Amsterdam: Elsevier. pp. 425-437.

17. Schwander M, Kachar B, Muller U (2010) Review series: The cell biology of hearing. J Cell Biol 190: 9-20.

18. Corey DP (2006) What is the hair cell transduction channel? J Physiol 576: 23-28.

19. Hudspeth AJ, Corey DP (1977) Sensitivity, polarity, and conductance change in the response of vertebrate hair cells to controlled mechanical stimuli. Proc Natl Acad Sci U S A 74: 2407-2411.

20. Holt JR, Corey DP (2000) Two mechanisms for transducer adaptation in vertebrate hair cells. Proc Natl Acad Sci U S A 97: 11730-11735.

21. Wangemann P (1995) Comparison of ion transport mechanisms between vestibular dark cells and strial marginal cells. Hear Res 90: 149-157.

22. Wangemann P (2002) K+ cycling and the endocochlear potential. Hear Res 165: 1-9.

23. Wangemann P, Liu J, Marcus DC (1995) Ion transport mechanisms responsible for K+ secretion and the transepithelial voltage across marginal cells of stria vascularis in vitro. Hear Res 84: 19-29.

24. Zdebik AA, Wangemann P, Jentsch TJ (2009) Potassium ion movement in the inner ear: insights from genetic disease and mouse models. Physiology (Bethesda) 24: 307-316.

25. Marcus DC, Chiba T (1999) K+ and Na+ absorption by outer sulcus epithelial cells. Hear Res 134: 48-56.

26. Chiba T, Marcus DC (2000) Nonselective cation and BK channels in apical membrane of outer sulcus epithelial cells. J Membr Biol 174: 167-179.

27. Von Bekesy G (1952) Resting potentials inside the cochlear partition of the guinea pig. Nature 169: 241-242.

28. Tasaki I, Spyropoulos C (1959) Stria vascularis as source of endocochlear potential. J Neurophysiol 22: 149-155.

29. Marcus DC, Wu T, Wangemann P, Kofuji P (2002) KCNJ10 (Kir4.1) potassium channel knockout abolishes endocochlear potential. Am J Physiol Cell Physiol 282: C403-C407.

30. Ito T, Choi BY, King KA, Zalewski CK, Muskett J, Chattaraj P, Shawker T, Reynolds JC, Butman JA, Brewer CC, Wangemann P, Alper SL, Griffith AJ (2011) SLC26A4 genotypes and phenotypes associated with enlargement of the vestibular aqueduct. Cell Physiol Biochem 28: 545-552.

31. Griffith AJ, Wangemann P (2011) Hearing loss associated with enlargement of the vestibular aqueduct: mechanistic insights from clinical phenotypes, genotypes, and mouse models. Hear Res 281: 11-17.

32. Pendred V (1896) DEAF-MUTISM AND GOITRE. The Lancet 148: 532.

33. Everett LA, Glaser B, Beck JC, Idol JR, Buchs A, Heyman M, Adawi F, Hazani E, Nassir E, Baxevanis AD, Sheffield VC, Green ED (1997) Pendred syndrome is caused by mutations in a putative sulphate transporter gene (PDS). Nat Genet 17: 411-422.

34. Li XC, Everett LA, Lalwani AK, Desmukh D, Friedman TB, Green ED, Wilcox ER (1998) A mutation in PDS causes non-syndromic recessive deafness. Nat Genet 18: 215-217.

35. Usami S, Abe S, Weston MD, Shinkawa H, Van Camp G, Kimberling WJ (1999) Non-syndromic hearing loss associated with enlarged vestibular aqueduct is caused by PDS mutations. Hum Genet 104: 188-192.

36. King KA, Choi BY, Zalewski C, Madeo AC, Manichaikul A, Pryor SP, Ferruggiaro A, Eisenman D, Kim HJ, Niparko J, Thomsen J, Butman JA, Griffith AJ, Brewer CC (2010) SLC26A4 genotype, but not cochlear radiologic structure, is correlated with hearing loss in ears with an enlarged vestibular aqueduct. Laryngoscope 120: 384-389.

37. Azaiez H, Yang T, Prasad S, Sorensen JL, Nishimura CJ, Kimberling WJ, Smith RJ (2007) Genotype-phenotype correlations for SLC26A4-related deafness. Hum Genet 122: 451-457.

38. Prasad S, Kolln KA, Cucci RA, Trembath RC, Van Camp G, Smith RJ (2004) Pendred syndrome and DFNB4-mutation screening of SLC26A4 by denaturing high-performance liquid chromatography and the identification of eleven novel mutations. Am J Med Genet A 124A: 1-9.

39. Yang T, Vidarsson H, Rodrigo-Blomqvist S, Rosengren SS, Enerback S, Smith RJ (2007) Transcriptional control of SLC26A4 is involved in Pendred syndrome and nonsyndromic enlargement of vestibular aqueduct (DFNB4). Am J Hum Genet 80: 1055-1063.

40. Yang T, Gurrola JG, Wu H, Chiu SM, Wangemann P, Snyder PM, Smith RJ (2009) Mutations of KCNJ10 together with mutations of SLC26A4 cause digenic nonsyndromic hearing loss associated with enlarged vestibular aqueduct syndrome. Am J Hum Genet 84: 651-657.

41. Landa P, Differ AM, Rajput K, Jenkins L, Bitner-Glindzicz M (2013) Lack of significant association between mutations of KCNJ10 or FOXI1 and SLC26A4 mutations in pendred syndrome/enlarged vestibular aqueducts. BMC Med Genet 14: 85.

42. Chen K, Wang X, Sun L, Jiang H (2012) Screening of SLC26A4, FOXI1, KCNJ10, and GJB2 in bilateral deafness patients with inner ear malformation. Otolaryngol Head Neck Surg 146: 972-978.

43. Stover EH, Borthwick KJ, Bavalia C, Eady N, Fritz DM, Rungroj N, Giersch AB, Morton CC, Axon PR, Akil I, Al Sabban EA, Baguley DM, Bianca S, Bakkaloglu A, Bircan Z, Chauveau D, Clermont MJ, Guala A, Hulton SA, Kroes H, Li VG, Mir S, Mocan H, Nayir A, Ozen S, Rodriguez SJ, Sanjad SA, Tasic V, Taylor CM, Topaloglu R, Smith AN, Karet FE (2002) Novel ATP6V1B1 and ATP6V0A4 mutations in autosomal recessive distal renal tubular acidosis with new evidence for hearing loss. J Med Genet 39: 796-803.

44. Karet FE, Finberg KE, Nelson RD, Nayir A, Mocan H, Sanjad SA, Rodriguez-Soriano J, Santos F, Cremers CW, Di Pietro A, Hoffbrand BI, Winiarski J, Bakkaloglu A, Ozen S, Dusunsel R, Goodyer P, Hulton SA, Wu DK, Skvorak AB, Morton CC, Cunningham MJ, Jha V, Lifton RP (1999) Mutations in the gene encoding B1 subunit of H+-ATPase cause renal tubular acidosis with sensorineural deafness. Nat Genet 21: 84-90.

45. Nikki R, Martin B, Gus O, Mato N, Elena T, Paul G (2012) Endolymphatic sac enlargement in a girl with a novel mutation for distal renal tubular acidosis and severe deafness. Case Rep Pediatr 2012: 605053.

46. Joshua B, Kaplan DM, Raveh E, Lotan D, Anikster Y (2008) Audiometric and imaging characteristics of distal renal tubular acidosis and deafness. J Laryngol Otol 122: 193-198.

47. Vargas-Poussou R, Houillier P, Le Pottier N, Strompf L, Loirat C, Baudouin V, Macher MA, Dechaux M, Ulinski T, Nobili F, Eckart P, Novo R, Cailliez M, Salomon R, Nivet H, Cochat P, Tack I, Fargeot A, Bouissou F, Kesler GR, Lorotte S, Godefroid N, Layet V, Morin G, Jeunemaitre X, Blanchard A (2006) Genetic investigation of autosomal recessive distal renal tubular acidosis: evidence for early sensorineural hearing loss associated with mutations in the ATP6V0A4 gene. J Am Soc Nephrol 17: 1437-1443.

48. Dou H, Finberg K, Cardell EL, Lifton R, Choo D (2003) Mice lacking the B1 subunit of H+ -ATPase have normal hearing. Hear Res 180: 76-84.

49. Paunescu TG, Russo LM, Da Silva N, Kovacikova J, Mohebbi N, Van Hoek AN, McKee M, Wagner CA, Breton S, Brown D (2007) Compensatory membrane expression of the V-ATPase B2 subunit isoform in renal medullary intercalated cells of B1-deficient mice. Am J Physiol Renal Physiol 293: F1915-F1926.

50. Norgett EE, Golder ZJ, Lorente-Canovas B, Ingham N, Steel KP, Frankl FE (2012) Atp6v0a4 knockout mouse is a model of distal renal tubular acidosis with hearing loss, with additional extrarenal phenotype. Proc Natl Acad Sci U S A 109: 13775-13780.

51. Lorente-Canovas B, Ingham N, Norgett EE, Golder ZJ, Karet Frankl FE, Steel KP (2013) Mice deficient in H+-ATPase a4 subunit have severe hearing impairment associated with enlarged endolymphatic compartments within the inner ear. Dis Model Mech 6: 434-442.

52. Hennings JC, Picard N, Huebner AK, Stauber T, Maier H, Brown D, Jentsch TJ, Vargas-Poussou R, Eladari D, Hubner CA (2012) A mouse model for distal renal tubular acidosis reveals a previously unrecognized role of the V-ATPase a4 subunit in the proximal tubule. EMBO Mol Med 4: 1057-1071.

53. Dorwart MR, Shcheynikov N, Yang D, Muallem S (2008) The solute carrier 26 family of proteins in epithelial ion transport. Physiology (Bethesda) 23: 104-114.

54. Gillam MP, Sidhaye AR, Lee EJ, Rutishauser J, Stephan CW, Kopp P (2004) Functional characterization of pendrin in a polarized cell system. Evidence for pendrin-mediated apical iodide efflux. J Biol Chem 279: 13004-13010.

55. Ko SB, Shcheynikov N, Choi JY, Luo X, Ishibashi K, Thomas PJ, Kim JY, Kim KH, Lee MG, Naruse S, Muallem S (2002) A molecular mechanism for aberrant CFTR-dependent HCO(3)(-) transport in cystic fibrosis. EMBO J 21: 5662-5672.

56. Garnett JP, Hickman E, Burrows R, Hegyi P, Tiszlavicz L, Cuthbert AW, Fong P, Gray MA (2011) Novel role for pendrin in orchestrating bicarbonate secretion in cystic fibrosis transmembrane conductance regulator (CFTR)-expressing airway serous cells. J Biol Chem 286: 41069-41082.

57. Bizhanova A, Chew TL, Khuon S, Kopp P (2011) Analysis of cellular localization and function of carboxy-terminal mutants of pendrin. Cell Physiol Biochem 28: 423-434.

58. Azroyan A, Morla L, Crambert G, Laghmani K, Ramakrishnan S, Edwards A, Doucet A (2012) Regulation of pendrin by cAMP: possible involvement in beta-adrenergic-dependent NaCl retention. Am J Physiol Renal Physiol 302: F1180-F1187.

59. Azroyan A, Laghmani K, Crambert G, Mordasini D, Doucet A, Edwards A (2011) Regulation of pendrin by pH: dependence on glycosylation. Biochem J 434: 61-72.

60. Dossena S, Maccagni A, Vezzoli V, Bazzini C, Garavaglia ML, Meyer G, Furst J, Ritter M, Fugazzola L, Persani L, Zorowka P, Storelli C, Beck-Peccoz P, Botta G, Paulmichl M (2005) The expression of wild-type pendrin (SLC26A4) in human embryonic kidney (HEK 293 Phoenix) cells leads to the activation of cationic currents. Eur J Endocrinol 153: 693-699.

61. Shcheynikov N, Yang D, Wang Y, Zeng W, Karniski LP, So I, Wall SM, Muallem S (2008) The Slc26a4 transporter functions as an electroneutral Cl-/I-/HCO3- exchanger: role of Slc26a4 and Slc26a6 in I- and HCO3- secretion and in regulation of CFTR in the parotid duct. J Physiol 586: 3813-3824.

62. Bogazzi F, Bartalena L, Raggi F, Ultimieri F, Martino E (2000) Pendrin does not increase sulfate uptake in mammalian COS-7 cells. J Endocrinol Invest 23: 170-172.

63. Scott DA, Wang R, Kreman TM, Sheffield VC, Karniski LP (1999) The Pendred syndrome gene encodes a chloride-iodide transport protein. Nat Genet 21: 440-443.

64. Rozenfeld J, Efrati E, Adler L, Tal O, Carrithers SL, Alper SL, Zelikovic I (2011) Transcriptional regulation of the pendrin gene. Cell Physiol Biochem 28: 385-396.

65. Soleimani M, Greeley T, Petrovic S, Wang Z, Amlal H, Kopp P, Burnham CE (2001) Pendrin: an apical Cl-/OH-/HCO3- exchanger in the kidney cortex. Am J Physiol Renal Physiol 280: F356-F364.

66. Royaux IE, Wall SM, Karniski LP, Everett LA, Suzuki K, Knepper MA, Green ED (2001) Pendrin, encoded by the Pendred syndrome gene, resides in the apical region of renal intercalated cells and mediates bicarbonate secretion. Proc Natl Acad Sci U S A 98: 4221-4226.

67. Yoshida A, Taniguchi S, Hisatome I, Royaux IE, Green ED, Kohn LD, Suzuki K (2002) Pendrin is an iodide-specific apical porter responsible for iodide efflux from thyroid cells. J Clin Endocrinol Metab 87: 3356-3361.

68. Pesce L, Bizhanova A, Caraballo JC, Westphal W, Butti ML, Comellas A, Kopp P (2012) TSH regulates pendrin membrane abundance and enhances iodide efflux in thyroid cells. Endocrinology 153: 512-521.

69. Royaux IE, Suzuki K, Mori A, Katoh R, Everett LA, Kohn LD, Green ED (2000) Pendrin, the protein encoded by the Pendred syndrome gene (PDS), is an apical porter of iodide in the thyroid and is regulated by thyroglobulin in FRTL-5 cells. Endocrinology 141: 839-845.

70. Shcheynikov N, Yang D, Wang Y, Zeng W, Karniski LP, So I, Wall SM, Muallem S (2008) The Slc26a4 transporter functions as an electroneutral Cl-/I-/HCO3- exchanger: role of Slc26a4 and Slc26a6 in I- and HCO3- secretion and in regulation of CFTR in the parotid duct. J Physiol 586: 3813-3824.

71. Pedemonte N, Caci E, Sondo E, Caputo A, Rhoden K, Pfeffer U, Di Candia M, Bandettini R, Ravazzolo R, Zegarra-Moran O, Galietta LJ (2007) Thiocyanate transport in resting and IL-4-stimulated human bronchial epithelial cells: role of pendrin and anion channels. J Immunol 178: 5144-5153.

72. Verlander JW, Hassell KA, Royaux IE, Glapion DM, Wang ME, Everett LA, Green ED, Wall SM (2003) Deoxycorticosterone upregulates PDS (Slc26a4) in mouse kidney: role of pendrin in mineralocorticoid-induced hypertension. Hypertension 42: 356-362.

73. Rossier BC, Staub O, Hummler E (2013) Genetic dissection of sodium and potassium transport along the aldosterone-sensitive distal nephron: importance in the control of blood pressure and hypertension. FEBS Lett 587: 1929-1941.

74. Rozenfeld J, Tal O, Kladnitsky O, Adler L, Efrati E, Carrithers SL, Alper SL, Zelikovic I (2012) The pendrin anion exchanger gene is transcriptionally regulated by uroguanylin: a novel enterorenal link. Am J Physiol Renal Physiol 302: F614-F624.

75. Forte LR, Fan X, Hamra FK (1996) Salt and water homeostasis: uroguanylin is a circulating peptide hormone with natriuretic activity. Am J Kidney Dis 28: 296-304.

76. Adler L, Efrati E, Zelikovic I (2008) Molecular mechanisms of epithelial cell-specific expression and regulation of the human anion exchanger (pendrin) gene. Am J Physiol Cell Physiol 294: C1261-C1276.

77. Frische S, Kwon TH, Frokiaer J, Madsen KM, Nielsen S (2003) Regulated expression of pendrin in rat kidney in response to chronic NH4Cl or NaHCO3 loading. Am J Physiol Renal Physiol 284: F584-F593.

78. Alesutan I, Daryadel A, Mohebbi N, Pelzl L, Leibrock C, Voelkl J, Bourgeois S, Dossena S, Nofziger C, Paulmichl M, Wagner CA, Lang F (2011) Impact of bicarbonate, ammonium chloride, and acetazolamide on hepatic and renal SLC26A4 expression. Cell Physiol Biochem 28: 553-558.

79. Haussinger D (1997) Liver regulation of acid-base balance. Miner Electrolyte Metab 23: 249-252.

80. Karim Z, Attmane-Elakeb A, Bichara M (2002) Renal handling of NH4+ in relation to the control of acid-base balance by the kidney. J Nephrol 15 Suppl 5: S128-S134.

81. Wangemann P, Nakaya K, Wu T, Maganti RJ, Itza EM, Sanneman JD, Harbidge DG, Billings S, Marcus DC (2007) Loss of cochlear HCO3- secretion causes deafness via endolymphatic acidification and inhibition of Ca2+ reabsorption in a Pendred syndrome mouse model. Am J Physiol Renal Physiol 292: F1345-F1353.

82. Nofziger C, Dossena S, Suzuki S, Izuhara K, Paulmichl M (2011) Pendrin function in airway epithelia. Cell Physiol Biochem 28: 571-578.

83. Galietta LJ, Pagesy P, Folli C, Caci E, Romio L, Costes B, Nicolis E, Cabrini G, Goossens M, Ravazzolo R, Zegarra-Moran O (2002) IL-4 is a potent modulator of ion transport in the human bronchial epithelium in vitro. J Immunol 168: 839-845.

84. Nakagami Y, Favoreto S Jr, Zhen G, Park SW, Nguyenvu LT, Kuperman DA, Dolganov GM, Huang X, Boushey HA, Avila PC, Erle DJ (2008) The epithelial anion transporter pendrin is induced by allergy and rhinovirus infection, regulates airway surface liquid, and increases airway reactivity and inflammation in an asthma model. J Immunol 181: 2203-2210.

85. Nakao I, Kanaji S, Ohta S, Matsushita H, Arima K, Yuyama N, Yamaya M, Nakayama K, Kubo H, Watanabe M, Sagara H, Sugiyama K, Tanaka H, Toda S, Hayashi H, Inoue H, Hoshino T, Shiraki A, Inoue M, Suzuki K, Aizawa H, Okinami S, Nagai H, Hasegawa M, Fukuda T, Green ED, Izuhara K (2008) Identification of pendrin as a common mediator for mucus production in bronchial asthma and chronic obstructive pulmonary disease. J Immunol 180: 6262-6269.

86. Larsson C, Hellqvist M, Pierrou S, White I, Enerback S, Carlsson P (1995) Chromosomal localization of six human forkhead genes, freac-1 (FKHL5), -3 (FKHL7), -4 (FKHL8), -5 (FKHL9), -6 (FKHL10), and -8 (FKHL12). Genomics 30: 464-469.

87. Hulander M, Wurst W, Carlsson P, Enerback S (1998) The winged helix transcription factor Fkh10 is required for normal development of the inner ear. Nat Genet 20: 374-376.

88. Blomqvist SR, Vidarsson H, Soder O, Enerback S (2006) Epididymal expression of the forkhead transcription factor Foxi1 is required for male fertility. EMBO J 25: 4131-4141.

89. Blomqvist SR, Vidarsson H, Fitzgerald S, Johansson BR, Ollerstam A, Brown R, Persson AE, Bergstrom GG, Enerback S (2004) Distal renal tubular acidosis in mice that lack the forkhead transcription factor Foxi1. J Clin Invest 113: 1560-1570.

90. Vidarsson H, Westergren R, Heglind M, Blomqvist SR, Breton S, Enerback S (2009) The forkhead transcription factor Foxi1 is a master regulator of vacuolar H-ATPase proton pump subunits in the inner ear, kidney and epididymis. PLoS One 4: e4471.

91. Dentice M, Luongo C, Elefante A, Ambrosio R, Salzano S, Zannini M, Nitsch R, Di Lauro R, Rossi G, Fenzi G, Salvatore D (2005) Pendrin is a novel in vivo downstream target gene of the TTF-1/Nkx-2.1 homeodomain transcription factor in differentiated thyroid cells. Mol Cell Biol 25: 10171-10182.

92. Carre A, Szinnai G, Castanet M, Sura-Trueba S, Tron E, Broutin-L'Hermite I, Barat P, Goizet C, Lacombe D, Moutard ML, Raybaud C, Raynaud-Ravni C, Romana S, Ythier H, Leger J, Polak M (2009) Five new TTF1/NKX2.1 mutations in brain-lung-thyroid syndrome: rescue by PAX8 synergism in one case. Hum Mol Genet 18: 2266-2276.

93. Civitareale D, Castelli MP, Falasca P, Saiardi A (1993) Thyroid transcription factor 1 activates the promoter of the thyrotropin receptor gene. Mol Endocrinol 7: 1589-1595.

94. Kawaguchi A, Ikeda M, Endo T, Kogai T, Miyazaki A, Onaya T (1997) Transforming growth factor-beta1 suppresses thyrotropin-induced Na+/I- symporter messenger RNA and protein levels in FRTL-5 rat thyroid cells. Thyroid 7: 789-794.

95. Kikkawa F, Gonzalez FJ, Kimura S (1990) Characterization of a thyroid-specific enhancer located 5.5 kilobase pairs upstream of the human thyroid peroxidase gene. Mol Cell Biol 10: 6216-6224.

96. Civitareale D, Lonigro R, Sinclair AJ, Di Lauro R (1989) A thyroid-specific nuclear protein essential for tissue-specific expression of the thyroglobulin promoter. EMBO J 8: 2537-2542.

97. Gray MA (2004) Bicarbonate secretion: it takes two to tango. Nat Cell Biol 6: 292-294.

98. Ko SB, Zeng W, Dorwart MR, Luo X, Kim KH, Millen L, Goto H, Naruse S, Soyombo A, Thomas PJ, Muallem S (2004) Gating of CFTR by the STAS domain of SLC26 transporters. Nat Cell Biol 6: 343-350.

99. Suzuki K, Royaux IE, Everett LA, Mori-Aoki A, Suzuki S, Nakamura K, Sakai T, Katoh R, Toda S, Green ED, Kohn LD (2002) Expression of PDS/Pds, the Pendred syndrome gene, in endometrium. J Clin Endocrinol Metab 87: 938.

100. Everett LA, Morsli H, Wu DK, Green ED (1999) Expression pattern of the mouse ortholog of the Pendred's syndrome gene (Pds) suggests a key role for pendrin in the inner ear. Proc Natl Acad Sci U S A 96: 9727-9732.

101. Wangemann P, Itza EM, Albrecht B, Wu T, Jabba SV, Maganti RJ, Lee JH, Everett LA, Wall SM, Royaux IE, Green ED, Marcus DC (2004) Loss of KCNJ10 protein expression abolishes endocochlear potential and causes deafness in Pendred syndrome mouse model. BMC Med 2: 30.

102. Kim HM, Wangemann P (2011) Epithelial cell stretching and luminal acidification lead to a retarded development of stria vascularis and deafness in mice lacking pendrin. PLoS One 6: e17949.

103. Everett LA, Belyantseva IA, Noben-Trauth K, Cantos R, Chen A, Thakkar SI, Hoogstraten-Miller SL, Kachar B, Wu DK, Green ED (2001) Targeted disruption of mouse Pds provides insight about the inner-ear defects encountered in Pendred syndrome. Hum Mol Genet 10: 153-161.

104. Hulander M, Wurst W, Carlsson P, Enerback S (1998) The winged helix transcription factor Fkh10 is required for normal development of the inner ear. Nat Genet 20: 374-376.

105. Dror AA, Politi Y, Shahin H, Lenz DR, Dossena S, Nofziger C, Fuchs H, Hrabe dA, Paulmichl M, Weiner S, Avraham KB (2010) Calcium oxalate stone formation in the inner ear as a result of an Slc26a4 mutation. J Biol Chem 285: 21724-21735.

106. Dror AA, Brownstein Z, Avraham KB (2011) Integration of human and mouse genetics reveals pendrin function in hearing and deafness. Cell Physiol Biochem 28: 535-544.

107. Lu YC, Wu CC, Shen WS, Yang TH, Yeh TH, Chen PJ, Yu IS, Lin SW, Wong JM, Chang Q, Lin X, Hsu CJ (2011) Establishment of a knock-in mouse model with the SLC26A4 c.919-2A>G mutation and characterization of its pathology. PLoS One 6: e22150.

108. Park HJ, Shaukat S, Liu XZ, Hahn SH, Naz S, Ghosh M, Kim HN, Moon SK, Abe S, Tukamoto K, Riazuddin S, Kabra M, Erdenetungalag R, Radnaabazar J, Khan S, Pandya A, Usami SI, Nance WE, Wilcox ER, Riazuddin S, Griffith AJ (2003) Origins and frequencies of SLC26A4 (PDS) mutations in east and south Asians: global implications for the epidemiology of deafness. J Med Genet 40: 242-248.

109. Lee H, Jung J, Shin J, Song M, Kim S, Lee JH, Lee KA, Shin S, Kim UK, Bok J, Lee KY, Choi J, Park H (2013) Correlation between genotype and phenotype in patients with bi-allelic SLC26A4 mutations. Clin Genet .

110. Lu YC, Wu CC, Yang TH, Lin YH, Yu IS, Lin SW, Chang Q, Lin X, Wong JM, Hsu CJ (2013) Differences in the pathogenicity of the p.H723R mutation of the common deafness-associated SLC26A4 gene in humans and mice. PLoS One 8: e64906.

111. Ishihara K, Okuyama S, Kumano S, Iida K, Hamana H, Murakoshi M, Kobayashi T, Usami S, Ikeda K, Haga Y, Tsumoto K, Nakamura H, Hirasawa N, Wada H (2010) Salicylate restores transport function and anion exchanger activity of missense pendrin mutations. Hear Res 270: 110-118.

112. Yoon JS, Park HJ, Yoo SY, Namkung W, Jo MJ, Koo SK, Park HY, Lee WS, Kim KH, Lee MG (2008) Heterogeneity in the processing defect of SLC26A4 mutants. J Med Genet 45: 411-419.

113. Dou H, Xu J, Wang Z, Smith AN, Soleimani M, Karet FE, Greinwald JH, Jr., Choo D (2004) Co-expression of pendrin, vacuolar H+-ATPase alpha4-subunit and carbonic anhydrase II in epithelial cells of the murine endolymphatic sac. J Histochem Cytochem 52: 1377-1384.

114. Choi BY, Kim HM, Ito T, Lee KY, Li X, Monahan K, Wen Y, Wilson E, Kurima K, Saunders TL, Petralia RS, Wangemann P, Friedman TB, Griffith AJ (2011) Mouse model of enlarged vestibular aqueducts defines temporal requirement of Slc26a4 expression for hearing acquisition. J Clin Invest 121: 4516-4525.

115. Li X, Sanneman JD, Harbidge DG, Zhou F, Ito T, Nelson R, Picard N, Chambrey R, Eladari D, Miesner T, Griffith AJ, Marcus DC, Wangemann P (2013) SLC26A4 targeted to the endolymphatic sac rescues hearing and balance in *Slc26a4* mutant mice. PLoS Genetics 9: e1003641.

116. Wangemann P, Kim HM, Billings S, Nakaya K, Li X, Singh R, Sharlin DS, Forrest D, Marcus DC, Fong P (2009) Developmental delays consistent with cochlear hypothyroidism contribute to failure to develop hearing in mice lacking Slc26a4/pendrin expression. Am J Physiol Renal Physiol 297: F1435-F1447.

117. Li X, Zhou F, Marcus DC, Wangemann P (2013) Endolymphatic Na(+) and K(+) concentrations during cochlear growth and enlargement in mice lacking Slc26a4/pendrin. PLoS One 8: e65977.

118. Nakaya K, Harbidge DG, Wangemann P, Schultz BD, Green ED, Wall SM, Marcus DC (2007) Lack of pendrin HCO3- transport elevates vestibular endolymphatic [Ca2+] by inhibition of acid-sensitive TRPV5 and TRPV6 channels. Am J Physiol Renal Physiol 292: F1314-F1321.

119. Unsold B, Kerst G, Brousos H, Hubner M, Schreiber R, Nitschke R, Greger R, Bleich M (2000) KCNE1 reverses the response of the human K+ channel KCNQ1 to cytosolic pH changes and alters its pharmacology and sensitivity to temperature. Pflugers Arch 441: 368-378.

120. Sadanaga M, Morimitsu T (1995) Development of endocochlear potential and its negative component in mouse cochlea. Hear Res 89: 155-161.

121. Hibino H, Horio Y, Inanobe A, Doi K, Ito M, Yamada M, Gotow T, Uchiyama Y, Kawamura M, Kubo T, Kurachi Y (1997) An ATP-dependent inwardly rectifying potassium channel, KAB-2 (Kir4. 1), in cochlear stria vascularis of inner ear: its specific subcellular localization and correlation with the formation of endocochlear potential. J Neurosci 17: 4711-4721.

122. Singh R, Wangemann P (2008) Free radical stress-mediated loss of Kcnj10 protein expression in stria vascularis contributes to deafness in Pendred syndrome mouse model. Am J Physiol Renal Physiol 294: F139-F148.

123. Hulander M, Kiernan AE, Blomqvist SR, Carlsson P, Samuelsson EJ, Johansson BR, Steel KP, Enerback S (2003) Lack of pendrin expression leads to deafness and expansion of the endolymphatic compartment in inner ears of Foxi1 null mutant mice. Development 130: 2013-2025.

124. Albert S, Blons H, Jonard L, Feldmann D, Chauvin P, Loundon N, Sergent-Allaoui A, Houang M, Joannard A, Schmerber S, Delobel B, Leman J, Journel H, Catros H, Dollfus H, Eliot MM, David A, Calais C, Drouin-Garraud V, Obstoy MF, Tran Ba HP, Lacombe D, Duriez F, Francannet C, Bitoun P, Petit C, Garabedian EN, Couderc R, Marlin S, Denoyelle F (2006) SLC26A4 gene is frequently involved in nonsyndromic hearing impairment with enlarged vestibular aqueduct in Caucasian populations. Eur J Hum Genet 14: 773-779.

125. Anwar S, Riazuddin S, Ahmed ZM, Tasneem S, Ateeq uJ, Khan SY, Griffith AJ, Friedman TB, Riazuddin S (2009) SLC26A4 mutation spectrum associated with DFNB4 deafness and Pendred's syndrome in Pakistanis. J Hum Genet 54: 266-270.

126. Choi BY, Stewart AK, Madeo AC, Pryor SP, Lenhard S, Kittles R, Eisenman D, Kim HJ, Niparko J, Thomsen J, Arnos KS, Nance WE, King KA, Zalewski CK, Brewer CC, Shawker T, Reynolds JC, Butman JA, Karniski LP, Alper SL, Griffith AJ (2009) Hypo-functional SLC26A4 variants associated with nonsyndromic hearing loss and enlargement of the vestibular aqueduct: genotype-phenotype correlation or coincidental polymorphisms? Hum Mutat 30: 599-608.

127. Pera A, Dossena S, Rodighiero S, Gandia M, Botta G, Meyer G, Moreno F, Nofziger C, Hernandez-Chico C, Paulmichl M (2008) Functional assessment of allelic variants in the SLC26A4 gene involved in Pendred syndrome and nonsyndromic EVA. Proc Natl Acad Sci U S A 105: 18608-18613.

128. Wu CC, Lu YC, Chen PJ, Yeh PL, Su YN, Hwu WL, Hsu CJ (2010) Phenotypic analyses and mutation screening of the SLC26A4 and FOXI1 genes in 101 Taiwanese families with bilateral nonsyndromic enlarged vestibular aqueduct (DFNB4) or Pendred syndrome. Audiol Neurootol 15: 57-66.

129. Yuan Y, You Y, Huang D, Cui J, Wang Y, Wang Q, Yu F, Kang D, Yuan H, Han D, Dai P (2009) Comprehensive molecular etiology analysis of nonsyndromic hearing impairment from typical areas in China. J Transl Med 7: 79.

130. Cheung CY, Brace RA (2005) Amniotic fluid volume and composition in mouse pregnancy. J Soc Gynecol Investig 12: 558-562.

131. Jayakannan M, Babourina O, Rengel Z (2011) Improved measurements of Na+ fluxes in plants using calixarene-based microelectrodes. J Plant Physiol 168: 1045-1051.

132. Barry PH (1994) JPCalc, a software package for calculating liquid junction potential corrections in patch-clamp, intracellular, epithelial and bilayer measurements and for correcting junction potential measurements. J Neurosci Methods 51: 107-116.

133. Untergasser A, Cutcutache I, Koressaar T, Ye J, Faircloth BC, Remm M, Rozen SG (2012) Primer3--new capabilities and interfaces. Nucleic Acids Res 40: e115.

134. Ramakers C, Ruijter JM, Deprez RH, Moorman AF (2003) Assumption-free analysis of quantitative real-time polymerase chain reaction (PCR) data. Neurosci Lett 339: 62-66.

135. Sadanaga M, Morimitsu T (1995) Development of endocochlear potential and its negative component in mouse cochlea. Hear Res 89: 155-161.

136. Lee JH, Marcus DC (2003) Endolymphatic sodium homeostasis by Reissner's membrane. Neuroscience 119: 3-8.

137. Yoo JC, Kim HY, Han KH, Oh SH, Chang SO, Marcus DC, Lee JH (2012) Na+ absorption by Claudius' cells is regulated by purinergic signaling in the cochlea. Acta Otolaryngol 132 Suppl 1: S103-S108.

138. Anniko M, Wroblewski R (1980) Elemental composition of the mature inner ear. Acta Otolaryngol 90: 425-430.

139. Anniko M, Nordemar H (1980) Embryogenesis of the inner ear. IV. Post-natal maturation of the secretory epithelia of the inner ear in correlation with the elemental composition in the endolymphatic space. Arch Otorhinolaryngol 229: 281-288.

140. Kim SH, Marcus DC (2011) Regulation of sodium transport in the inner ear. Hear Res 280: 21-29.

141. Kim CH, Kim HY, Chang O, Oh SH, Lee JE, Lee JH (2009) Developmental change of Na(+)-absorptive function in Reissner's membrane epithelia. Neuroreport 20: 1275-1278.

142. Lelli A, Asai Y, Forge A, Holt JR, Geleoc GS (2009) Tonotopic gradient in the developmental acquisition of sensory transduction in outer hair cells of the mouse cochlea. J Neurophysiol 101: 2961-2973.

143. Kim SH, Park HY, Choi HS, Chung HP, Choi JY (2009) Functional and molecular expression of epithelial sodium channels in cultured human endolymphatic sac epithelial cells. Otol Neurotol 30: 529-534.

144. Griffith AJ, Arts A, Downs C, Innis JW, Shepard NT, Sheldon S, Gebarski SS (1996) Familial large vestibular aqueduct syndrome. Laryngoscope 106: 960-965.

145. Phelps PD, Coffey RA, Trembath RC, Luxon LM, Grossman AB, Britton KE, Kendall-Taylor P, Graham JM, Cadge BC, Stephens SG, Pembrey ME, Reardon W (1998) Radiological malformations of the ear in Pendred syndrome. Clin Radiol 53: 268-273.

146. Valvassori GE, Clemis JD (1978) The large vestibular aqueduct syndrome. Laryngoscope 88: 723-728.

147. Takeda T, Taguchi D (2009) Aquaporins as potential drug targets for Meniere's disease and its related diseases. Handb Exp Pharmacol 171-184.

148. Jacques T, Picard N, Miller RL, Riemondy KA, Houillier P, Sohet F, Ramakrishnan SK, Busst CJ, Jayat M, Corniere N, Hassan H, Aronson PS, Hennings JC, Hubner CA, Nelson RD, Chambrey R, Eladari D (2013) Overexpression of Pendrin in Intercalated Cells Produces Chloride-Sensitive Hypertension. J Am Soc Nephrol .

149. Miller RL, Zhang P, Smith M, Beaulieu V, Paunescu TG, Brown D, Breton S, Nelson RD (2005) V-ATPase B1-subunit promoter drives expression of EGFP in intercalated cells of kidney, clear cells of epididymis and airway cells of lung in transgenic mice. Am J Physiol Cell Physiol 288: C1134-C1144.

150. Royaux IE, Belyantseva IA, Wu T, Kachar B, Everett LA, Marcus DC, Green ED (2003) Localization and functional studies of pendrin in the mouse inner ear provide insight about the etiology of deafness in pendred syndrome. J Assoc Res Otolaryngol 4: 394-404.

151. Thibaut J, Picard N, Miller RL, Riemondy KA, Houillier P, Sohet F, Ramakrishnan S, Büsst C, Jayat M, Corniere N, Aronson PS, Hennings JC, Hübner C, Nelson R, Chambrey R, Eladari D (2013) Mice with overexpression of hte renal Cl-/HCO3- exchanger Pendrin (Slc26a4) develop chloride-sensitive hypertension. J Am Soc Nephrol in press: .

152. Miller RL, Lucero OM, Riemondy KA, Baumgartner BK, Brown D, Breton S, Nelson RD (2009) The V-ATPase B1-subunit promoter drives expression of Cre recombinase in intercalated cells of the kidney. Kidney Int 75: 435-439.

153. Huntzinger E, Izaurralde E (2011) Gene silencing by microRNAs: contributions of translational repression and mRNA decay. Nat Rev Genet 12: 99-110.

154. Frisina RD, Singh A, Bak M, Bozorg S, Seth R, Zhu X (2011) F1 (CBAxC57) mice show superior hearing in old age relative to their parental strains: hybrid vigor or a new animal model for "golden ears"? Neurobiol Aging 32: 1716-1724.

155. Ison JR, Allen PD, O'Neill WE (2007) Age-related hearing loss in C57BL/6J mice has both frequency-specific and non-frequency-specific components that produce a hyperacusis-like exaggeration of the acoustic startle reflex. J Assoc Res Otolaryngol 8: 539-550.

156. Ohlemiller KK, Gagnon PM (2004) Cellular correlates of progressive hearing loss in 129S6/SvEv mice. J Comp Neurol 469: 377-390.

157. Ouagazzal AM, Reiss D, Romand R (2006) Effects of age-related hearing loss on startle reflex and prepulse inhibition in mice on pure and mixed C57BL and 129 genetic background. Behav Brain Res 172: 307-315.

158. Zheng QY, Johnson KR, Erway LC (1999) Assessment of hearing in 80 inbred strains of mice by ABR threshold analyses. Hear Res 130: 94-107.

159. Rugh R (1968) The mouse; its reproduction and development. Burgess Pub Co .

160. Theiler K (1972) The house mouse; development and normal stages from fertilization to 4 weeks of age. Springer-Verlag .

161. Kiernan AE (2006) The paintfill method as a tool for analyzing the three-dimensional structure of the inner ear. Brain Res 1091: 270-276.

162. Martin P, Swanson GJ (1993) Descriptive and experimental analysis of the epithelial remodellings that control semicircular canal formation in the developing mouse inner ear. Dev Biol 159: 549-558.

163. Kim YH, Kwon TH, Frische S, Kim J, Tisher CC, Madsen KM, Nielsen S (2002) Immunocytochemical localization of pendrin in intercalated cell subtypes in rat and mouse kidney. Am J Physiol Renal Physiol 283: F744-F754.

164. Marcus DC, Rokugo M, Thalmann R (1985) Effects of barium and ion substitutions in artificial blood on endocochlear potential. Hear Res 17: 79-86.